

Characterization of SrAl₂O₄:Eu²⁺,Dy³⁺ nano thin films prepared by pulsed laser deposition

By

**Patrick Damson Nsimama
(MSc)**

A thesis submitted in fulfillment of the requirements for the degree

PHILOSOPHIAE DOCTOR

in the

Faculty of Natural and Agricultural Sciences

Department of Physics

at the

University of the Free State

Promoter: Prof. H.C. Swart

Co-Promoter: Prof. O.M. Ntwaeaborwa

November 2010

Dedication

Dedicated to the memory of my lovely mother; the late Mbozyo Mwangaya (1924-1990)

ACKNOWLEDGEMENTS

First and foremost, I express my heartfelt gratitude to The Almighty God; my Father, for granting me the opportunity to pursue this study. I thank him also for enabling me to complete my studies successfully. I have done all things through Christ who has been strengthening me.

With an immense sense of humility, I express my sincere thanks and enormous gratitude to my supervisor Professor H.C. Swart for his esteemed guidance, invaluable help and fruitful suggestions throughout the course of my work. He played a great role in securing funds for my study program. He is a man of people who clearly knows how to lead the group as a family. I have learned a lot on technical aspects of research from him.

I would particularly like to express my indebtedness to my co-supervisor Prof. O. M. Ntwaeaborwa for his guidance and encouragement during the entire course of my studies. He has taught me a lot on the writing skills of which he is very good. He also introduced me to the sol-gel process of phosphor preparations of which I am very grateful. I thank him for his technical advice in the organization of ideas.

I am greatly indebted to the African Laser Center (ALC), National Research Foundation (NRF) and the Cluster Programme of the University of the Free State for their financial support.

I would like to extend my special gratitude to Thomas du Plooy and Brian Yalisi of the National Laser Center (NLC) for their valuable support during my visits to the NLC for my experimental work.

Special thanks go to my employer, the Principal of Dar es Salaam Institute of Technology, Prof. J.W.A. Kondoro for granting me permission to come to study here, his financial and moral support. He is a man of understanding.

I express my thanks to the Head, Department of Laboratory Technology at the Dar es Salaam Institute of Technology, Dr. Leonia for his cooperation and my colleagues employee (L.L.

Mkiramweni, D. Ntisy, Dr. Ezekiel, Mrs C. Kimaro, A. Mmari and C. Muhale) for their moral support.

I especially thank my fellow researchers (Dr. E. Coetsee, G. Tshabalala, P.S. Mbule, D.B. Bem, JJ. Dolo, Dr. P. Shreyas, Dr. I.M Nagpure, Dr. B.M. Mothudi, H.J. Van Heerden, S. Kronje, Dr. Marek Gusowski, M.M.Duvenhage, P.A. Moleme, P. Nkundabakura, B. Oruru, H. S Ahmed, M.J Madito, B. Ogundenji & family for their continuous academic and social support. Last but not least, I would like to acknowledge the moral support from Prof. JJ. Terblans, Prof. W.D. Roos, Prof. P.J. Meintjes, Prof. M.J.H Hoffman, Dr. T. Kroon and Mr. D.P. van Jaarsveldt.

I express my thanks to the technical staff, Prof. PWJ Van Wyk and B. Janecke of the Center of Microscopy for their great support and advice during SEM measurements.

I would also like to extend my heartfelt appreciations to Prof. J.R. Botha and Dr. Julien Dangbegnon from the Nelson Mandela Metropolitan University for the technical support during the photoluminescence measurements using their PL system.

My special thanks go to my pastors L. Mbega of Tanzania Assemblies of God (TAG) and F. Aboakye of Christ Embassy Church, Bloemfontein for their spiritual fatherhood and prayers.

I also acknowledge the support of the administrative staff in the Physics Department, namely E. Pretorius, K. Cronje, P. Ntulini and Y. Fick.

My appreciations also go to Prof. J.T. Abiade from Virginia Tech. for his assistance in doing Transmission electron microscopy measurements for my samples.

Dr. W.L. Anangisye is highly acknowledged for his advice, encouragement and brotherly love. My brother J.M. Nsimama and my nephew T.M. Sijabaje, my sister Anastazia Nsimama, Godwin Nsimama, Augustino Nsimama and Kaole Mwangaya are highly appreciated for their encouragement and moral support.

I would also like to express my sincere gratitude to my brethren; Mr and Mrs Yinka, Pastor Tatu, Mr. G. Komba, Mr. N. Materu, Mr. M. Kazilo, Mr. Mwangata, Mr. Kigaila and the

rest of Christ Embassy, Bloemfontein and TAG Mbezi Luis church members for their encouragements.

I owe my loving thanks to my lovely family; my wife Lucy, my daughters Happy, Diana and Dorcas, my sons; Benny and Adam for their patience and prayers during all the time of my study. I am very proud of having them in my life.

ABSTRACT

Thin films of $\text{SrAl}_2\text{O}_4:\text{Eu}^{2+},\text{Dy}^{3+}$ phosphor were deposited on silicon (Si (100)) substrates using a 248 nm KrF pulsed laser. Deposition parameters, namely; substrate temperature, pulse repetition rate, number of laser pulses, base pressure and the working atmosphere were varied during the film deposition processes. Atomic force microscopy (AFM), Scanning electron microscopy (SEM), X-ray Diffraction (XRD), energy dispersive x-ray spectroscopy (EDS), and the fluorescence spectrophotometry were used to characterize the thin films. The surface characterization was done by using Auger electron spectroscopy (AES) combined with CL spectroscopy and X-ray photoelectron spectroscopy (XPS). PL data were collected in air at room temperature using a 325 nm He-Cd laser PL system and the UV Xenon lamp Cary Eclipse fluorescence spectrophotometer.

The particle morphologies, surface topographies and photoluminescence (PL) properties were varying with the deposition parameters. Rougher film surfaces gave better PL properties. The optimum substrate temperature for $\text{SrAl}_2\text{O}_4:\text{Eu}^{2+},\text{Dy}^{3+}$ films with intense PL emission was in the 350-400° C range. $\text{SrAl}_2\text{O}_4:\text{Eu}^{2+},\text{Dy}^{3+}$ thin films ablated using a higher number of pulses gave superior PL properties to those deposited at lower number of pulses. As-deposited films prepared in the gas atmospheres gave AFM images with well defined particles and better PL properties than those deposited in vacuum. The average particle sizes for films deposited in gas atmospheres were ranging from 25 nm to 40 nm. The results from XRD and HRTEM showed that the as-deposited $\text{SrAl}_2\text{O}_4:\text{Eu}^{2+},\text{Dy}^{3+}$ thin films were amorphous. Upon annealing at 800° in vacuum for 2 hours, the PL of the films deposited in the gas atmospheres decreased. However, the crystallinity and the PL properties of the annealed vacuum deposited thin film improved considerably. The CL spectra gave only green emission peaks ranging from 507 nm to 522 nm. Both the PL and CL emissions were ascribed to the $4f^65d^1 \rightarrow 4f^7$ Eu^{2+} ion transitions.

The AES elemental composition results for the undegraded and electron degraded thin films gave all the main elements in the $\text{SrAl}_2\text{O}_4:\text{Eu}^{2+},\text{Dy}^{3+}$ material, i.e. Sr, Al and O. The ratios of Al and Sr APPHs to that of O increased slightly during removal of the C from the surface. The C/O ratio decreased with an increase in electron dose. Results from the RBS showed thin film $\text{SrAl}_2\text{O}_4:\text{Eu}^{2+},\text{Dy}^{3+}$ stoichiometric ratios comparable to the commercial powder. The sharp decrease in the C/O APPH ratio was due to removal of C from the surface due to the

electron stimulated surface chemical reactions (ESSCRs) which took place during electron bombardment. During the ESSCR process, the electron beam dissociates the O₂ and other background species such as H₂O to atomic species which subsequently react with C to form volatile compounds (CO_x, CH₄, etc.). The CL intensity degraded during prolonged electron beam irradiation due to the ESSCR process. The CL degradation increased with the increase in the chamber base pressure. The XPS data collected from the degraded films proved that strontium oxide (SrO) and aluminium oxide (Al₂O₃) were formed on the surface of the films as a result of the ESSCR in line with the increase of Sr/O and Al/O from the AES results.

KEYWORDS

SrAl₂O₄:Eu²⁺, Dy³⁺, Pulsed laser deposition, thin films, photoluminescence, afterglow, cathodoluminescence, atomic force microscopy, scanning electron microscopy, Auger electron spectroscopy, X-ray photoelectron spectroscopy.

ACRONYMS AND SYMBOLS

- PL- Photoluminescence
- CL - Cathodoluminescence
- AES - Auger electron spectroscopy
- APPHs - Auger peak-to-peak heights
- XPS -X-ray photoelectron spectroscopy
- XRD -X-ray diffraction
- HRTEM – High resolution Transmission electron microscopy
- SEM- Scanning electron microscopy
- EDS -Energy dispersive spectroscopy
- PLD -Pulsed laser deposition
- AFM- Atomic force microscopy
- XPS- X-ray photoelectron spectroscopy
- RBS – Rutherford back scattering
- FTIR – Fourier-Transform infrared
- He-Cd- Helium Cadmium
- RE- Rare earth
- KrF-Krypton fluoride
- Sr- Strontium
- Al- Aluminium
- O₂- Oxygen molecule
- O- Oxygen atom
- VB- Valence band
- CB- Conduction band
- V_O- Oxygen vacancy
- V_{Sr}-Strontium vacancy

TABLE OF CONTENTS

ACKNOWLEDGEMENTS.....	iii
ABSTRACT.....	vi
KEYWORDS.....	vii
ACRONYMS.....	viii

CHAPTER 1: INTRODUCTION

1.1 OVERVIEW.....	1
1.2 STATEMENT OF THE RESEARCH PROBLEM.....	3
1.3 RESEARCH OBJECTIVES.....	4
1.4 THESIS LAYOUT.....	5
REFERENCES.....	6

CHAPTER 2: THEORY

2.1 AN OVERVIEW TO PHOSPHORS.....	8
2.2 FLUORESCENCE.....	10
2.3 PHOSPHORESCENCE.....	10
2.4 PHOTOLUMINESCENCE MEASUREMENT PRINCIPLES.....	11
2.5 CATHODOLUMINESCENCE MEASUREMENT PRINCIPLES.....	13
2.5.1 GENERATION OF ELECTRON-HOLE (EH) PAIRS.....	13
2.5.2 DEGRADATION OF CATHODOLUMINESCENCE.....	15
2.6 STRUCTURE AND PROCESSES DETERMINING THE EMISSION PROPERTIES OF $\text{SrAl}_2\text{O}_4:\text{Eu}^{2+},\text{Dy}^{3+}$	16
2.6.1 THE f-d TRANSITIONS.....	16
2.6.2 AFTERGLOW (PHOSPHORESCENCE) MECHANISM OF $\text{SrAl}_2\text{O}_4:\text{Eu}^{2+},\text{Dy}^{3+}$..	18
2.6.3 THE CRYSTAL STRUCTURE OF SrAl_2O_4	21
REFERENCES.....	23

CHAPTER 3: RESEARCH TECHNIQUES

3.1 INTRODUCTION.....	25
3.2 PULSED LASER DEPOSITION (PLD) TECHNIQUE.....	25

3.3 PHOTOLUMINESCENCE (PL).....	27
3.4 SCANNING ELECTRON MICROSCOPY (SEM).....	31
3.5 ATOMIC FORCE MICROSCOPY (AFM).....	32
3.6 HIGH RESOLUTION TRANSMISSION ELECTRON MICROSCOPY (HRTEM).....	32
3.7 X-RAY DIFFRACTION (XRD).....	33
3.8 AUGER ELECTRON SPECTROSCOPY (AES).....	31
3.9 X-RAY PHOTOELECTRON SPECTROSCOPY (XPS)	34
3.10 RUTHERFORD BACKSCATTERING (RBS).....	35
REFERENCES.....	38

CHAPTER 4: THE EFFECTS OF SUBSTRATE TEMPERATURE ON THE STRUCTURE, MORPHOLOGY AND PHOTOLUMINESCENCE PROPERTIES OF PULSED LASER DEPOSITED SrAl₂O₄:Eu²⁺,Dy³⁺ THIN FILMS

4.1 INTRODUCTION.....	39
4.2 EXPERIMENTAL DETAILS.....	40
4.3 RESULTS AND DISCUSSION.....	40
4.4 CONCLUSION.....	44
REFERENCES.....	46

CHAPTER 5: THE INFLUENCE OF THE NUMBER OF PULSES ON THE MORPHOLOGICAL AND PHOTOLUMINESCENCE PROPERTIES OF SrAl₂O₄:Eu²⁺,Dy³⁺ THIN FILMS PREPARED BY PULSED LASER DEPOSITION

5.1 INTRODUCTION.....	47
5.2 MATERIALS AND METHODS.....	48
5.3 RESULTS AND DISCUSSION.....	48
5.4 CONCLUSION.....	54
REFERENCES.....	55

CHAPTER 6: PHOTOLUMINESCENCE PROPERTIES OF SrAl₂O₄:Eu²⁺,Dy³⁺ THIN PHOSPHOR FILMS GROWN BY PULSED LASER DEPOSITION

6.1 INTRODUCTION.....	56
-----------------------	----

6.2 EXPERIMENTAL DETAILS.....	57
6.3 RESULTS AND DISCUSSIONS.....	58
6.4 CONCLUSION.....	64
REFERENCES.....	65

CHAPTER 7: THE EFFECT OF DIFFERENT GAS ATMOSPHERES ON THE LUMINESCENT PROPERTIES OF PULSED LASER ABLATED SrAl₂O₄:Eu²⁺,Dy³⁺ THIN FILMS

7.1 INTRODUCTION.....	66
7.2 EXPERIMENTAL DETAILS.....	67
7.3 RESULTS AND DISCUSSION.....	68
7.3.1 SEM RESULTS.....	68
7.3.2 AFM RESULTS.....	69
7.3.3 XRD RESULTS.....	72
7.3.4 PHOTOLUMINESCENCE RESULTS.....	73
7.3.5 LONG AFTERGLOW CHARACTERISTICS.....	75
7.3.6 THE XRD AND PL RESULTS FOR THE ANNEALED FILM.....	77
7.3.7 DEPTH PROFILE ANALYSIS.....	79
7.4 CONCLUSION.....	81
REFERENCES.....	82

CHAPTER 8: ELEMENTAL COMPOSITION AND CATHODOLUMINESCENT STUDIES OF PULSED LASER ABLATED SrAl₂O₄:Eu²⁺, Dy³⁺ THIN FILMS

8.1 INTRODUCTION.....	84
8.2 EXPERIMENTAL DETAILS.....	85
8.3 RESULTS AND DISCUSSION.....	86
8.3.1 THE SEM RESULTS.....	86
8.3.2 THE AES RESULTS.....	88
8.3.3 CL RESULTS.....	89
8.4 CONCLUSION.....	91
REFERENCES.....	92

**CHAPTER 9: AUGER ELECTRON/X-RAY PHOTOELECTRON AND
CATHODOLUMINESCENT SPECTROSCOPIC STUDIES OF PULSED LASER
ABLATED SrAl₂O₄:Eu²⁺, Dy³⁺ THIN FILMS**

9.1 INTRODUCTION.....93
9.2 EXPERIMENTAL DETAILS.....94
9.3 RESULTS AND DISCUSSION.....95
 9.3.1 THE AUGER ELECTRON SPECTROSCOPY (AES) RESULTS.....95
 9.3.2 CL RESULTS.....98
 9.3.3 THE XPS RESULTS.....101
9.4 CONDLUSION.....106
REFERENCES.....108

CHAPTER 10: SUMMARY AND SUGGESTIONS FOR FUTURE WORK

11.1 THESIS SUMMARY.....110
11.2 SUGGESTIONS FOR THE FUTURE WORK.....113

PUBLICATIONS

PUBLICATIONS RESULTING FROM THIS WORK.....115
PRESENTATIONS IN CONFERENCES/WORKSHOPS.....116

CHAPTER 1

INTRODUCTION

1.1 OVERVIEW

The phenomenon of persistent luminescence has been known to mankind thousands of years ago. This phenomenon was first demonstrated by ancient Chinese paintings that remained visible at night when different colours were mixed with a special kind of pearl shell [1]. The first scientifically described observation of persistent luminescence (afterglow) dates back to 1602, when shoemaker and alchemist Vincenzo Casciarolo discovered the famous Bologna stone. The afterglow of this stone was described by Fortunius Licetus in the *Litheosporus Sive De Lapide Bononiensi* in 1640, and he attributed it to the natural barium sulphide impurity present in the stone [1].

For many decades, zinc sulphide (ZnS) doped with copper (and later co doped with cobalt) was the most famous and widely used persistent phosphor [2, 3, 4]. In August 1996, Matsuzawa *et al.* [5] published an article on the $\text{SrAl}_2\text{O}_4:\text{Eu}^{2+}$, where they reported the afterglow from this material that lasted for several hours. Takasaki *et al.* [6] co doped SrAl_2O_4 with divalent europium (Eu^{2+}) and trivalent dysprosium (Dy^{3+}), resulting in a phosphor that emitted bright light for hours after cutting off the excitation.

Today, the $\text{SrAl}_2\text{O}_4:\text{Eu}^{2+}, \text{Dy}^{3+}$ phosphor has attracted a lot of attention due to its high quantum efficiency, long afterglow and good stability [7]. Its long afterglow properties have resulted in its application in a wide variety of light emitting devices. For example, it is used in luminous paint for highway, airport escape routes and buildings. In addition, it can also be used in textile printing, the dial plates of glow watch, warning signs, etc. [8]. SrAl_2O_4 has a stuffed tridymite structure, which is constructed by corner-shared AlO_4 tetrahedrons, and large divalent cations, Sr^{2+} ions, that occupy the interstitial sites to compensate for the charge

imbalance [9]. Since the ionic radii of Sr^{2+} (1.21 Å) and Eu^{2+} (1.20 Å) ions are almost equal, Eu^{2+} tends to substitute Sr^{2+} sites in the stuffed tridymite structure. The $4f^65d^1 \rightarrow 4f^7$ transitions of Eu^{2+} ions in the SrAl_2O_4 matrix provides a broad band emission centered at 520 nm [10]. High luminescent intensity and longer decay times are very important features of long afterglow phosphors. The long afterglow of $\text{SrAl}_2\text{O}_4:\text{Eu}^{2+},\text{Dy}^{3+}$ is believed to originate from the photo-oxidation of the Eu^{2+} cation under UV-irradiation [11]. According to this model, an electron from the $4f^7$ ground state is excited to the $4f^65d^1$ level of Eu^{2+} followed by an electron capture from the valence band reducing Eu^{2+} to Eu^+ . The hole generated in the valence can migrate and be captured by Dy^{3+} converting it to Dy^{4+} . Relaxation to the ground state, which is accompanied by green emission, is triggered by the thermo-activated promotion of an electron from the valence band to the first unoccupied levels of Dy^{4+} followed by a migration of the trapped hole to the photon-generated Eu^+ cation [5].

Conventionally, strontium aluminates (SrAlO_4) are prepared by solid-state reactions between SrO or SrCO_3 and Al_2O_3 . Without flux, the preparation of the SrAl_2O_4 phase generally requires high temperatures (i.e. 1400-1600° C) [12, 13] and produces grains of large size. Other chemical methods that have been developed for the synthesis of strontium aluminates, are, sol-gel [8], detonation [14], combustion [15], chemical precipitation [16] etc. In most of the reported works [7, 8, 13, 15, 16], the $\text{SrAl}_2\text{O}_4:\text{Eu}^{2+},\text{Dy}^{3+}$ phosphors have been prepared and investigated in the form of powders. However, for various industrial applications such as device fabrication and surface coatings it is important to investigate the performance of these phosphors in the form of thin films as well. Moreover, it is well documented that thin film phosphors have several advantages over powders, such as higher lateral resolution from smaller grains, better thermal stability, reduced out gassing, and better adhesion to solid substrates [17]. They can also be used in fabrication of smaller pixels to enhance resolutions of information display screens [18].

Amongst the techniques used to prepare luminescent thin films, pulsed-laser deposition has several attractive features, including stoichiometric transfer of the target material, generation of quality plume of energetic species, hyper thermal reaction between the ablated cations and molecular O_2 in the ablation plasma, and compatibility with background pressures ranging from UHV to 100 Pa [17]. The plasma fabricated during pulsed laser ablation is very energetic, and its mobility can be easily controlled by changing processing parameters [19].

The presence of a background gas in the chamber has a strong influence on the quality of the plasma produced by the laser. The gas can modify the kinetic energy and the spatial distribution of the ejected species present in the plasma, and it may also induce compositional changes in the deposited films [20]. Plume collisions may also provide an increase in the vibration energy of molecular species [21]. Thus, the background gas affects the spatial distribution, the deposition rate, the energy and distribution of ablated particles thereby controlling the cluster formation, cluster size, cluster energy and particle distribution [21].

Another important deposition parameter is the substrate temperature. The mobility of the atoms deposited on the surface is directly dependent on temperature, a dependence which can influence the activation energy of each process [22]. Reports have also shown that the crystallinity of the as-grown films is highly dependent upon the processing temperature. However, a high temperature will cause the inter-diffusion reaction at the interface between the film and substrate or substrate surface reconstruction that strongly alters the physical properties of the as-grown films [23]. The substrate temperature has a dominant influence on the film structure like crystallinity, orientation and surface morphology.

Apart from the above mentioned deposition parameters, there are several others which have a significant influence on the properties of laser ablated thin films, namely, the laser fluence, laser wavelength, laser energy, shape of the laser pulse, focusing geometry, number of pulses (thickness), repetition rate, laser-target distance, substrate-target distance, substrate type, etc. In particular, the choice of the laser has a greater effect on the parameters of the ablative particle fluxes and hence on the film properties [24]. By varying the deposition conditions, the morphological, topographical and structural properties change and luminescent properties of the phosphor can also change. Current research topics on the $\text{SrAl}_2\text{O}_4:\text{Eu}^{2+}$, Dy^{3+} include among other things, the study of the synthesis, luminescent properties (photoluminescence (PL), cathodoluminescence (CL), electroluminescence (EL), etc.) and decay characteristics and phosphorescence mechanisms.

1.2 STATEMENT OF THE RESEARCH PROBLEM

$\text{SrAl}_2\text{O}_4:\text{Eu}^{2+}$, Dy^{3+} material is a potential candidate for applications in the infrastructures, especially in form of long afterglow luminous paints. Measures to meet the increased demand ought to involve large scale production plans. Among other things, intensive laboratory

research works need to be done in order to understand the science of $\text{SrAl}_2\text{O}_4:\text{Eu}^{2+},\text{Dy}^{3+}$ material. The laboratory results are the needed outputs for the large scale engineering work. $\text{SrAl}_2\text{O}_4:\text{Eu}^{2+},\text{Dy}^{3+}$ has been investigated extensively in the powder form. However, there is very limited reports in the literature on $\text{SrAl}_2\text{O}_4:\text{Eu}^{2+}, \text{Dy}^{3+}$ thin films. There are even fewer results on pulsed laser deposited $\text{SrAl}_2\text{O}_4:\text{Eu}^{2+}, \text{Dy}^{3+}$ thin films despite the fact that the technique is among the best for thin film depositions. There isn't any literature on the elemental composition analysis of $\text{SrAl}_2\text{O}_4:\text{Eu}^{2+}, \text{Dy}^{3+}$ thin films. Additionally, no CL study has been reported on pulsed laser deposited (PLD) $\text{SrAl}_2\text{O}_4:\text{Eu}^{2+}, \text{Dy}^{3+}$ thin films.

Due to the potential future applications of $\text{SrAl}_2\text{O}_4:\text{Eu}^{2+}, \text{Dy}^{3+}$ material, the need to understand its science for large scale production plans and the suitability of the PLD process for preparing $\text{SrAl}_2\text{O}_4:\text{Eu}^{2+}, \text{Dy}^{3+}$ in thin films, there is a need to do more researches on PLD $\text{SrAl}_2\text{O}_4:\text{Eu}^{2+}, \text{Dy}^{3+}$ thin films. It is also essential to study the stability of the material to various irradiation sources such as ultraviolet light and electron beams for stable lighting and display applications.

1.3 RESEARCH OBJECTIVES

- To prepare $\text{SrAl}_2\text{O}_4:\text{Eu}^{2+}, \text{Dy}^{3+}$ thin films using the PLD technique.
- To study the changes on the thin film properties with the PLD deposition parameters
- To study the PL and CL characteristics of the $\text{SrAl}_2\text{O}_4:\text{Eu}^{2+}, \text{Dy}^{3+}$ thin films.
- To study the structural and morphological properties of the PLD $\text{SrAl}_2\text{O}_4:\text{Eu}^{2+}, \text{Dy}^{3+}$ thin films using X-ray Diffraction (XRD), Atomic Force Microscopy (AFM) and Scanning Electron Microscopy (SEM) respectively.
- To study the afterglow properties of $\text{SrAl}_2\text{O}_4:\text{Eu}^{2+},\text{Dy}^{3+}$ thin films and the CL stability to electron beam irradiation.
- To investigate the relationship between the PL/ CL and the structural/morphological properties of $\text{SrAl}_2\text{O}_4:\text{Eu}^{2+},\text{Dy}^{3+}$ thin films.
- To investigate the elemental composition of pulsed laser deposited thin films using the AES, XPS and EDS.
- To determine the stoichiometric ratios of the elements in PLD $\text{SrAl}_2\text{O}_4:\text{Eu}^{2+},\text{Dy}^{3+}$ thin films using the RBS technique.

1.4 THESIS LAYOUT

This thesis is divided into three main parts; namely theory (chapters 2-3), photoluminescence investigation (Chapters 4-7) and cathodoluminescence investigation (Chapters 8-9). Chapter 2 provides an overview of phosphors and their fundamental properties. A detailed account on the structure and processes determining the properties of the $\text{SrAl}_2\text{O}_4:\text{Eu}^{2+},\text{Dy}^{3+}$ material, namely f-d transition, phosphorescence mechanism and the crystal structure is also given. Chapter 3 gives a brief description of the research techniques involved in this work including the film preparation technique, i.e. PLD and the film surface characterization techniques.

The PL investigation (Chapters 4-7) comprises of results obtained through varying PLD deposition parameters, namely substrate temperature (Chapter 4), number of pulses (Chapter 5), pulse repetition rate and base pressure (Chapter 6) and the deposition atmospheres (Chapter 7). This part discusses mainly the Photoluminescence (PL) properties and its relation to the surface properties of the films.

Chapters 8-9 discusses mainly the surface analysis (Auger electron spectroscopy (AES) and X-ray photoelectron spectroscopy (XPS)) and cathodoluminescence results of $\text{SrAl}_2\text{O}_4:\text{Eu}^{2+},\text{Dy}^{3+}$ thin films.

Chapter 10 gives the summary of the thesis results and suggestions for future work. The last part of the thesis gives a list of publications resulting from this work and the conferences/workshops presentations.

REFERENCES

1. E.N. Harvey, *A History of Luminescence from the Earliest Times until 1900*; American Philosophical Society: Philadelphia, PA, USA, 1957.
2. H.C. Swart, J.S. Sebastian, T.A. Trottier, S.L. Jones, P.H. Holloway, *J. Vac. Sci. Technol. A* **14** (1996) 1697.
3. H.C. Swart, T.A. Trottier, J.S. Sebastian, S.L. Jones, P.H. Holloway, *J. Appl. Phys.* **83** (1998) 4578.
4. O.M. Ntwaeaborwa, H.C. Swart, R.E. Kroon, *J. Vac. Sci. Technol. A* **25** (2007) 1152.
5. T. Matsuzawa, Y. Aoki, N. Takeuchi, Y.A Murayama, *J. Electrochem. Soc.*, **143**, (1996) 2670.
6. H. Takasaki, S. Tanabe, T. Hanada, *J. Ceram. Soc.* **104** (1996), 322.
7. O.M. Ntwaeaborwa, P.D. Nsimama, J.T. Abiade, E. Coetsee, H.C. Swart, *Phys. B: Condens. Matter* **404** (2008) 4436.
8. T. Peng, L. Huajun, H. Yang, C. Yan, *Mater. Chem. & Phys.* **85** (2004) 68-72.
9. D.Ravichandran, S.T. Johnson, S. Erdei, R. Roy, W.B. White, *Displays* **19** (1999) 197.
10. H.C. Swart, E. Coetzee, J.J. Terblans, O.M. Ntwaeaborwa, P.D. Nsimama, F.B. Dejene, J.J. Dolo, *Appl. Phys. A* **101** (2010) 633.
11. F. Clabau, X. Rocquefelte, S. Jobic, P. Denieard, M.-H. Whangbo, A. Garcia, T. Mercier, *Solid State Sci.* **9** (2007) 608.
12. Y.-L. Chang, H.-I. Hsiang, M.-T Liang, *J of Alloys and Compounds* **461** (2008) 598.
13. P.D. Sarkisov, N.V. Popovich, A.G. Zhelnin, *Glass Ceramics* **60** (2003) 9.
14. X. Li, Y. Qu, X. Xie, Z. Wang, R. Li, *Mater. Lett.* **60** (2006) 3673.
15. H. Chander, D. Haranath, V. Shanker, P. Sharma, *J. of Cryst. Growth* **271** (2004) 307.
16. X. Lü, M. Zhong, W. Shu, Q. Yu, X. Xiong, R. Wang, *Powder Technology* **177** (2007) 83.
17. D.P. Norton, *Mater. Sci. and Engineering R* **43** (2004) 139.
18. M.S. Dhlamini, PhD thesis University of the Free State (2008).
19. Z.G. Zhang, F. Zhou, X.Q. Wei, M. Liu, G. Sun, C.S. Chen, C.S. Xue, H.Z. Zhuang, B.Y. Man, *Physica E* **39** (2007) 253.
20. J. Gonzalo, R. Gómez, S. Román J. Errière, C.N. AFonso, R. Pérez Casero, *Appl. Phys. A* **66** (1998) 487.

21. A. Bailini, P.M. Ossi, A. Rivolta, Appl. Surf. Sci. **253** (2007) 7682.
22. S. Christoulakis, M. Suche, N. Katsarakis, E. Koudoumas, Appl. Surf. Sci. **253** (2007) 8169.
23. R. Eason (editor), *Pulsed laser deposition of thin films applications-led growth of functional materials*, John Wiley & Sons, Inc. Hoboken, New Jersey, 2006.
24. M. Ozegowski, K. Meteva, S. Metev, G. Sepold, Appl. Surf. Sci. **138-139** (1999) 68.

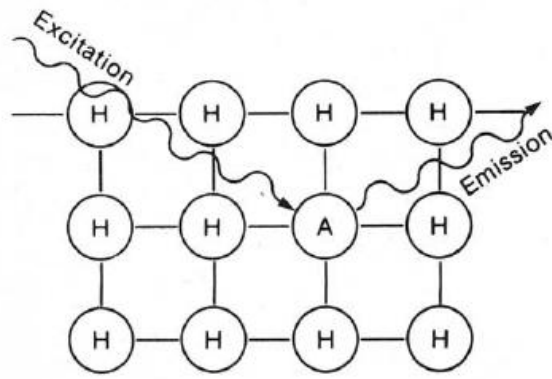
CHAPTER 2

THEORY

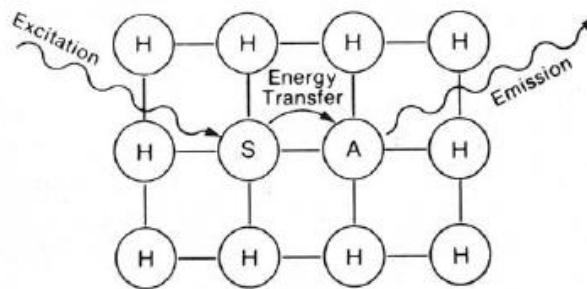
2.1 AN OVERVIEW TO PHOSPHORS

Luminescence can be defined as a process by which chemical substances/materials emit photons during an electron transition from the excited to the ground state. The materials can be excited by irradiating them with high energy electrons or photons. Accordingly, the luminescence resulting from excitation by high energy electrons is called cathodoluminescence and that from the excitation by high energy photons is called photoluminescence. The principles of photoluminescence and cathodoluminescence will be discussed in detail in section 2.4 and 2.5. The class of materials which emit characteristic luminescence are called **phosphors**. Phosphors consist of a host material which constitutes the bulk and intentional impurities introduced to the host. The characteristic luminescence properties are obtained either directly from the host or activators/dopants introduced intentionally to the host material. An activator is an impurity ion which when incorporated into the host lattice gives rise to a center which can be excited to luminesce. If more than one activator is used, they are called co-activators or co-dopants. One activator (sensitizer) tends to absorb energy from the primary excitation and transfer to the other activator to enhance its luminescent intensity [1].

Figure 2.1 displays a schematic diagram showing the role of an activator and sensitizer in the luminescence process of a phosphor [1]. In Figure 2.1 (a), light emission is a result of direct excitation of the activator atom A (the absorber) surrounded by the host lattice atoms, H, while Figure 2.1 (b) shows light emission from A as a result of excitation of and energy transfer from the co-activator atom (the sensitizer) S.



(a)



(b)

Figure 2.1. (a) The schematic diagram showing the role of an activator (A) in a host (H) lattice in a phosphor luminescence process. (b) The schematic diagram showing the role of a sensitizer (S) and an activator (A) in a phosphor luminescence process.

Figure 2.2 indicates the schematic diagram of the energy levels of the sensitizer and absorber showing the excitation, energy transfer and the emission processes.

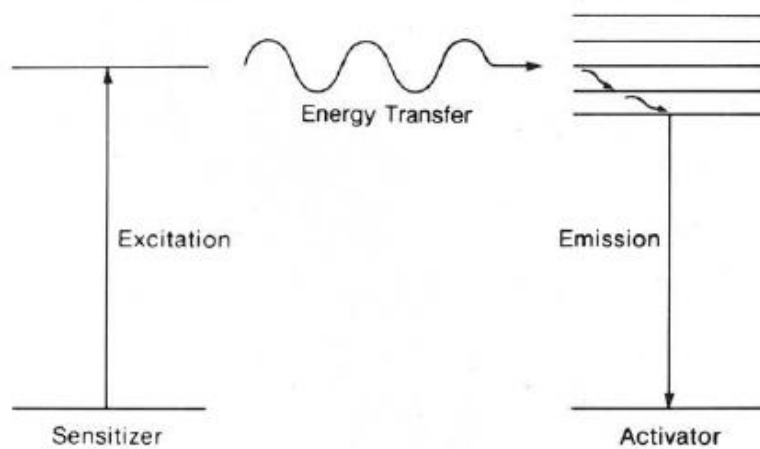


Figure 2.2. Schematic diagram illustrating the energy transfer between a sensitizer and activator.

Luminescence in solids, i.e. inorganic insulators and semiconductors, is classified in terms of the nature of the electronic transitions producing it. It can either be intrinsic or extrinsic. In the intrinsic process, the luminescence results from the inherent defects present in the crystal structure [2]. This type of luminescence does not involve impurity atoms. Extrinsic photoluminescence on the other hand, results from the intentionally incorporated impurities in the crystal structure [3]. This type can be divided into two categories; namely localized and delocalized luminescence. In the localized luminescence excitation and emission processes are confined to a localized luminescence center, whereas in the delocalized luminescence the electrons and holes participate in the luminescence process (free electron in the conduction band and free holes in the valence band) [4]. Luminescence processes can be divided into two main categories, namely fluorescence and phosphorescence based on the time the excited electrons takes to return to their ground states after the excitation has been stopped.

2.2 FLUORESCENCE

Fluorescence is the process in which emission of photons stops immediately when excitation is cut off. It is the process in which the excited electrons return to the ground state in a time not greater than 10^{-6} sec, the resulting emissions is described as fluorescence [5]. In fluorescence there are no traps but many luminescent centers.

2.3 PHOSPHORESCENCE

Phosphorescence occurs when the recombination of the photo-generated electrons and holes is significantly delayed in a phosphor. If one of the excited states of a luminescent center is a quasistable state (i.e., an excited state with very long life time) a percentage of the centers will be stabilized in that state during excitation. Excited electrons and holes in the conduction and valence bands of a phosphor can often be captured by impurity centers or crystal defects before they reach emitting centers. When the probability for the electron (hole) captured by an impurity or defect center to recombine with a hole (electron) or to be reactivated into the conduction band (valence band) is negligibly small, the center or defect is called a trap [6]. The decay time of phosphorescence due to traps can be as long as several hours and is often

accompanied by the photoconductive phenomena [6]. The principles of light emission by photoluminescence and cathodoluminescence are discussed in sections 2.4 and 2.5.

2.4 PHOTOLUMINESCENCE MEASUREMENT PRINCIPLES

Photoluminescence is the luminescence of a material after excitation by high energy photons. Photoluminescence properties of a material are characterized by both absorption (excitation) of the material by a primary excitation source and emission of light by the material. A typical experimental arrangement for determining excitation spectra is shown in Figure 2.3. In this example the excitation source is the output of a monochromator which, like a prism, resolves the excitation light source into its component wavelengths.

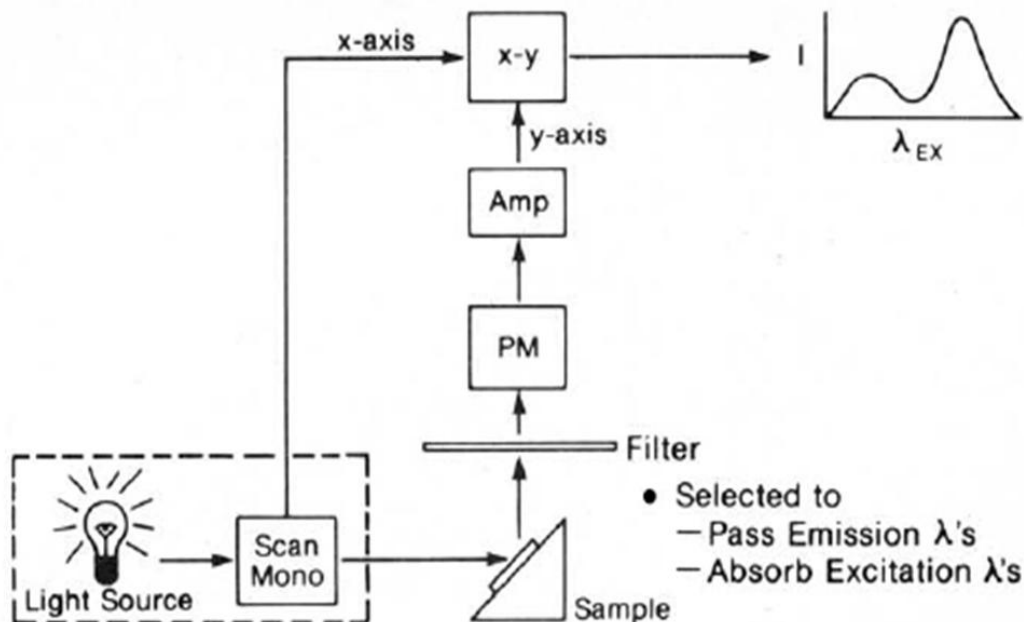


Figure 2.3. Schematic diagram for the measurement of excitation spectra [1].

The excitation wavelength of interest illuminates the sample. Then intensity of the luminescence emission is measured by a photomultiplier tube. The optical cut-off filter placed between the sample and the photomultiplier tube is selected so that it will pass the luminescence emission but will absorb the reflected excitation radiation. The output of the photomultiplier tube is amplified and then fed into the y axis of an x-y recorder. The value of the excitation wavelength selected is plotted on the x-axis. Thus, one obtains an x-y plot which shows the intensity of the luminescence emission as a function of the wavelength of the excitation radiation. The spectrum is obtained using a monochromator equipped with an

appropriate light detector. In the case of an excitation spectrum, the relationship is obtained by observing changes in the emitted light intensity at a set wavelength while varying the excitation energy [1].

The excitation source consists of the light source and a monochromator, which selects a specific wavelength range from the incoming light. A filter can do a similar job. The light emitted from the sample is analyzed by a monochromator equipped with a light detector. The light detector transforms the photons into electrical signals. A laser is an excellent monochromatic light source and has a radiative power at a given frequency several orders of magnitude greater than that of other light sources. They can either operate in continuous or pulsed mode. Common gas lasers used for the study of luminescence are the He-Ne, Ar⁺ ion, Kr⁺ ion and He-Cd. The He-Cd laser uses a mixture of the He gas and Cd metal vapour, and has emission peaks in the ultraviolet and visible region. When it is operated in the continuous wave (CW) mode, the 325 nm peak is most prominent, with output powers of 100 mW. This laser is very useful as an ultraviolet excitation source for measuring photoluminescence spectra.

The luminescence properties of a phosphor can be characterized by its emission spectrum (wavelength), brightness and decay time. The emission spectrum is obtained by plotting the intensity against the wavelength of the emitted light from a sample excited by an appropriate excitation source of constant energy. The experimental arrangement for the determination of an emission spectrum is shown schematically in Figure 2.4. A single excitation wavelength is selected. The optical cut-off filter serves the same purpose as previously described. The emission of the sample is analyzed by means of a monochromator [1].

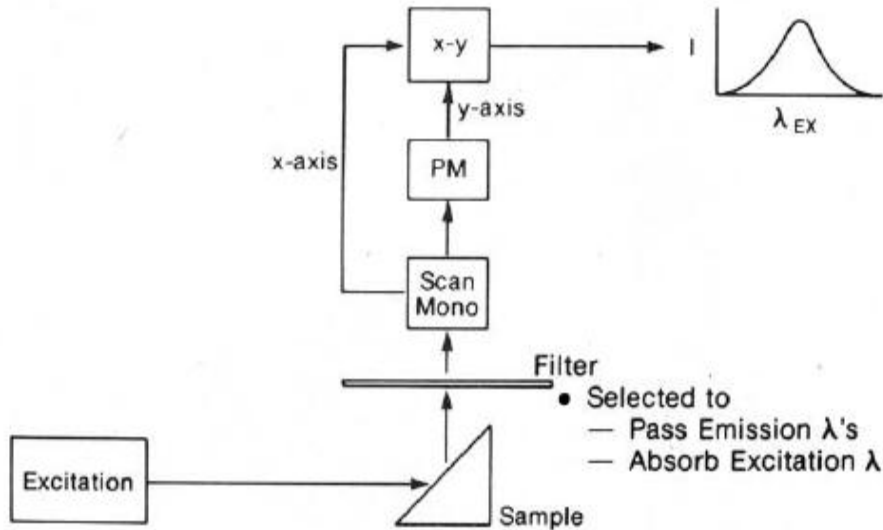


Figure 2.4. Schematic diagram of a typical experimental arrangement for recording the emission spectrum of a phosphor [1].

2.5 CATHODOLUMINESCENCE MEASUREMENT PRINCIPLES

Cathodoluminescence (CL) is defined as the luminescence stimulated by a collision between an energetic beam of electrons (primary electrons) and a solid material (phosphor). This process involves the generation of electron-hole pairs and emission of photons during recombination of the holes and electrons.

2.5.1 GENERATION OF ELECTRON-HOLE (EH) PAIRS

When an energetic electron beam is incident on a phosphor, a number of physical processes take place including emission of secondary electrons, Auger electrons and back-scattered electrons. Hundreds of free electrons and free holes are produced along the path of the incident electron (primary electron) as illustrated in Figure 2.5.

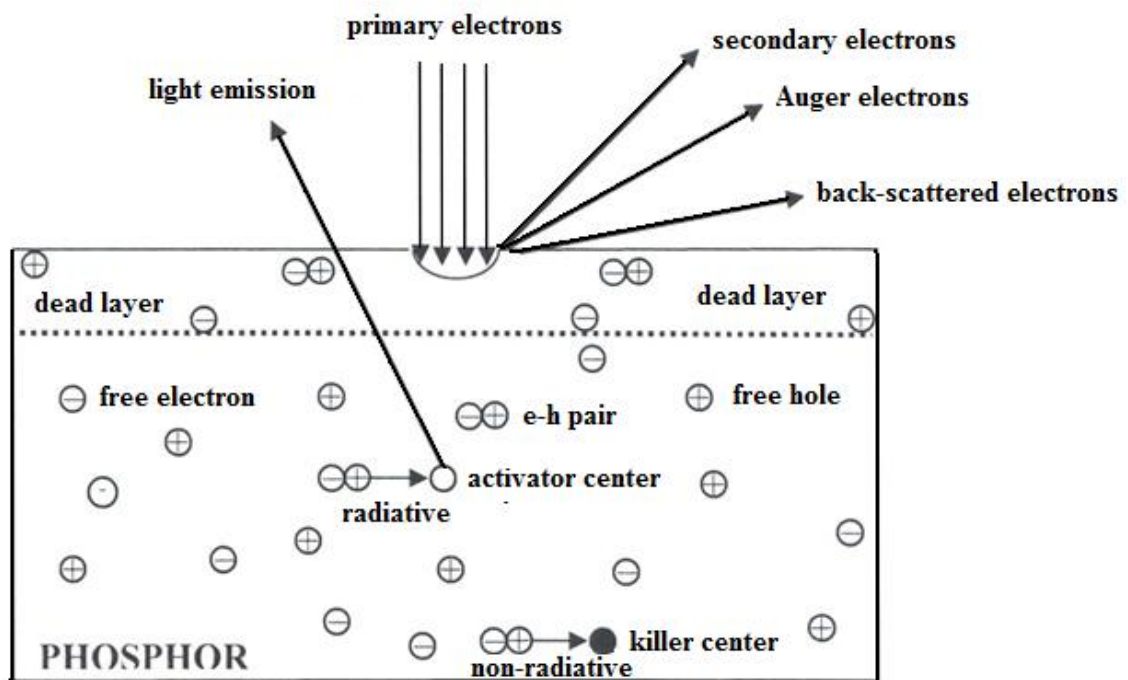


Figure 2.5. CL process in a phosphor grain [7].

The e-h pairs can diffuse through the phosphor and transfer their energy to activator ions and subsequently emit light. This process is referred to as radiative recombination. Unwanted process in which the e-h pairs recombine non-radiatively by transferring their energy to killer centres (incidental impurities and inherent lattice defects) is also possible. The e-h pair can also diffuse to the surface of the phosphor and recombine non-radiatively. A thin dead (non-luminescent) layer may be formed on the surface [7].

The luminescence centers can be excited either directly or indirectly. In the direct excitation, there is a direct recombination of free electrons and holes for a perfect (free from impurities and lattice defects) crystal [7] as shown in Figure 2.6 (i). The indirect excitation takes place when a crystal is distorted and localized energy levels (impurity levels) are created in the band-gap of a given material. Common impurities include the activator impurities, incidental impurities and lattice defects. This provides effective recombination paths of the free electrons and holes as represented by 2.5 (ii), (iii) and (iv) as shown in the figure below. The photon energy of these transitions is smaller than that of the direct ones [7].

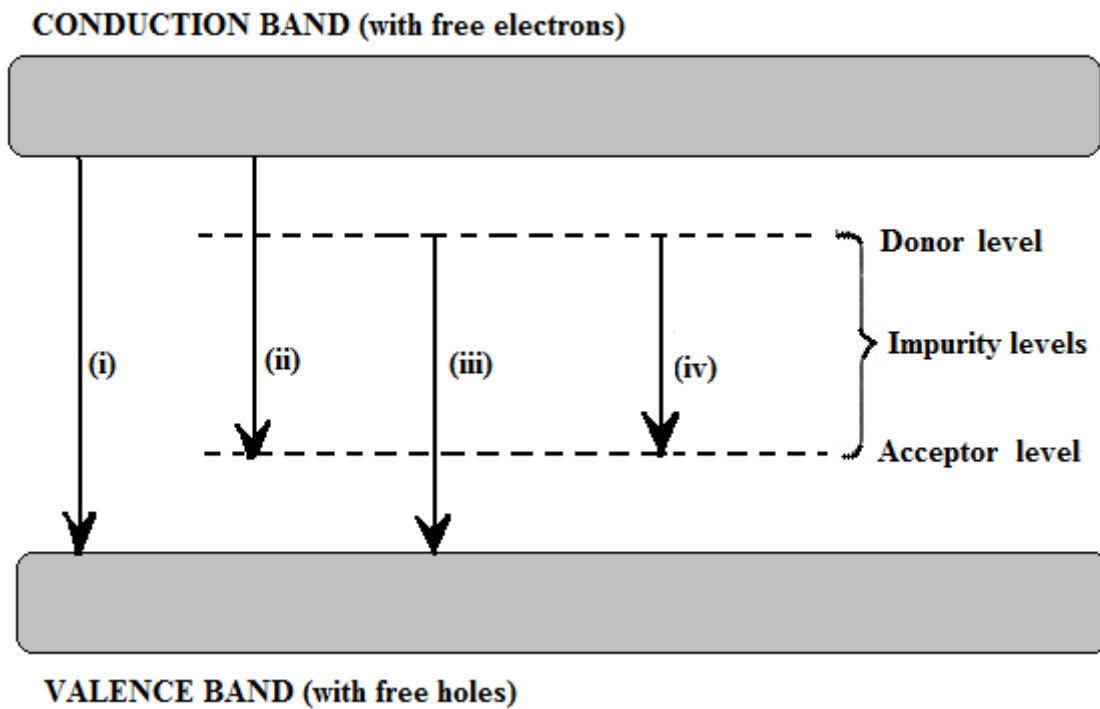


Figure 2.6 Models of catholuminescent transitions [7].

2.5.2 DEGRADATION OF CATHODOLUMINESCENCE

Degradation of the CL intensity has been a subject of research since the 1960s. It is defined as a reduction of cathodoluminescence efficiency of phosphors during electron beam bombardment. Pfanhl’s law [8] describes well the rate of degradation of the CL intensity and development of an electron stimulated surface chemical reaction (ESSCR) model. The law is defined as;

$$I(N) = \frac{I_0}{(I+CN)} \dots\dots\dots(2.1)$$

where I is the aged CL intensity, I_0 is the initial CL intensity, N is the number of electrons per unit area and C is the burn parameter which is equal to the inverse of the number of electrons per unit area required to reduce the intensity to half of its original value. It proposes that the CL degradation depends on the type of gas in the vacuum, the gas pressure, the beam voltage and the electron (coulombic) dose [9, 10].

The next section discusses some characteristics related to $\text{SrAl}_2\text{O}_4:\text{Eu}^{2+}, \text{Dy}^{3+}$, such as the f-d optical transitions, the phosphorescence (afterglow) mechanism and the crystal structure of

the $\text{SrAl}_2\text{O}_4:\text{Eu}^{2+},\text{Dy}^{3+}$. The last section will focus on the comparison of powder and thin films.

2.6 STRUCTURE AND PROCESSES DETERMINING THE EMISSION PROPERTIES OF $\text{SrAl}_2\text{O}_4:\text{Eu}^{2+},\text{Dy}^{3+}$

$\text{SrAl}_2\text{O}_4:\text{Eu}^{2+},\text{Dy}^{3+}$ is a green emitting long afterglow phosphor. The green emission comes from the f-d transitions of Eu^{2+} ions which substitute the Sr^{2+} ions in the SrAl_2O_4 lattice. Dy^{3+} ion plays the role of trapping the charge carriers [11, 12]. The next sections give a brief discussion on the f-d transition, the phosphorescence mechanism and the crystal structure of a $\text{SrAl}_2\text{O}_4:\text{Eu}^{2+},\text{Dy}^{3+}$ phosphor.

2.6 .1 THE f-d TRANSITIONS

The Eu^{2+} ion with the $4f^7$ electron configuration show efficient luminescence resulting from the $4f \rightarrow 5d$ transition, and is an important activator for various kinds of practical phosphors. The luminescence colours or wavelengths of this ion varies widely from near-ultraviolet to red regions depending on the nature of the host lattice. The ground state of the $4f^7$ configuration is ^8S , while the lowest excited state is $^6\text{P}_J$. In most Eu^{2+} -activated phosphors, 5d levels are located below the $^6\text{P}_J$ state, causing broadband luminescence owing to the allowed $4f^65d \rightarrow 4f^7$ transition. However, in some phosphors the 6P_J state is lower, and in such cases the observed luminescence is due to the $4f^{7*} \rightarrow 4f^7$ transition [13].

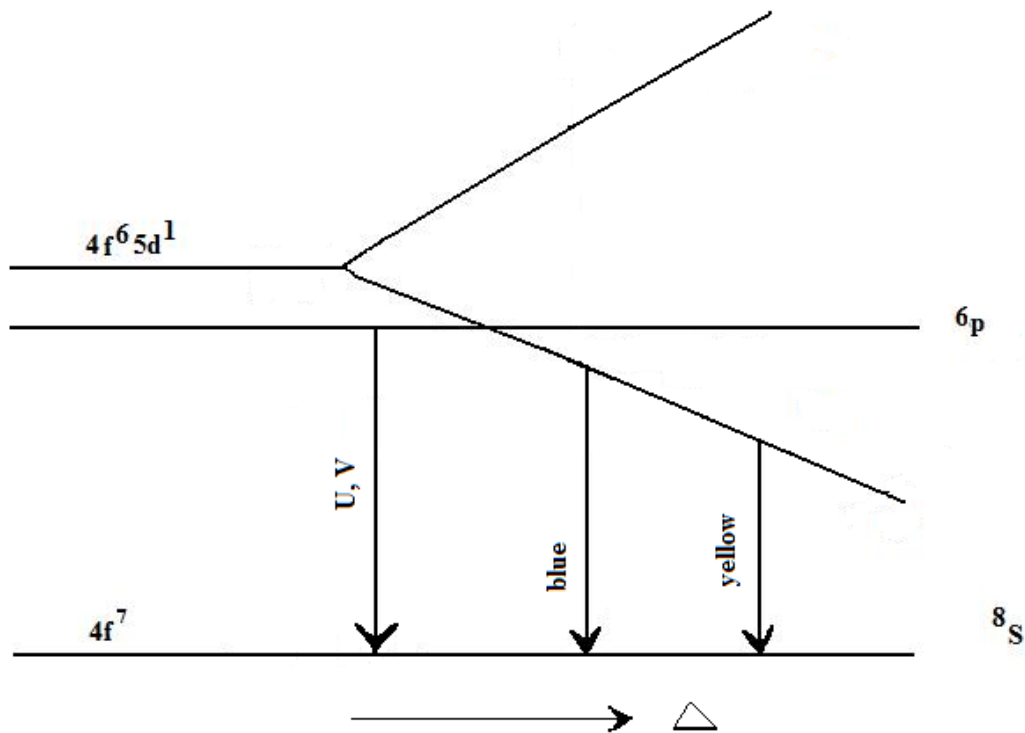


Figure 2.7. Schematic energy level diagram of Eu^{2+} as a function of the crystal field strength Δ [13].

The d-orbit is fivefold degenerate in free space. In crystal of cubic symmetry it is split into the threefold d- and twofold d-orbits. The split interval is proportional to the crystal field strength (Figure 2.7). Sharp luminescence lines are characteristic of the $f \rightarrow f$ transition. At room temperature, the excited electrons are raised to the 5d state, so that broadband luminescence at 390 nm resulting from the $5d \rightarrow 4f$ transition is observed. With increasing crystal field strength, the 5d state becomes lower than the $4f^{7*}$ state, so that luminescence at 520 nm from the $5d \rightarrow 4f$ transition is produced [13].

There are two types of localized centers in Eu^{2+} -activated phosphors. The first one is type C in which Eu^{2+} ions are photo-ionized by vacuum-ultraviolet excitation changing to Eu^{3+} and photoconductivity resulting from electron is observed. The second is type D (to which $\text{SrAl}_2\text{O}_4:\text{Eu}^{2+}$ belongs) in which the excitation of Eu^{2+} by ultraviolet light leads to the liberation of holes to the valence band accompanied by the reduction of Eu^{2+} to Eu^{1+} and the photoconductivity resulting from holes [11].

2.6.2 AFTERGLOW (PHOSPHORESCENCE) MECHANISM OF SrAl₂O₄:Eu²⁺,Dy³⁺

The afterglow (also called phosphorescence) refers to a luminescence with delayed radiative transition and it is caused by the trapping of photo-generated electrons and/or holes at intrinsic or extrinsic defect sites of the material [14]. When freed by thermal energy, these trapped charge carriers recombine at the ionized luminescent centers. The amount of thermal energy needed to free the charge carriers depends on the trap depth, E_T . Thus phosphorescence is a thermo-activated physical phenomenon in which charge carriers are released at well-defined characteristic temperatures of the trap depth; it is a thermoluminescence with de-trapping at room temperature. The radiative life time of phosphorescence is about 10^{-3} - 10^{-4} s.

Formally, the phosphorescent decay time τ follows an exponential law

$$\frac{1}{\tau} = s \exp\left(-\frac{E_T}{kT}\right) \dots \dots \dots (2.2)$$

where s is a prefactor proportional to the vibration frequency of the trapped charge carrier within the trap (often taken to be equal to 10^{12} s⁻¹). Normally, E_T values lower than 0.2 eV lead to fast de-trapping at room temperature and prevent a long afterglow, while E_T values higher than 1.5 eV require annealing at high temperature or laser light to de-trap charge carriers as observed in photostimulable phosphors [12]. It is also possible to determine the fast, intermediate and slow decays of the afterglow characteristics, since they are indicative of the different rates of decay. The decay curves can be fitted by the third order exponential equation:

$$I = A_1 \exp\left(-\frac{t}{\tau_1}\right) + A_2 \exp\left(-\frac{t}{\tau_2}\right) + A_3 \exp\left(-\frac{t}{\tau_3}\right) \dots \dots (2.3)$$

where I represents the phosphorescent intensity: A_1 , A_2 and A_3 are constants: t is the decay time; and τ_1 , τ_2 and τ_3 are the decay constants [14].

For a long time, the mechanism of the persistent luminescence of SrAl₂O₄:Eu²⁺,Dy³⁺ was understood according to the Matsuzawa model [11], which stipulates that the UV excitation of Eu²⁺ cations from the ground state $4f^7$ to an excited state $4f^65d^1$, $\text{Eu}^{2+}(4f^7) + h\nu \rightarrow \text{Eu}^{2+*}(4f^65d^1)$, generates a hole in the f orbitals. This transition is followed by an electron capture from the valence band (VB) leading to the reduction $\text{Eu}^{2+*} + e^- \rightarrow \text{Eu}^+$. The hole created in

the VB can migrate and can be captured by a Dy^{3+} cation to form a Dy^{4+} cation, $\text{Dy}^{3+} + \text{h}^+ \rightarrow \text{Dy}^{4+}$. It is supposed that the return to the ground state of Eu^{2+} with light emission is triggered by the thermo-activated promotion of an electron from the VB to the first unoccupied levels of Dy^{4+} , followed by the migration of trapped hole to a photo-generated Eu^+ cation.

The Matsuzawa model is based on highly improbable assumptions. First, the reduction of Eu^{2+*} to Eu^+ is highly unlikely and so is the oxidation $\text{Dy}^{3+} + \text{h}^+ \rightarrow \text{Dy}^{4+}$ due to the chemical instabilities of E^{u+} and Dy^{4+} . Second, as pointed out by Dorenbos [15], the proposed VB Eu^{2+*} ($4f^65d^1$) transitions leading to the final $4f^75d^1$ electronic configuration of Eu^{2+} is based on an incorrect concept of a hole state. The shortcomings of Dorenbos model are firstly, the lack of explanation of the intrinsic phosphorescence of the un-codoped $\text{SrAl}_2\text{O}_4:\text{Eu}^{2+}$, which lasts longer than 1 hour, because there is no trap without codopants in this model. Secondly, the divalent cations such as Dy^{2+} , Nd^{2+} , Ho^{2+} , Er^{2+} are not chemically stable species in oxides. Third, the features of the thermoluminescence peak of $\text{SrAl}_2\text{O}_4:1\%\text{Eu}^{2+}$ and $\text{SrAl}_2\text{O}_4:1\%\text{Eu}^{2+}, 2\%\text{Dy}^{3+}$ are very similar suggesting that the chemical nature of the trap is not changed by codoping [12]

Aitasalo et al. [16] modified the Matsuzawa model. In their model it was assumed that the photo-excitation of Eu^{2+} is activated by an energy transfer associated with the return of an electron trapped at certain defect levels of unknown origin or oxygen vacancy (V_{O}) levels to the ground state and that these defect levels are populated by a depletion of the VB under UV excitation, which gives rise to holes trapped at cation vacancies. The modification of Aitasalo model was done by Clabau et al. [12]. Clabau et al. model suggests the theoretical and experimental positions of the oxygen and strontium vacancies responsible for the electron and hole trapping processes. Their model relies on the facts that (a) the d-block levels of Eu^{2+} cations partially overlap with the bottom of the conduction band (CB) as suggested from electronic band structure calculations performed for a hypothetical composition $\text{Sr}_{0.75}\text{Eu}_{0.25}\text{Al}_2\text{O}_4$, (b) the f^7 ground state of Eu^{2+} lies in the middle of the forbidden band gap as suggested by x-ray photoelectron spectroscopy (XPS) data [12], (c) the Eu^{2+} cations can be oxidized under irradiation because both Eu^{2+} and Eu^{3+} species are stable species in oxides and (d) the concentration of Eu^{2+} cations can change under UV irradiation.

Under UV irradiation, electrons are promoted from the occupied 4f levels of Eu^{2+} to the empty 5d levels and from the VB top to the unoccupied 4f levels of residual Eu^{3+} (i.e.,

charge transfer) as indicated in Figure 2.7. The electrons promoted to the 5d levels can be trapped at the V_O defects located in the vicinity of the photo-generated Eu^{3+} cations, while the holes created in the VB can be trapped at the V_{Sr} or V_{Al} levels. Due to these trapping processes, Eu^{2+} is oxidized to Eu^{3+} while residual Eu^{3+} is reduced to Eu^{2+} . The thermal energy at ambient temperature causes the detrapping of the trapped electrons directly to the 5d levels of Eu^{2+} , hence leading to the $4f^65d^1 \rightarrow 4f^7$ ($^8S_{7/2}$) green phosphorescence. The hole conductivity of $\text{SrAl}_2\text{O}_4:\text{Eu}$ is assigned to the residual Eu^{3+} cations that remain unreduced in $\text{SrAl}_2\text{O}_4:\text{Eu}$, as evidenced from Mossbauer experiments [12].

Spectral analysis of thermoluminescent peaks shows that the holes generated in the VB are trapped at cation vacancy levels (i.e., the oxygen lone pair levels surrounding each cation vacancy) and the de-trapped holes would recombine with electrons at the photo-generated Eu^{2+} sites with the emission at 450 nm. The peak at 450 nm is only for low-temperature luminescence spectrum of $\text{SrAl}_2\text{O}_4:\text{Eu}$ samples prepared in air [17]. The blue emission is likely coming from the de-excitation process [18].

This model is displayed schematically in Figure 2.8.

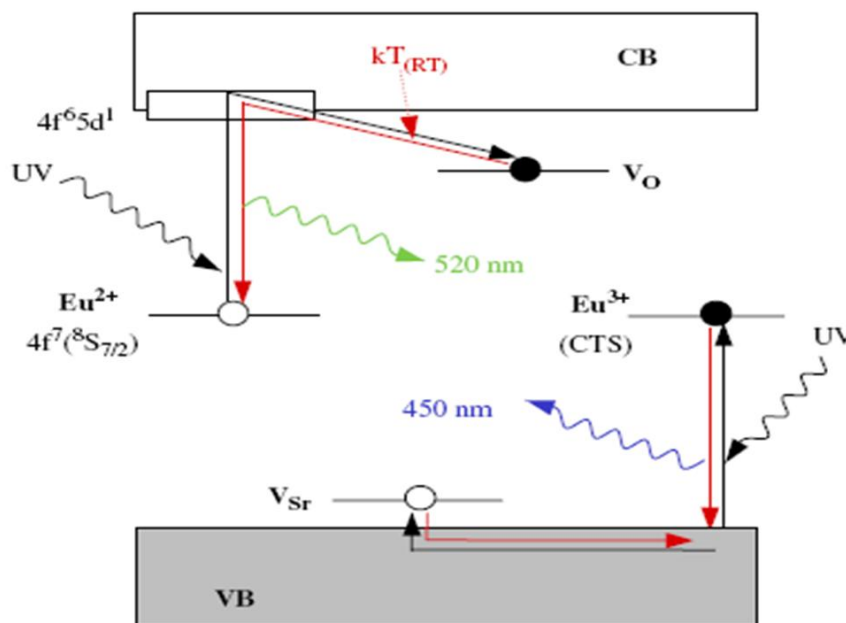


Figure 2.8. Phosphorescence mechanism of $\text{SrAl}_2\text{O}_4:\text{Eu}$ and its codoped derivatives proposed by Clabau et al. Black and red arrows refer to the trapping and the de-trapping processes, respectively (adapted from Ref. [19]).

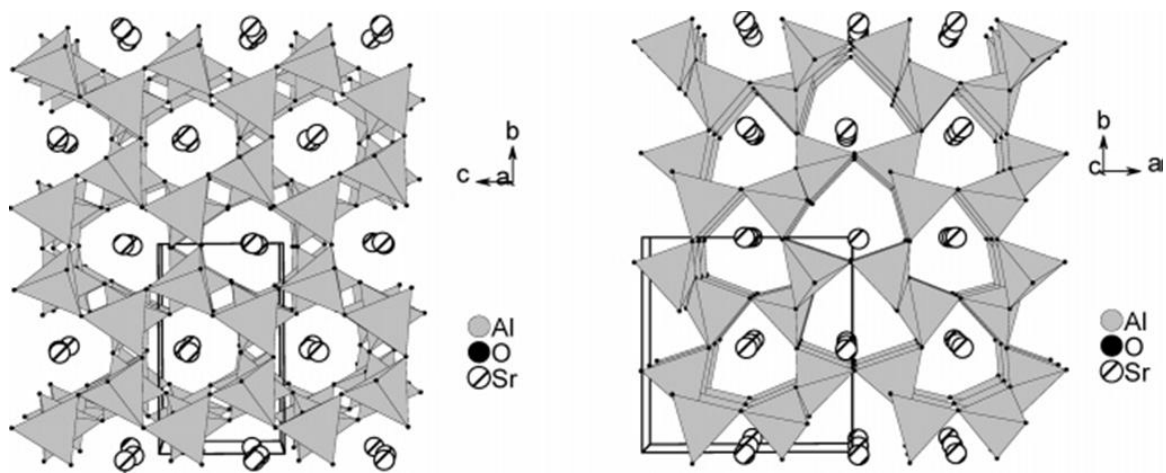
The electronic band structure calculations of SrAl₂O₄ with Sr and O vacancies show that the V_{Sr} is located at 0.15 eV above the VB top and the V_O level is at 0.60 eV below the CB bottom [18]. They also found that the lengthening of the phosphorescence decay time by codoping with Dy³⁺ ions results from the stabilization of the pre-existing electron traps caused by the presence of interactions between dopant (codopants) cations and oxygen vacancies in the lattice of SrAl₂O₄. The variation of the TL curve upon codoping also suggests that the Dy³⁺ cation increases the number and depth of the electron traps [17]. This is based on the fact that, Eu²⁺ cation strongly attracts positively charged oxygen vacancies, which require electron density to get stabilized, because the electron density of Eu²⁺ is more polarisable than that of Sr²⁺. When introduced as a codopant in substitution for Sr²⁺, a second Dy³⁺ ion has the tendency to migrate towards Eu²⁺ and gains stability due to the excess positive charge. To some extent, therefore, Eu²⁺ cations should be regarded as an electron reservoir even if no electron is transferred to an oxygen vacancy level V_O or the Dy³⁺ cation at the Sr²⁺ site. Then, the electron density of Dy³⁺ being again more polarisable than that of Sr²⁺, the anion vacancies located near Eu²⁺ are more attracted and stabilized, which favour an increase in trap concentration [12].

With regards to the above mentioned phosphorescence mechanisms, I would recommend Clabaus's model because it is based on the experimental results. However, more studies ought to take place in future.

2.6.3 THE CRYSTAL STRUCTURE OF SrAl₂O₄

SrAl₂O₄ adopt a stuffed tridymite-type structure consisting of corner sharing AlO₄ tetrahedral which connect together to form six-membered rings. Each oxygen ion is shared by two aluminium ions so that each tetrahedron has one net negative charge. The charge balance is achieved by the large divalent cation Sr²⁺, which occupies interstitial site within the tetrahedral frame-work [22]. SrAl₂O₄ exists in two different phases, namely monoclinic (M) i.e. P2₁ (a = 8.447 Å, b = 8.816 Å, c = 5.163 Å, β = 93.42°) and hexagonal P6₃22, (a = 5.140 Å, c = 8.462 Å (H) i.e. P6₃22 [18]. It undergoes a phase transition from a low-temperature monoclinic distorted structure to hexagonal tridymite structure at 650° C [21].

The ideal undistorted structure of SrAl_2O_4 is described by cell parameters close to those of high tridymite [19]. The monoclinic SrAl_2O_4 , being stable at temperatures below 950 K is a distorted form of a hexagonal SrAl_2O_4 . The distortion involves a reduction in the symmetry of the trigonally distorted rings. The monoclinic SrAl_2O_4 has two strontium sites. The distances between the strontium ion and its neighbouring oxygen ions are different for the two strontium sites. In one site, the oxygen atoms are at a larger distance from the strontium ion than the other [24]. The structure has channels in the a - and c -directions where Sr^{2+} ions are located [23]. This can be revealed by the parallel projections of the polyhedral forms for the directions- c and $-a$ shown in Figure 2.9.



Schematic views of the monoclinic phase of SrAl_2O_4 along the a - and c -directions.

The Sr^{2+} and Eu^{2+} ions are very similar in their ionic size (i.e., 1.21 and 1.20 Angstrom respectively). Consequently, when occupied by Eu^{2+} ions, the two different Sr^{2+} ions located at the two different Sr^{2+} sites will have very similar local environments [24]. The sites of the dopants and codopants of SrAl_2O_4 are dictated by their ionic radii.

REFERENCES

1. J. A. DeLuca, *Journal of Chemical Education*, **57** (1980) 541.
2. S. Boggs, D. Krinsley, *Application of Cathodoluminescence imaging to the study of sedimentary rocks*, Cambridge University Press, England, 2006.
3. R.D. Blackledge, *Forensic analysis on the cutting edge*, John Willey & Sons Publications, USA, 2007.
4. D. R. Vij, *Luminescence of Solids*, Science, Plenum Press, New York & London, 1998.
5. J. Ball, A. D. Moore, *Essential physics for radiographers*, Blackwell Publishing, First edition, Oxford, 1979.
6. S. Shionoya, W.M. Yen, *Phosphors Handbook*, CRC Press, USA, 1998.
7. O.M. Ntwaeaborwa, Ph.D. dissertation, University of the Free State, South Africa (2006)
8. A. Pfahnl, *Advances in electron tube techniques*, Pergamon, New York, (1961) 204.
9. L. Ozawa, *Cathodoluminescence and photoluminescence, Theories and Practical Applications*, CRC Press Taylor & Francis Group, Boca Raton London New York, (2007) 8.
10. K.T. Hillie, Ph.D. dissertation, University of the Free State, South Africa (2001).
11. T. Matsuzawa, Y. Aoki, N. Takeuchi, Y. Maruyama, *J. Electrochem. Soc.* **143** (1996) 2670.
12. F. Clabau, Xavier Rocquefelte, Ste´phane Jobic, Philippe Deniard, Myung-Hwan Whangbo, Alain Garcia, Thierry Le Mercier, *Solid state Sciences* **9** (2007) 612.
13. G. Blasse in *Luminescence of Solids*, edited by D.R. Vij, Plenum Publishing Corporation 233 Spring Street, New York (1998) 122.
14. B.M Mothudi, O.M. Ntwaeaborwa, J.R Botha and H.C. Swart, *Physica B: Condensed Matter*, **404** (2009) 4440.
15. P. Dorenbos, *J. Electrochem. Soc.* **152** (2005) H107.
16. T. Aitasalo, P. Deren, J. Ho¨lisa, H. Jungner, J. Krupa, M. Lastusaari, J. Legendziewicz, J. Niittykoski, W. Streck, *J. Solid State Chem.* **171** (2003) 114.
17. Y. Lin, Z. Tang, Z. Zhang, *Mater. Lett.* **51** (2001) 14.
18. F. Clabau, X. Rocquefelte, S. Jobic, P. Deniard, M.-H. Whangbo, A. Garcia, T. Le Mercier, *Chem. Mater.* **17** (2005) 3904.
19. A. Lo´pez, M. G. da Silva, E. B-Saitovitch, A. R. Camara, R. N. Silveira Jr, R. J.M. Fonseca, **43** (2008) 464.

20. E. Cordoncillo, B. J-Lopez, Marta Martínez, M. L. Sanjuán, P. Escribano, J. Alloys and Comp. **484** (2009) 693-697.
21. T. Katsumata, K. Sasajima, S. Komuro, T. Morikawa, J. Amer. Ceram. Soc. **81** (1998) 413.
22. S. Ito, S. Banno, K. Suzuki, M. Inagaki, Z. Phys. Chem. **105** (1977) 377.
23. J.C. Klein, D.M. Hercules, J. Catal. **82** (1983) 424.
24. D. Ravichandran, S.T. Johnson, S. Erdei, Rustum Roy, W.B. White, Displays **19** (1999) 197.

CHAPTER 3

RESEARCH TECHNIQUES

3.1 INTRODUCTION

This chapter gives a brief account of the pulsed laser deposition and other characterization techniques including atomic force microscopy (AFM) and scanning electron microscopy (SEM), for morphological and topographical analysis; X-ray Diffraction (XRD), and high resolution transmission electron microscopy (HRTEM) for structural analysis; the fluorescence spectrophotometry, photoluminescence (PL) and cathodoluminescence (CL) spectroscopies for luminescence measurements; and Auger electron spectroscopy (AES) and X-ray photoelectron spectroscopy (XPS) for elemental composition analyses; Rutherford backscattering (RBS) was employed for the stoichiometric ratios analysis.

3.2 PULSED LASER DEPOSITION (PLD) TECHNIQUE

In the PLD technique, the laser is focused onto a rotating target where it evaporates the material to form a plume. The plume travels in either vacuum or gas background region between the target and the substrate before depositing on the substrate to form a film. Figure 3.1 shows the schematic diagram for the PLD process. The process is preceded by the evacuation of the chamber to a high vacuum. The lasers which are commonly used are the UV excimer lasers; namely, ArF (193 nm), KrF (248 nm) and XeCl (308 nm). Generally, there are about five stages involved in the PLD process. In the first stage, the laser is absorbed by the target material. The second stage involves the one-dimensional plume expansion of the ablated materials during laser irradiation. In the third stage there is a three-dimensional plume expansion into vacuum or background gas. Slowing down and stopping of

the plume in a background gas then follows in the fourth stage. In the fifth stage the ablated atoms are collected on a substrate, leading to the film growth [1].

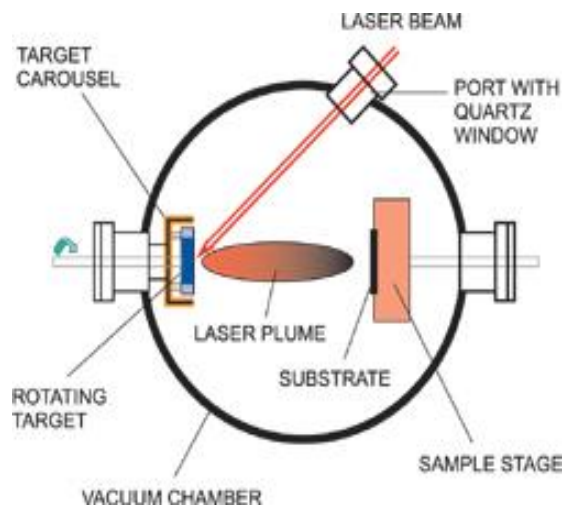


Figure 3.1. Schematic diagram for the PLD set up and process [2].

Typically, the deposition rate per laser pulse is on the order of 0.0001 to 1 Å per pulse [3].

In the current work, a KrF 248 nm laser wavelength was used. A photograph of the PLD system is shown in Figure 3.2. The two main components of the system are the laser and vacuum chamber.

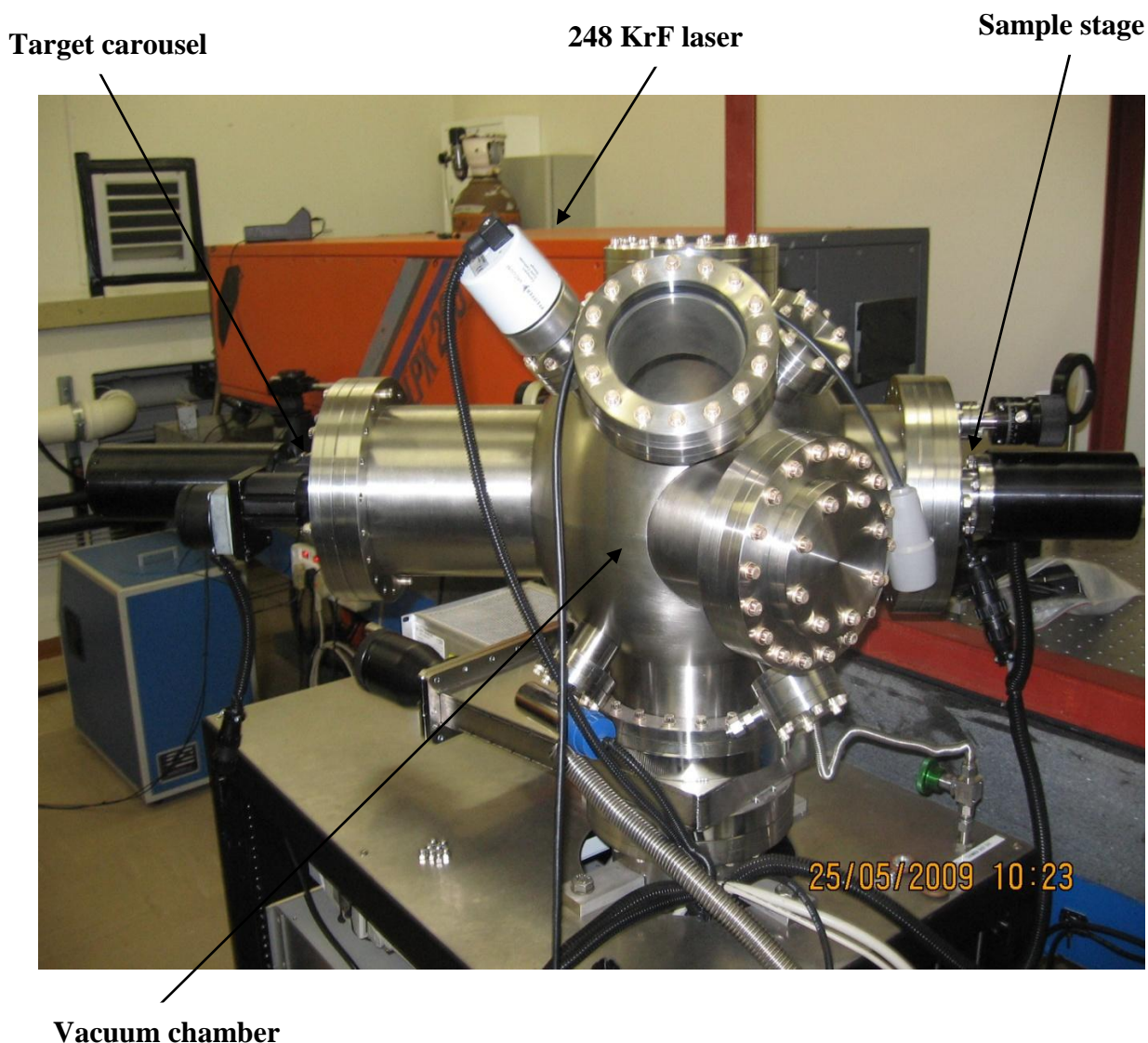


Figure 3.2. The pulsed laser deposition (PLD) system at the National Laser Centre (NLC, CSIR), Pretoria.

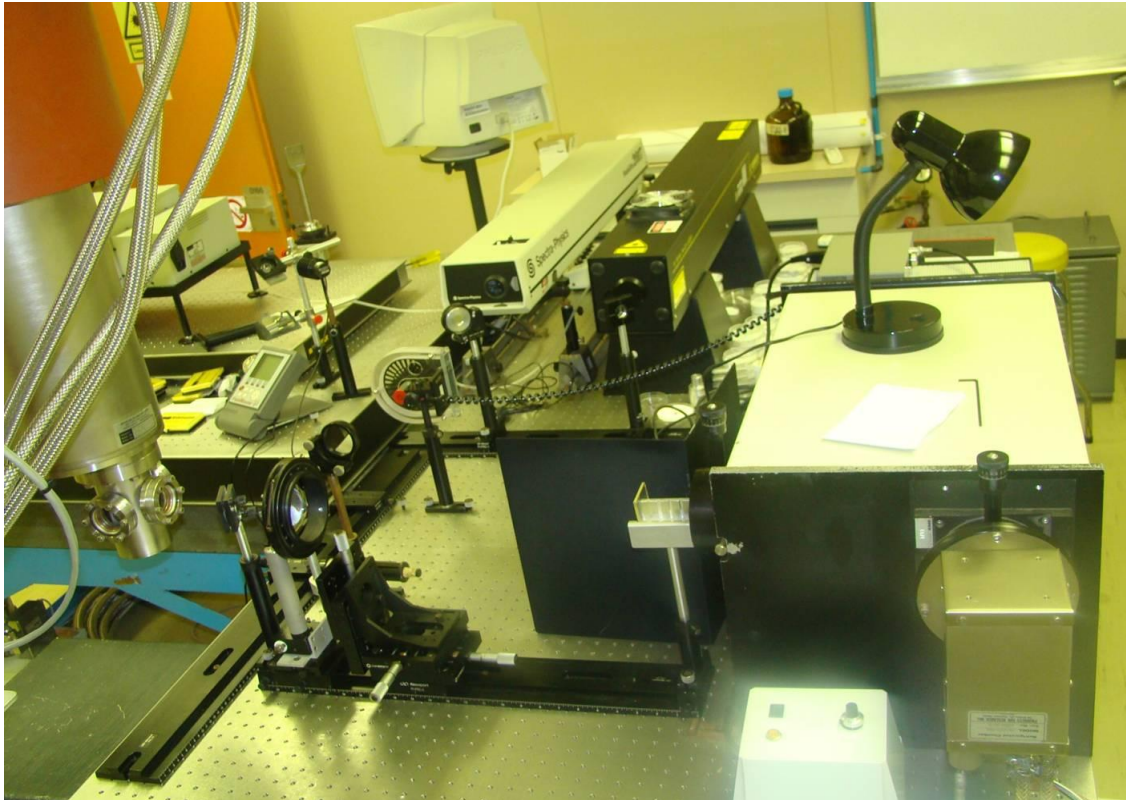
3.3 PHOTOLUMINESCENCE (PL)

The PL system consists of the source of primary excitation (laser/light). The excitation source can be the UV light, electron beam or laser. The spectrum is obtained using a monochromator equipped with an appropriate light detector [4]. In the current work, two PL systems were employed for the measurements; namely the Carry Eclipse spectrophotometer and the He-Cd laser ($\lambda = 325$ nm). The Carry Eclipse spectrophotometer uses the monochromatized xenon

lamp as the excitation source whose wavelength can be varied on the whole UV region. The He-Cd laser system on the other hand excites using only a fixed wavelength of 325 nm. The photographs for the two PL systems are shown in Figure 3.3 (a) and Figure 3.3 (b).



(a)

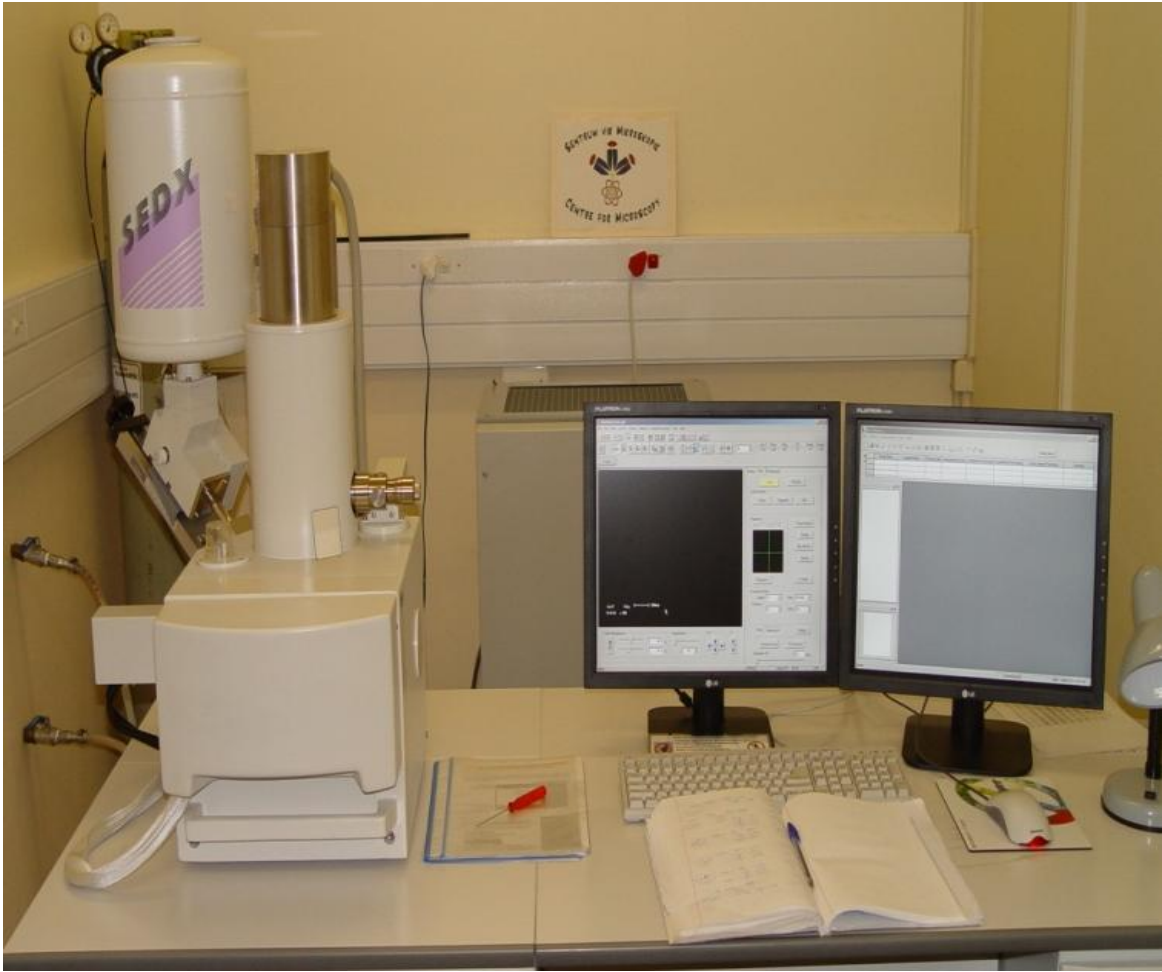


(b)

Figure 3.3. (a) The Cary Eclipse Fluorescence spectrophotometer at the Physics Department, University of the Free State. (b) The He-Cd laser photoluminescence unit at Nelson Mandela Metropolitan University (NMMU) in Port Elizabeth.

3.4 SCANNING ELECTRON MICROSCOPY (SEM)

In a scanning electron microscope (SEM), a narrow electron beam with energy typically in the 5-35 keV range is focused on a sample and scanned along a pattern of parallel lines. The interaction of the electron beam with the sample produces secondary electrons, backscattered electrons and characteristic X-rays, in a volume of the sample whose size depends on the kinetic energy, the density and atomic number of the material analyzed [5]. These signals are processed with internal electronics cards and software to form an image and to analyse the scanned surface. The analysis of the characteristic X-ray radiation emitted from samples yields quantitative elemental information. Modern energy-dispersive spectrometers are capable of detecting characteristic X-rays of all elements above atomic number 4–5 [5]. In the current work two SEMs were used namely the Shimadzu Superscan SSX-550 system and the PHI 700 Auger Nanoprobe. The photographs for the two systems are shown in Figure 3.4.



(a)



(b)

Figure 3.4. (a) The Shimadzu Superscan SSX-550 SEM system at the Microscopy Center, University of the Free State. (b) The PHI 700 Auger Nanoprobe SEM unit at the Department of Physics of the University of the Free State.

3.5 ATOMIC FORCE MICROSCOPY (AFM)

The AFM uses a probe, silicon tip and cantilever spring, to record the surface topography of samples. While scanning, the force between the tip and the sample is measured by monitoring the deflection of the cantilever. The deflection of the cantilever is controlled by using the optical lever technique. A beam from a laser diode is focused onto the end of the cantilever and the position of the reflected beam is monitored by a position sensitive detector (PSD) [6]. A topographic image of the sample is obtained by plotting the deflection of the cantilever versus its position on the sample. Alternatively, it is possible to plot the height position of the translation stage. This height is controlled by a feedback loop, which maintains a constant force between the tip and sample. Atomic force microscopes can be operated in air, different gases, vacuum or liquid. The AFM can be operated in three modes namely, the contact, non-contact and tapping mode [7]. In the current study the AFM images were collected by using the Shimadzu SPM - 9600 model whose photograph is shown in Figure 3.5.



Figure 3.5. The atomic force microscopy (AFM) unit at the Physics Department, University of the Free State.

3.6 HIGH RESOLUTION TRANSMISSION ELECTRON MICROSCOPY (HRTEM)

High-resolution transmission electron microscopy (HRTEM) is one of the most powerful tools for characterizing nanomaterials. It uses the same principle as that of SEM but only differs by the fact that it transmits the incoming electron beam instead of scanning across the sample surface [8]. Figure 3.6 shows the picture of the HRTEM used in characterizing $\text{SrAl}_2\text{O}_4:\text{Eu}^{2+},\text{Dy}^{3+}$ thin films in this work.



Figure 3.6. The FEI Titan 300 HRTEM system at Virginia Tech. Institute, USA.

3.7. X-RAY DIFFRACTION (XRD)

X-ray diffraction is a technique used to determine the arrangement of atoms within a crystalline material in which a beam of X-ray strikes a crystal and diffracts into many specific directions. The interaction of an X-ray beam with the sample produces constructive interference and when conditions satisfy Bragg's Law ($n\lambda = 2d\sin\theta$), the diffracted rays are

collected, processed and counted [9]. By scanning the sample through a range of 2θ angles, all possible peaks to d-spacings allows identification of the sample based on its unique d-spacings. In the current work the X-ray diffraction data was collected by using a SIEMENS D5000 diffractometer using $\text{CuK}\alpha$ radiation of $\lambda = 1.5405 \text{ nm}$. A photograph of the X-ray diffractometer used in this study is shown in Figure 3.7.



Figure 3.7. SIEMENS D5000 model X-ray diffractometer at the Geology Department, University of the Free State.

3.8. AUGER ELECTRON SPECTROSCOPY (AES)

In the AES technique, electrons with a specific energy are used for identification of chemical elements present in a material. To induce electron emission, excitation is required. When a material is irradiated with energetic electrons, electrons are emitted from the inner shells [10]. The kinetic energy of the emitted electrons corresponds to the difference between the energies of the electron energy levels involved and the work function. Because these three parameters are specific to each element, the resulting energy distribution reflects the elementary composition of the material [11]. In the current work, the CL data were collected

via an optical fibre set attached to one of the ports of the UHV chamber and a computer. One end of the fibre was positioned inside the chamber close to the sample, while the other end was connected to the spectrometer. The coupling efficiency to the spectrometer is always better since additional optics is kept to a minimum. The Ocean Optics S2000 spectrometer type with OOIBase32 computer software was employed for the CL data collection in this work. Figure 3.8 shows the photo of the AES combined with the CL system used in AES surface and CL emission data collection.

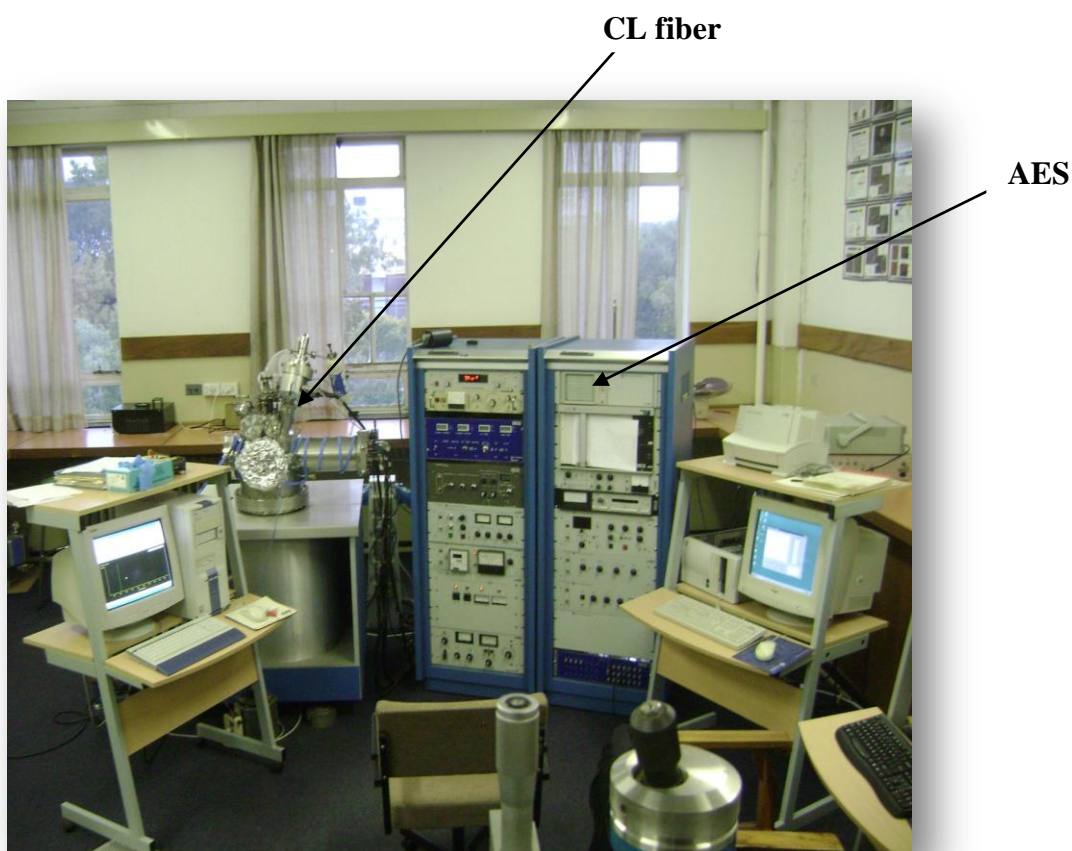


Figure 3.8. The PHI model 545 Auger electron spectroscopy (AES) unit combined with the CL unit at the Physics Department, University of the Free State.

3.9 X-RAY PHOTOELECTRON SPECTROSCOPY (XPS)

In the x-ray photoelectron spectroscopy, the photoelectrons are ejected from the core-level by an X-ray photon of energy $h\nu$. The energy of the emitted photoelectron is then analysed by the electron spectrometer and the data presented as a graph of intensity (usually expressed as counts or counts/s) versus electron binding energy. The kinetic energy (E_K) of the electron is

the experimental quantity measured by the spectrometer, and it depends on the photon energy of the X-rays employed and is therefore not an intrinsic material property [10]. The binding energy of the electron (E_B) is the parameter which identifies the electron specifically, both in terms of its parent element and atomic energy level [10]. The photoelectron spectrum will reproduce the electronic structure of an element quite accurately since all electrons with a binding energy less than the photon energy will feature in the spectrum. The PHI5000 XPS Versaprobe (monochromatic $AlK\alpha$ lines) system was used in this work for data collection (Figure 3.9).



Figure 3.9. The PHI 5000 XPS Versaprobe (monochromatic $AlK\alpha$ lines) machine at the Physics Department of the University of the Free State.

3.10 RUTHERFORD BACKSCATTERING (RBS)

Rutherford backscattering spectrometry (RBS) is a very popular thin-film characterization technique. RBS uses a very high energy and low-mass ion beam, such as He^+ , with a 2 MeV

energy, that penetrates up to a depth of a few microns into the films and film-substrate [12]. This deep penetration results in a subsequent collection of the elastically scattered ions from the coulomb repulsion that occurs between the ion and nucleus and is known as Rutherford backscattering. By analyzing the energy spectrum from the scattered ions, one can determine the stoichiometry of thin-film compositions with accuracies of $\pm 1.0\%$. If the incident high-energy beam is aligned along a particular crystal channel structure, the channeling spectroscopy can yield details about the crystallinity, interface phenomena, thickness and epitaxial quality [13]. Figure 3.10 shows a photograph of the RBS system used to analyze films in this study.



Figure 3.10. The RBS system at Ithemba Labs, Cape Town, South Africa.

The following chapters (4-9) will be presenting results in form of wholly or partly published/submitted papers, in/to the international Journals so there might be some repetitions in the introduction parts and experimental details. The study aimed at investigating the optimum deposition parameters for the highly emitting pulsed laser

deposited $\text{SrAl}_2\text{O}_4:\text{Eu}^{2+},\text{Dy}^{3+}$ thin films. Among many PLD deposition parameters only few were considered, i.e. the substrate temperature, number of pulses, repetition rate and the working atmosphere. Also, the initial plan was to optimize one deposition condition and use the obtained optimum value when optimizing the next deposition condition. However, due to the short time allocated to the users of the PLD system (the only PLD national facility for students) some deposition parameters couldn't be done and also in some cases the optimization consistency of deposition parameters couldn't be followed.

REFERENCES

1. J. Schou, Appl. Surf. Sci. **255** (2009) 5191.
2. www.physandtech.net/pld/PLD_schem
3. D.P. Norton, Mater. Sci. **R 43** (2004) 139.
4. J.A. Deluca, J. Chem. Edu. **57** (1980) 541.
5. K.D. Vernon-Parry, III-Vs Review **13** (2000) 40.
6. N. Jalili, K. Laxminarayana, Mechatronics **14** (2004) 907.
7. R. Fung, S. Huang, J. Vib. Acoust. **123** (2001) 502.
8. Q. Y. Zhang, X. Y. Huang, Prog. Mater. Sci. **55** (2010) 353.
9. http://serc.carleton.edu/research_education/geochemsheets/techniques/XRD.html
10. J. F. Watts, J. Wolstenholme, *An Introduction to Surface Analysis by XPS and AES*, Copyright © John Wiley & Sons Ltd, the Atrium, Southern Gate, Chichester, West Sussex PO19 8SQ, England, 2003.
11. M. Kohler, W. Fritzsche, *Nanotechnology, an introduction to nano structuring techniques*, Wiley-VCH Verlag GmbH & Co. KGaA, Weinheim, 2004.
12. J. Perriere, Vacuum **37** (1987) 429.
13. D. R. Pesiri, R. C. Snow, N. Elliott, C. Maggiore, R. C. Dye, Journal of Membrane Science **176** (2000) 209.

CHAPTER 4

THE EFFECTS OF SUBSTRATE TEMPERATURE ON THE STRUCTURE, MORPHOLOGY AND PHOTOLUMINESCENCE PROPERTIES OF PULSED LASER DEPOSITED $\text{SrAl}_2\text{O}_4:\text{Eu}^{2+},\text{Dy}^{3+}$ THIN FILMS

4.1 INTRODUCTION

The long afterglow properties of $\text{SrAl}_2\text{O}_4:\text{Eu}^{2+},\text{Dy}^{3+}$ material has made it to be a potential candidate for applications in infrastructure in future. These applications, include among others the luminous paints in highway, airport, building and ceramics, textile, dial plate of glowing watch, warning signs and escape route ways [1]. Additionally, $\text{SrAl}_2\text{O}_4:\text{Eu}^{2+},\text{Dy}^{3+}$ has good stability and is safe and friendly to the environment [2]. Conventionally, $\text{SrAl}_2\text{O}_4:\text{Eu}^{2+},\text{Dy}^{3+}$ is prepared in powder form using the solid state reaction technique. However, thin films offer several advantages due to their good luminescence characteristics, higher image resolution from small grains, better thermal stability and good adhesion to the substrate [3]. Among the techniques used to synthesize luminescent thin films, pulsed laser deposition (PLD) is a unique process for stoichiometric ablation of the target material offering an excellent control of the film morphology [4].

During PLD, the kinetics of atomic arrangement is mainly determined by substrate temperature and the energy of the deposition atoms [5]. Additionally, the mobility of the atoms deposited on the surface is directly dependent on temperature, a dependence which can influence the activation energy of each process [6]. Reports have also shown that the crystallinity of the as-grown films is highly dependent upon the processing temperature [7]. Studies on the influence of substrate temperature on $\text{SrAl}_2\text{O}_4:\text{Eu}^{2+}, \text{Dy}^{3+}$ thin films is of great importance to establish the optimum substrate temperature range for high PL intensity. Additionally, there are limited reports in the literature on $\text{SrAl}_2\text{O}_4:\text{Eu}^{2+}, \text{Dy}^{3+}$ thin films. In this chapter, we report on the variation of photoluminescence and morphological properties

of $\text{SrAl}_2\text{O}_4:\text{Eu}^{2+}, \text{Dy}^{3+}$ thin films with substrate temperature on the 40-700 °C range. The ablation took place in the oxygen gas background.

4.2 EXPERIMENTAL DETAILS

$\text{SrAl}_2\text{O}_4:\text{Eu}^{2+}, \text{Dy}^{3+}$ powder phosphor from Phosphor Technology (UK) was pressed without binders to make a pellet (target) for ablation. The pellet was annealed in air at 600° C for 24 hours to remove water vapour and other adsorbed volatile substances. The chamber was first evacuated to a base pressure of 8×10^{-6} mbar before backfilling with 2.7×10^{-2} mbar oxygen gas. The pellet was then ablated and the film was deposited on ultrasonically cleaned Si (100) using a 248 nm KrF laser with 4000 pulses and a of 8 Hz repetition rate. The films were deposited at different substrate temperatures ranging from 40-700° C while fixing other deposition parameters. The Shimadzu Superscan SSX-550 system was used to collect the Scanning Electron Microscopy (SEM). Atomic Force Microscopy (AFM) micrographs were obtained from the Shimadzu SPM - 9600 model. PL excitation and emission spectra were recorded using a 325 nm He-Cd laser PL system. High resolution transmission electron microscopy (HRTEM) was employed for crystal structure analysis.

4.3 RESULTS AND DISCUSSIONS

AFM images of $\text{SrAl}_2\text{O}_4:\text{Eu}^{2+}, \text{Dy}^{3+}$ thin films deposited at varying substrate temperatures in the range of 40 – 700° C are shown in Figure 4.1. It can be observed from the results that different morphologies were obtained by changing the substrate temperature during film deposition. It is clear that the particle sizes of the film deposited at higher substrate temperature (700° C) were much larger than the particle sizes of the films deposited at lower substrate temperatures suggesting that the growth rate of deposited particles was much faster at higher substrate temperatures. The increase in the crystallite size possibly results from the enhancement of the film surface atomic mobility with increasing substrate temperature, which enables the thermodynamically favored grains to grow [8]. Similar results were reported by Jones et al. [9]. The films deposited at lower substrate temperatures of 40° C (NS-09) and 400° C (NS-4) had smoother surfaces than the film deposited at higher substrate temperature of 700° C (NS-8). The surface topography changed from smooth to nodular with

an increase in substrate temperature. Increasing the substrate temperature to 700° C yielded a complete development of nodular surface with well defined grain boundaries.

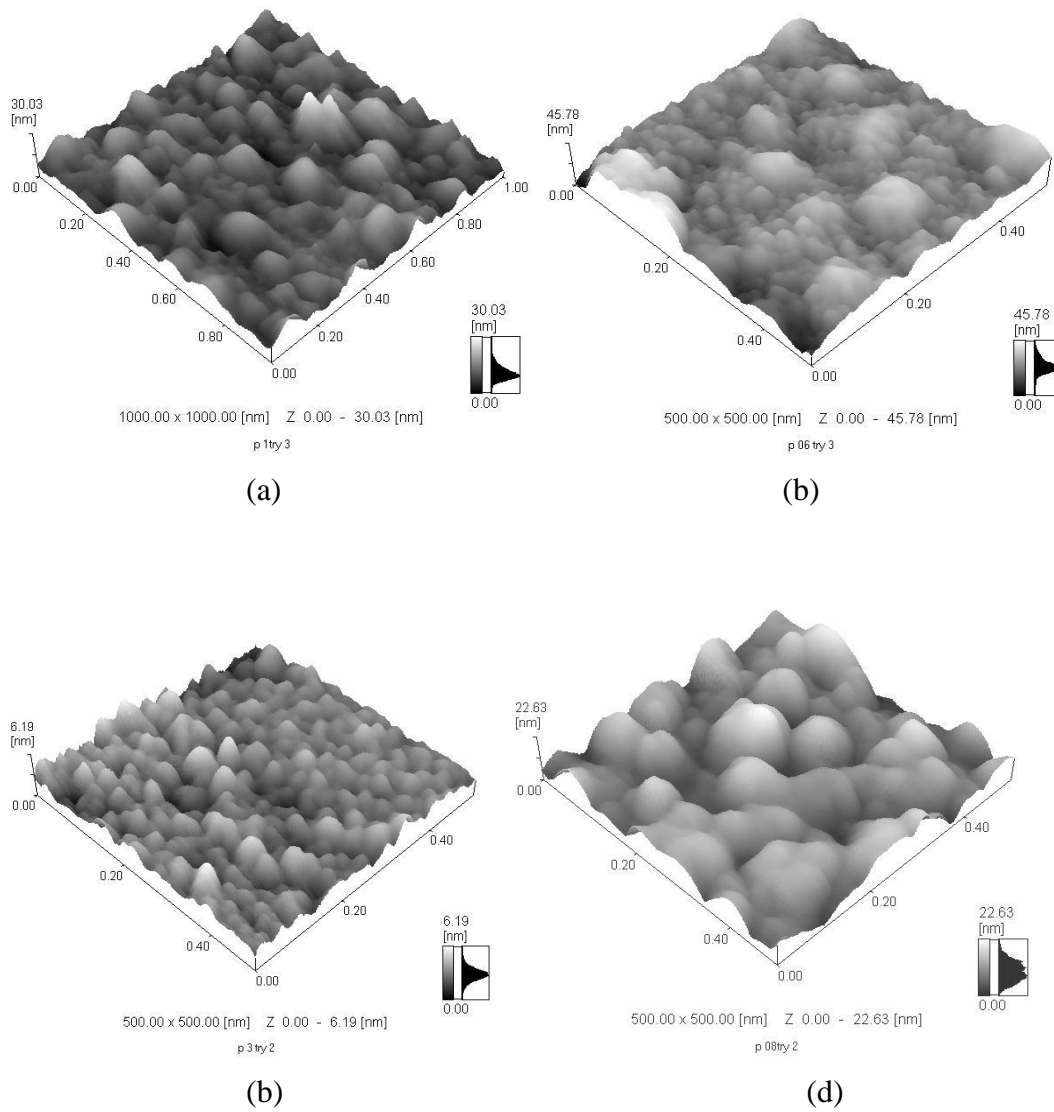


Figure 4.1. AFM images of the films deposited at (a) 40° C (b) 200° C, (c) 400° C and (d) 700° C.

Figure 4.2 shows the SEM images of the films grown at different substrate temperatures. The film was coated with a thin layer of platinum layer for focus ion beam (FIB) sample preparation as shown in Figure 4.3 (left). The HRTEM image in Figure 4.3 (right) shows that

the SrAl_2O_4 layer was amorphous. This result was consistent with the XRD data (not shown) collected from all the films.

Figure 4.4 shows the PL spectra of the films deposited at substrate temperatures ranging from 40 – 700° C.

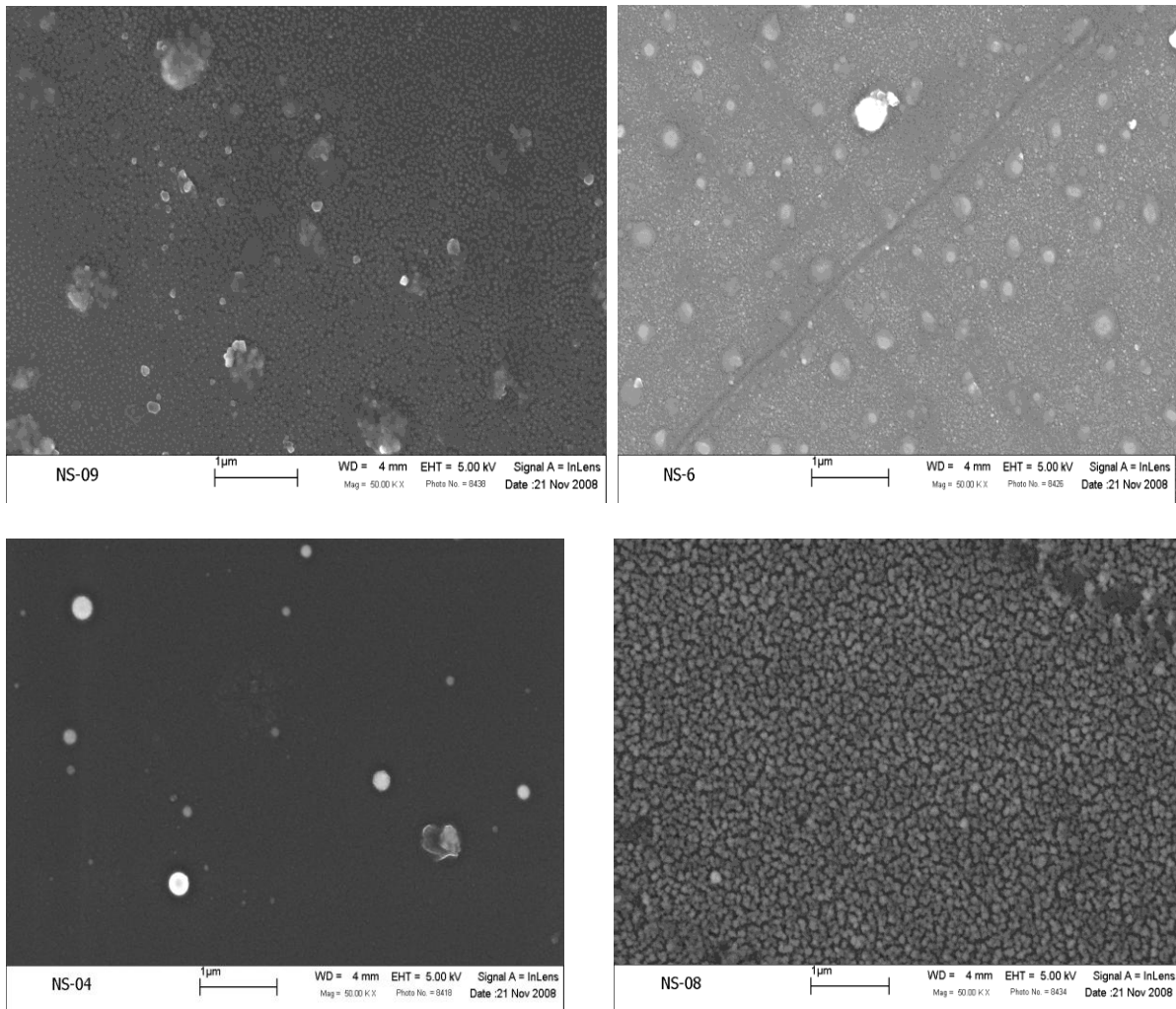


Figure 4.2. SEM micrographs of the films deposited at (NS-09) 40° C (NS-6) 200° C, (NS-4) 400° C and (NS-08) 700° C.

Figure 4.3 shows the HRTEM micrographs of the film deposited at 0.2 Torr O_2 and 400° C.

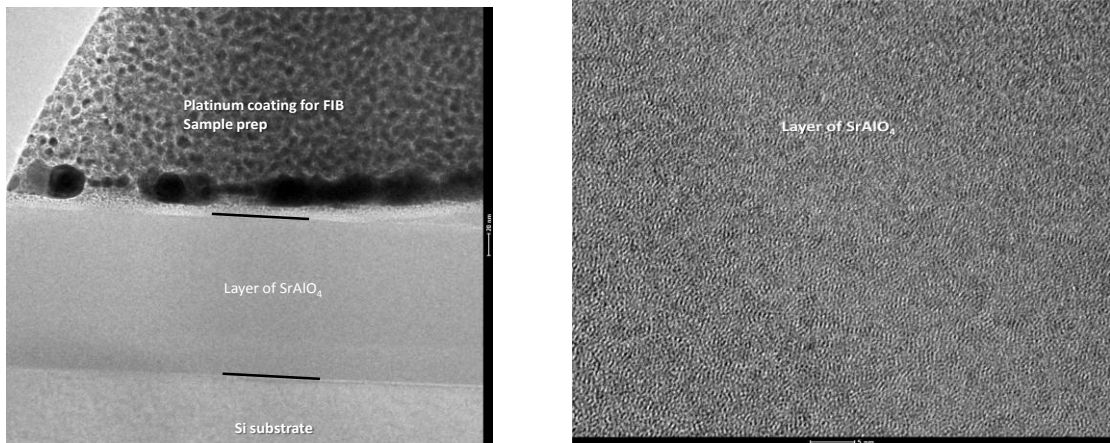
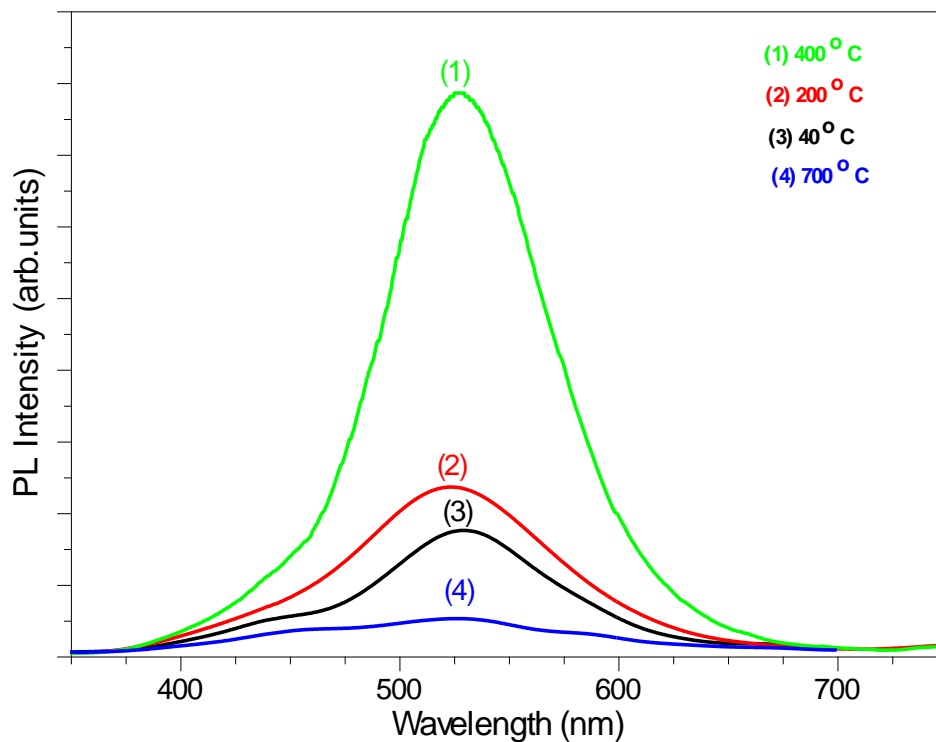


Figure 4.3. HRTEM images of the film deposited 1.1 Torr O_2 and $400^\circ C$. The image on the left shows the Platinum layer deposited for FIB sample preparation and the image on the right shows an amorphous layer $SrAl_2O_4$. The scale is 5 nm.



Figures 4.4. PL spectra of the films deposited at temperatures ranging from $40 - 700^\circ C$.

The increase in the substrate temperature resulted in an increase in particle sizes which in turn increased the PL intensity of the films. The highest PL intensity was observed from the film deposited at 400° C and the intensity dropped when the substrate temperature was increased to 700° C. The decrease in the PL at the substrate temperature of 700° C is attributed to the inter-diffusion at the film substrate interface [7]. The increase in the PL intensity with the increase of the substrate temperature can be associated with rougher surfaces and improved optical properties of larger crystallite sizes at higher temperatures. It is well known that rough surfaces increases the probability of light emission from the surface by limiting the chances of total internal reflection at the film-substrate interface [9]. Dhlamini et al. [10] found that the PL intensity of the SiO₂:PbS layers obtained with PLD increased relatively with the increase in the substrate temperature. This relative increase of the PL intensity with the substrate temperature suggests the decrease of the grains which plays a major role in increasing defect densities. Similar behaviour was observed by Mckittrick et al [11], in their study of characterization of photoluminescent (Y_{1-x}Eu_x)₂O₃ thin films prepared by metallorganic chemical vapour deposition. They measured an increase in the PL intensity with an increase in substrate temperature (500° C, 600° C and 700° C) of the films grown on sapphire substrates. They ascribed the increase in the PL intensity to both grain growth (minimizing grain-boundary area) and a reduction of disorder around the Eu³⁺ in the lattice. Coetsee et al. [12] also found that the increase in substrate temperature from 400 to 600 °C resulted in increased luminescence due to a rougher surface. For better luminescent intensity the thin films should have a rougher surface. The SEM and AFM images of the 700° C shows that the surface structure of the sample is completely different from the rest of the films, with relatively bigger and more robust particles and was therefore expected to give the highest PL intensity. The reason why the PL intensity decreased at 700° C is attributed to the diffusion at the film-substrate temperature [7].

4.4 CONCLUSION

SrAl₂O₄:Eu²⁺,Dy³⁺ thin film phosphors were deposited on Si (100) substrates at different substrate temperatures ranging from 40 – 700° C. The films deposited at higher substrate temperatures were shown to have rougher surface and larger particle sizes than those deposited at lower substrate temperature. The PL intensity increased with temperature from 40 – 400° C, with the maximum at 400°C, and then dropped when the temperature was

increased to 700° C. The increase in the PL intensity was associated with rougher surfaces and improved optical properties at high temperatures.

REFERENCES

1. F. Gao, Z. Xiong, H. Xue, Y. Liu, J. Phys. Conference Series **152** (2009) 1.
2. O. M. Ntwaeaborwa, P. D. Nsimama, Shreyas Pitale, I. M. Nagpure, Vinay Kumar, E. Coetsee, J. J. Terblans, P. T. Sechogela and H. C. Swart, J. Vac. Sci. Technol. A **28** (2010) 901.
3. J.S. Bae, K.S. Shim, S.B. Kim, J.H. Jeong, S.S. Yi, J.C. Park, J. Cryst. Growth **264** (2004) 290.
4. A.M. Hristea, O. Alm, E-J. Popovici, M. Boman, Thin Solid Films **516** (2008) 8431.
5. X.M. Fan, J.S. Lian, Z.X. Guo, H.J. Lu, Appl. Surf. Sci. **239** (2005) 176.
6. S. Christoulakis, M. Sucheá, N. Katsarakis, E. Koudoumas, Appl. Surf. Sci. **253** (2007) 8169.
7. R. Eason (Editor), *Pulsed laser deposition of thin films applications-led growth of functional materials*, Wiley Interscience, 2006.
8. C.B. Wang, R. Tu, T. Goto, Q. Shen, L.M. Zhang, Mater. Chem. Phys. **113** (2009) 130.
9. S.L. Jones, D. Kumar, R.K. Singh, P.H. Holloway, Appl. Phys. Lett. **71** (1997) 404.
10. M.S. Dhlamini, J.J. Terblans, O.M. Ntwaeaborwa, J.M. Ngaruiya, K.T. Hillie, J.R. Botha and H.C. Swart, J. of Lumin, **128** (2008) 1997.
11. J. McKittrick, C.F. Bacalski, G.A. Hirata, K.M. Hubbard, S.G. Pattillo, K.V. Salazar, M. Trkula, J. Am. Ceram. Soc. **83** (2000) 1241.
12. E. Coetsee, J.J. Terblans, H.C. Swart, J.M. Fitz-Gerald and J.R. Botha, e-J. Surf. Sci. Nanotech. **7** (2009) 369.

CHAPTER 5

THE INFLUENCE OF THE NUMBER OF PULSES ON THE MORPHOLOGICAL AND PHOTOLUMINESCENCE PROPERTIES OF $\text{SrAl}_2\text{O}_4:\text{Eu}^{2+},\text{Dy}^{3+}$ THIN FILMS PREPARED BY PULSED LASER DEPOSITION

5.1 INTRODUCTION

The green emitting $\text{SrAl}_2\text{O}_4:\text{Eu}^{2+},\text{Dy}^{3+}$ is a well-known phosphor for its high quantum efficiency and long afterglow characteristics. It has a high potential to be used in various display devices, luminescent paints, screens, glow signs, emergency escape route guidance systems, detection for structural damage, etc. [1]. $\text{SrAl}_2\text{O}_4:\text{Eu}^{2+},\text{Dy}^{3+}$ has commonly been prepared using several techniques, such as the solid-state reaction [2, 3], sol-gel [4], combustion [5], detonation [6], etc. Most of the reported works are on powder samples. However, thin film phosphors have several advantages over powders, such as higher lateral resolution from smaller grains, better thermal stability, reduced out gassing, and better adhesion to the solid surface [7]. Amongst the techniques used to prepare/grow/ablate luminescent thin films, Pulsed Laser Deposition (PLD) is a unique process for stoichiometric transfer of the target material with excellent morphology [8]. It is also well known that the structure and other properties of the film can be affected by varying the deposition process parameters. Crystallinity and surface roughness of the phosphor thin films have strong effects on the photoluminescence response of the films [9]. Christoukis et al. [10] reported that the roughness of laser ablated calcium sulfide thin films increased with the increase in the number of pulses.

There are limited reports in the literature [11] on $\text{SrAl}_2\text{O}_4:\text{Eu}^{2+},\text{Dy}^{3+}$ thin films deposited using the PLD technique. Sato et al. [11] investigated the PL properties of pulsed laser ablated $\text{SrAl}_2\text{O}_4:\text{Eu}^{2+},\text{Dy}^{3+}$ thin films at lower temperatures (-264- 0° C). They also found that the as-deposited thin films were amorphous and the annealed ones had the common $\text{SrAl}_2\text{O}_4:\text{Eu}^{2+},\text{Dy}^{3+}$ monoclinic phase. Further investigations on the influence of different

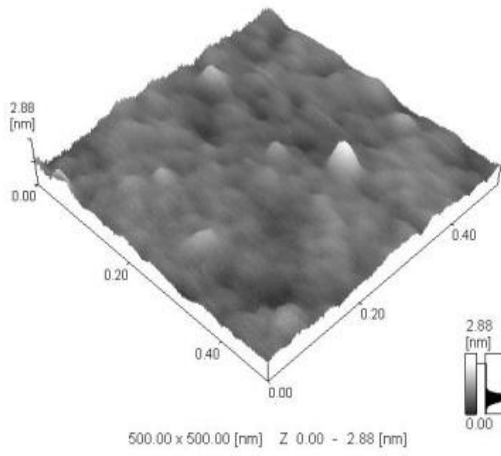
deposition parameters to the properties of $\text{SrAl}_2\text{O}_4:\text{Eu}^{2+}$, Dy^{3+} films are crucial in the production of highly emitting films. In the current work, the influence of the number of laser pulses on the morphological, structural and photoluminescence properties of $\text{SrAl}_2\text{O}_4:\text{Eu}^{2+}$, Dy^{3+} thin films prepared by the PLD technique is reported.

5.2 MATERIALS AND METHODS

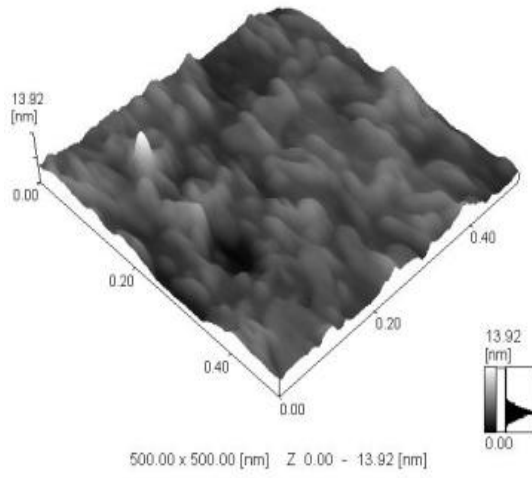
Silicon (100) wafers were used as substrates and they were first cleaned as described elsewhere [12]. A commercial $\text{SrAl}_2\text{O}_4:\text{Eu}^{2+}$, Dy^{3+} phosphor powder was pressed without binders to prepare a pellet that was used as an ablation target. The target was annealed at 600°C for 24 hours in air before placing it on the target holder of the PLD system. The deposition chamber was evacuated to a base pressure of 6.7×10^{-6} mbar. A Lambda Physic 248 nm KrF excimer laser was used to ablate the phosphor pellet in vacuum. The laser energy density and fluency were 0.74 J/cm^2 and 8 Hz respectively. The substrate temperature was fixed at 200°C and the target to substrate distance was 6 cm. The ablated area was 1 cm^2 . The films were deposited at 4000, 8000 and 16000 number of pulses. A Shimadzu Superscan SSX-550 system was used to collect the SEM and EDX data. AFM micrographs and surface roughness measurements were obtained from a Shimadzu SPM - 9600. XRD data was collected by using a D5000 diffractometer using $\text{CuK}\alpha$ radiation of $\lambda = 1.5405 \text{ nm}$. Photoluminescence excitation and emission spectra were recorded using a Cary Eclipse fluorescence spectrophotometer (Model: LS 55) with a built-in xenon lamp and a grating to select a suitable wavelength for excitation. The excitation wavelength was 340 nm.

5.3 RESULTS AND DISCUSSION

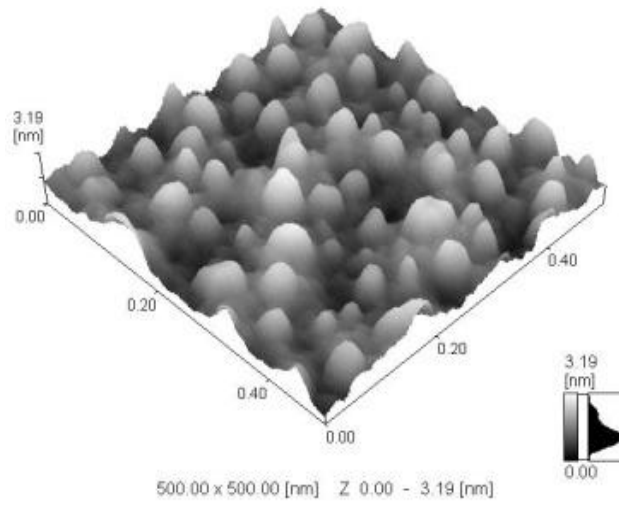
Figure 5.1(a) shows the AFM pictures of the three films deposited at (i) 4000 (ii) 8000 and (iii) 16000 pulses. The sample deposited at 4000 pulses showed a smooth continuous phase with poorly defined boundaries of particles. Cylindrical shaped grains with poorly defined boundaries were observed in the AFM picture of the sample deposited at 8000 pulses in Fig. 5.1(a) (ii). The sample deposited at 16000 pulses (Fig. 5.1(a) (iii)) gave well defined boundaries of spheroidal particles aligned in the vertical direction. The surface roughness for the films are shown in Figure 5.1(b).



(i)



(ii)



(iii)

(a)

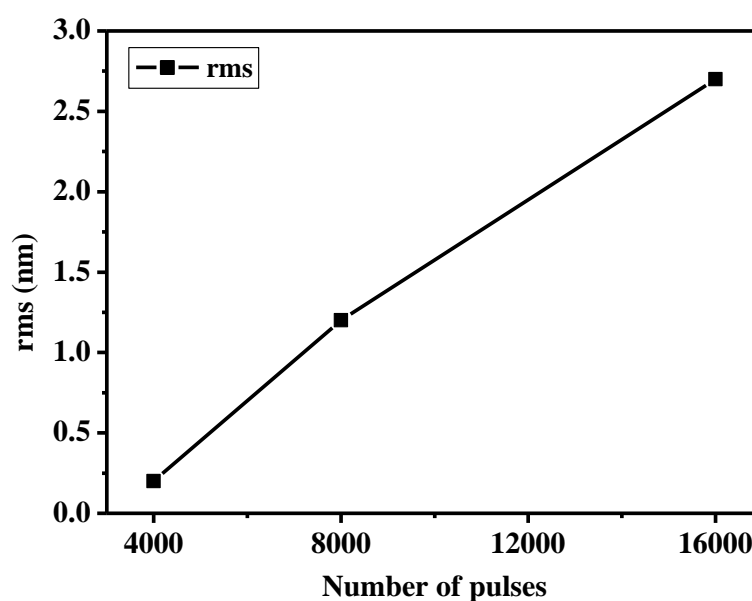


Figure 5.1. (a) The AFM pictures of PLD SrAl₂O₄:Eu²⁺, Dy³⁺ thin films deposited at (i) 4000, (ii) 8000, (iii) 16000 pulses. (b) The variation of SrAl₂O₄:Eu²⁺, Dy³⁺ thin film rms roughness with the number of pulses.

It is therefore reasonable to conclude that the surface roughness and well defined boundaries of particles are only obtained when depositing at a higher number of pulses. Similar results were reported by Christoukis et al. [10] on laser ablated Calcium sulfide thin films.

XRD diffractographs of the thin films deposited at the different number of pulses (Figure 5.2), showed that the films were amorphous with only a very small indication of the monoclinic SrAl₂O₄:Eu²⁺, Dy³⁺ (220) peak at $2\theta = 29.2^\circ$ measured for the 8000 and 16000 pulses samples. Amorphous SrAl₂O₄:Eu²⁺, Dy³⁺ films have also been reported by other authors [11] from unannealed films.

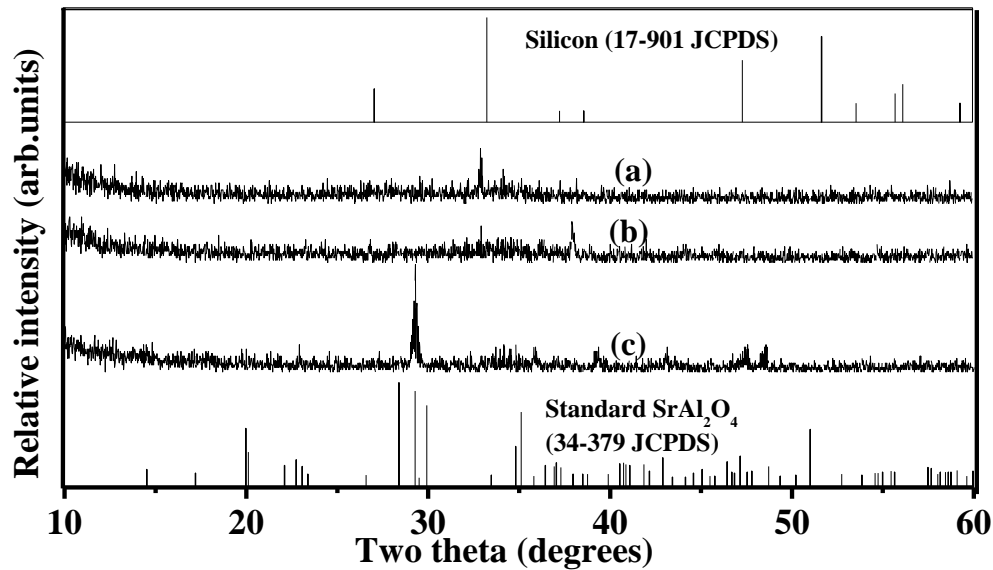


Figure 5.2. The XRD diffraction graphs for the $\text{SrAl}_2\text{O}_4:\text{Eu}^{2+}, \text{Dy}^{3+}$ films deposited at: (a) 4000 (b) 8000 (c) 16000 number of pulses. The silicon substrate and the standard 34-379 JCPDS file of $\text{SrAl}_2\text{O}_4:\text{Eu}^{2+}, \text{Dy}^{3+}$ also shown.

Figure 5.3 shows the room temperature PL emission data of the $\text{SrAl}_2\text{O}_4:\text{Eu}^{2+}, \text{Dy}^{3+}$ films deposited at 4000, 8000 and 16000 pulses (spectra (b)-(d)) and of the commercial $\text{SrAl}_2\text{O}_4:\text{Eu}^{2+}, \text{Dy}^{3+}$ powder (spectrum (e)). All the samples were excited at 340 nm using a monochromatized xenon lamp. Two emission peaks were observed at 517 and 630 nm from all the films. The emission at 517 nm can be ascribed to $4f^65d^1 \rightarrow 4f^7$ transitions of Eu^{2+} [13] and that at 630 nm can be ascribed to ${}^5\text{D}_0 \rightarrow {}^7\text{D}_2$ transitions of Eu^{3+} [14]. The Eu^{3+} is either due to incomplete reduction of Eu^{3+} during sample preparation [15] or it is most likely that Eu^{2+} was oxidized to Eu^{3+} during pulsed laser deposition. The highest PL intensity was observed from the film deposited at 16000 pulses (spectrum (d)) with the major emission in the green region at 517 nm and the least intense green emission was observed from the film deposited at 4000 pulses (spectrum (b)). The higher PL intensity from the film deposited at 16000 pulses can be ascribed to the film's relatively rougher surface as well as the thicker layer as observed from the AFM data in Figure 5.1(b). It is well known that rough surfaces increases the probability of light emission from the surface by limiting the chances of total internal reflection at the film-substrate interface [16].

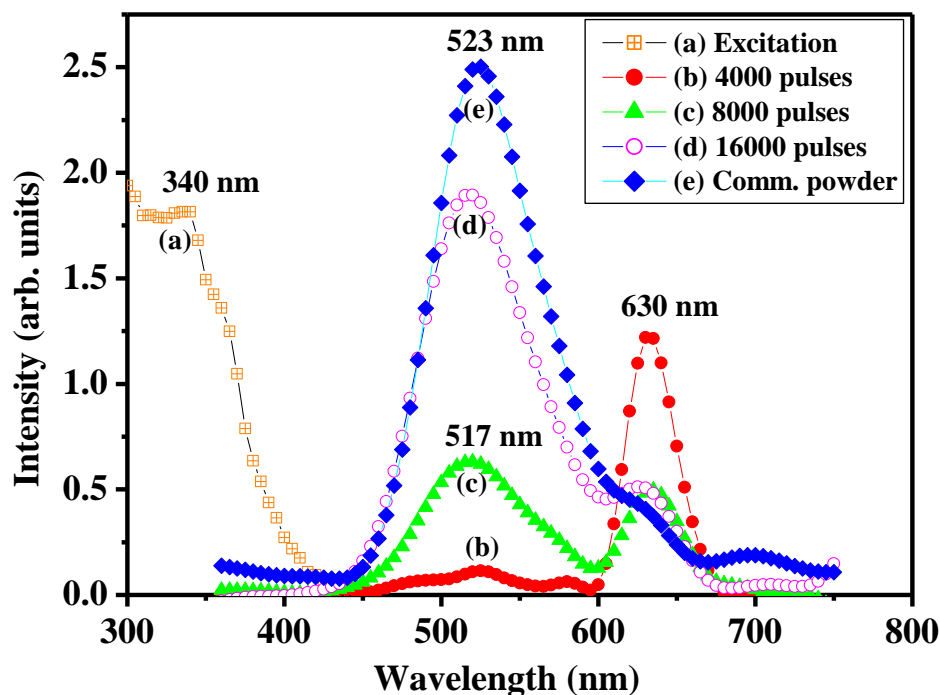


Figure 5.3. The PL (a) excitation and emission spectra of the $\text{SrAl}_2\text{O}_4:\text{Eu}^{2+}, \text{Dy}^{3+}$ thin films deposited at (a) 4000 (b) 8000 (c) 16000 pulses and that of (e) the commercial $\text{SrAl}_2\text{O}_4:\text{Eu}^{2+}, \text{Dy}^{3+}$ powder.

The red emission at 630 nm was more intense than the green emission at 517 nm in the film deposited at 4000 pulses. It is most likely that Eu^{2+} was initially oxidized to Eu^{3+} at a relatively faster rate when depositing at 4000 pulses. It should be noted that the 517 nm peak in spectra (b) – (d) is slightly blue-shifted from the peak observed in $\text{SrAl}_2\text{O}_4:\text{Eu}^{2+}, \text{Dy}^{3+}$ powder at 523 nm. Among other things, the blue-shifting suggests that the particle sizes of the films were smaller than those of the commercial powder. The excitation spectrum for the 517 nm emission is shown in Figure 5.3 (a). The red peak was only recorded by the Xenon lamp Carry Eclipse spectrophotometer but not by the laser system. The reason behind this difference is not yet clear at the moment.

The afterglow characteristics of the thin films are shown in Figure 5.4. Consistent with the PL data, the data in Figure 5.4 show that the film deposited with 16000 pulses had relatively longer decay times. The decay curves of the films were characterized by an initial rapid decay followed by long lasting phosphorescence.

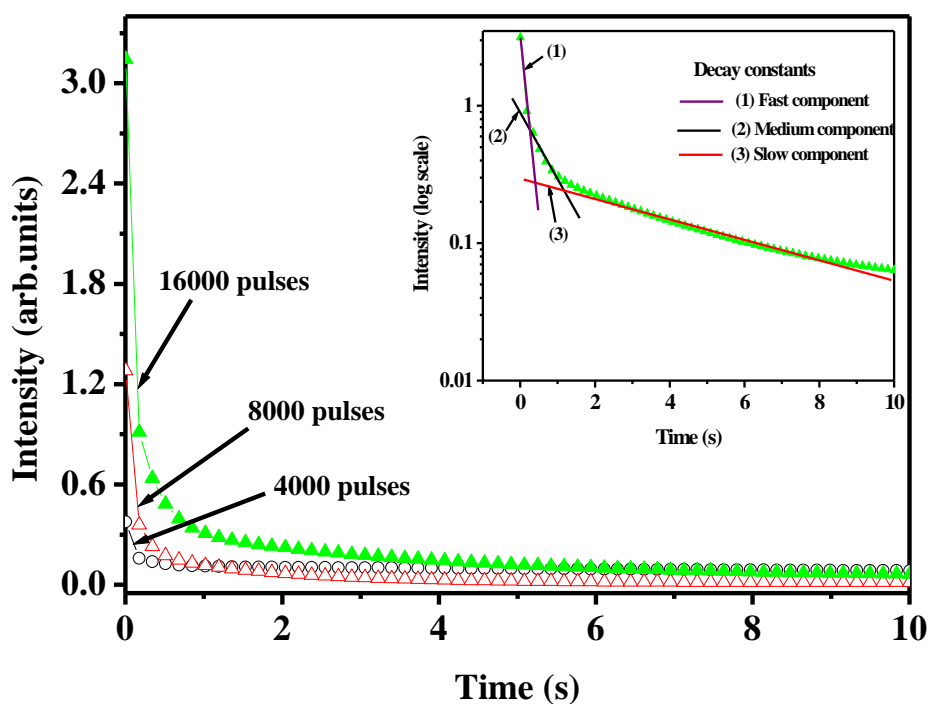


Figure 5.4. Afterglow characteristics of PLD SrAl₂O₄:Eu²⁺, Dy³⁺ thin films deposited at the different number of pulses: (a) 4000, (b) 8000 and (c) 16000.

The decay curves were fitted by using equation (2.3). Consistent with the equation, the decay curves are characterized by three different regions labeled fast, medium and slow in the inset of Figure 5.3; and they are indicative of different rates of decay for the films. The half life times for the fitted data are listed in Table 5.1.

Table 5.1. The afterglow lifetimes for the SrAl₂O₄:Eu²⁺, Dy³⁺ films deposited at a different number of pulses as indicated.

Film Pulses	Half life times		
	τ_1 (s)	τ_2 (s)	τ_3 (s)
(a) 4000	0.001 ± 0.001	0.008 ± 0.001	0.64 ± 0.05
(b) 8000	0.004 ± 0.001	0.160 ± 0.001	1.60 ± 0.05
(c) 16000	0.018 ± 0.001	0.265 ± 0.001	3.43 ± 0.05

The phosphorescence of $\text{SrAl}_2\text{O}_4:\text{Eu}^{2+},\text{Dy}^{3+}$ is believed to originate from the photo-oxidation of Eu^{2+} cation under UV-irradiation [15]. According to this model, an electron from the $4f^7$ ground state is excited to the $4f^65d^1$ level of Eu^{2+} followed by an electron capture from the valence band reducing Eu^{2+} to Eu^+ . The hole generated in the valence can migrate and be captured by Dy^{3+} converting it to Dy^{4+} . Relaxation to the ground state, which is accompanied by green emission, is triggered by the thermo-activated promotion of an electron from the valence band to the first unoccupied levels of Dy^{4+} followed by a migration of the trapped hole to the photon-generated Eu^+ cation [15].

It can be concluded from the results in Table 1 that there was an increase in the values of decay times with the increase in the number of pulses. The sample deposited at 16000 pulses showed superior decay properties.

5.4 CONCLUSION

$\text{SrAl}_2\text{O}_4:\text{Eu}^{2+},\text{Dy}^{3+}$ thin films were successfully grown on Si(100) substrates by the pulsed laser deposition technique. The samples deposited at a higher number of pulses have well packed grains, while those prepared at lower number of pulses has a smooth uniform surface. The XRD results show that films are generally amorphous with only one small common $\text{SrAl}_2\text{O}_4:\text{Eu}^{2+}, \text{Dy}^{3+}$ (220) peak featuring in the samples prepared at the higher number of pulses (8000 and 16000). The intense green emission from the brightest film deposited at 16000 laser pulses was at 517 nm and the less intense green emission was observed from the film deposited at 4000 laser pulses. The emission at 630 nm from $^5\text{D}_0 \rightarrow ^7\text{D}_2$ transitions of Eu^{3+} was also detected. The film with the higher PL intensity had superior afterglow characteristics.

REFERENCES

1. P. Sharma, D. Haranath, H. Chander, S. Singh, *Appl. Surf. Sci.* **254** (2008) 4052.
2. Y-L. Chang, H-I. Hsiang, M-T. Liang, *Journal of Alloys and Compounds* **461** (2008) 598.
3. P.D. Sarkisov, N.V. Popovich, A.G. Zhelnin, *Glass and Ceramics* **60** (2003) 9.
4. T. Peng, L. Huajun, H. Yang, *J. Mater. Chem. & Phys* **85** (2004) 68.
5. T. Peng, H. Yang, X. Pu, B. Hu, Z. Jian, C. Yan, *Mater. Lett.* **58** (2004) 352.
6. X. Li, Y. Qu, X. Xie, Z. Wang, R. Li, *Mater. Lett.* **60** (2006) 3673.
7. J.S. Bae, K.S. Shim, S.B. Kim, J.H. Jeong, S.S. Yi, J.C. Park, *J. Cryst. Growth* **264** (2004) 290.
8. A. Mesaros-Hristea, O. Alm, E. Jeane, P. Boman, *Thin Solid Films* **516** (2004) 343.
9. L. Fang, M. Shen, *J. of Cryst. Growth* **310** (2008) 3470.
10. S. Christoulakis, M. Suche, N. Katsarakis, E. Koudoumas, *Appl. Surf. Sci.* **253** (2007) 8169.
11. K. Sato, S. Komuro, T. Morikawa, H. Aizawa, T. Katsumata, S. Harakob, X. Zhao, *J. Cryst. Growth* **275** (2005) 1137.
12. E. Coetsee, H.C. Swart, J.J. Terblans, O.M. Ntwaeaborwa, K.T. Hillie, W.A. Jordaan U. Buttner, *Optical Materials* **29** (2007) 1338.
13. D. Jia, *Optical Materials* **22** (2003) 65.
14. N. Perea-Lopez, J.A. Gonzalez-Ortega, G.A. Hirata, *Optical Materials* **29** (2006) 43.
15. F. Clabau, X. Rocquefelte, S. Jobic, P. Denieard, M-H. Whangbo, A. Garcia, T. Mercier, *Solid State Sciences* **9** (2007) 608.
16. S.L. Jones, D. Kumar, K-G. Cho, R. Singh, P.H. Holloway, *Displays* **19** (1999) 151.

CHAPTER 6

PHOTOLUMINESCENCE PROPERTIES OF $\text{SrAl}_2\text{O}_4:\text{Eu}^{2+},\text{Dy}^{3+}$ THIN PHOSPHOR FILMS GROWN BY PULSED LASER DEPOSITION

6.1 INTRODUCTION

There has been a growing research interest on the study of photoluminescence and phosphorescence properties of $\text{SrAl}_2\text{O}_4:\text{Eu}^{2+},\text{Dy}^{3+}$ phosphor because of its chemical stability, high quantum yield and long lasting phosphorescence, among other things, for possible application in different types of light emitting devices. $\text{SrAl}_2\text{O}_4:\text{Eu}^{2+},\text{Dy}^{3+}$ has emerged, in the past two decades, as a preferred phosphorescent green phosphor over traditional $\text{ZnS}:\text{Cu}$ for use in lighting. Compared to the $\text{ZnS}:\text{Cu}$ phosphor, $\text{SrAl}_2\text{O}_4:\text{Eu}^{2+},\text{Dy}^{3+}$ exhibits higher brightness and persistent phosphorescence without introducing radioisotopes, suggesting that it is safe and friendly to the environment. $\text{SrAl}_2\text{O}_4:\text{Eu}^{2+},\text{Dy}^{3+}$ can be used in construction materials to detect damages in bridges, low level escape system during general power failures, textile printing, clock watches, electronic dial plates and luminous paints [1, 2].

Photoluminescence and phosphorescence properties of the $\text{SrAl}_2\text{O}_4:\text{Eu}^{2+},\text{Dy}^{3+}$ phosphor have widely been investigated in the form of powders with particle sizes ranging from micron to nanometer scale. For many industrial and technological applications such as surface coatings and device fabrication it is also important to investigate the properties of this phosphor in the thin film form. Due to this demand, research interest in the growth and characterization of $\text{SrAl}_2\text{O}_4:\text{Eu}^{2+},\text{Dy}^{3+}$ thin films has grown significantly in the past few years. $\text{SrAl}_2\text{O}_4:\text{Eu}^{2+},\text{Dy}^{3+}$ thin films have been prepared by different techniques including RF sputtering and/or ion beam evaporation [3-8], and pulsed laser deposition (PLD) technique [9]. PLD is a versatile film growth technique with many advantages over other techniques. In this technique, a pulsed laser beam strikes a source material (target) producing a flash of evaporants (in the form of a plume) that deposit on the substrate producing a film with the composition usually identical to that of the target material. Different processing parameters such as background reactive gas pressure, substrate temperature, target-substrate distance,

laser energy and frequency can be varied in order to improve microstructure, particle morphology and optical properties of the films. In our previous results [10, 11] we reported on the influence of power and the number of pulses on the PL properties of laser ablated films. Films deposited at 400° C and highest number of pulses gave the brightest green emissions. In this chapter, the PLD technique was used to grow SrAl₂O₄:Eu²⁺,Dy³⁺ thin films by varying different processing parameters (namely, the pulse repetition rates, base pressures and substrate temperatures) with the aim of optimizing the photoluminescence intensity and decay times of the films. The substrate temperature range was 200-500° C, aimed at locating the more accurate optimum deposition temperature.

6.2 EXPERIMENTAL DETAILS

The PLD target was prepared by pressing, without a binder, a commercial SrAl₂O₄:Eu²⁺,Dy³⁺ powder from Phosphor Technology in the United Kingdom. The target was annealed in air at 600° C for 24 hours to remove water vapour and other incidental impurities adsorbed during preparation of the target. The target was deposited on ultrasonically degreased Si (100) substrates in a vacuum chamber using a 248 nm KrF excimer laser. The deposition was carried out at different pulse repetition rates (4-10 Hz), substrate temperatures (200 – 500° C), and base pressures (9.2×10^{-6} – 8.8×10^{-4} mbar). A summary of deposition parameters that show parameters that were varied versus those that were fixed is given in Table 6.1. The target-to-substrate distance was maintained at 6 cm. The films were analyzed by X-ray diffraction (XRD) (SIEMENS D5000 diffractometer), Rutherford backscattering spectroscopy (RBS), Atomic force microscopy (AFM) (Shimadzu, SPM-9600) and fluorescent spectroscopy (Carry Eclipse).

Table 6.1 Varied vs fixed parameters during film deposition

Varied parameter	Fixed parameter					
	Working atmosphere	Base pressure (mbar)	Working pressure (mbar)	Substrate temperature (°C)	No. of pulses	Laser energy density (J/cm ²)
Substrate temperature	Oxygen	9.25×10^{-6}	4.5×10^{-2}	-	12000	0.98
Base pressure	Base pressure	-	-	200 °C	8000	0.97
Repetition rate	Base pressure	6.01×10^{-6}	6.01×10^{-6}	200 °C	12000	1.05

6.3 RESULTS AND DISCUSSIONS

The XRD data were collected from all the films and were compared to the commercial $\text{SrAl}_2\text{O}_4:\text{Eu}^{2+},\text{Dy}^{3+}$ powder. Although the XRD patterns from the powder [not shown] were consistent with monoclinic phase of $\text{SrAl}_2\text{O}_4:\text{Eu}^{2+},\text{Dy}^{3+}$ as reported elsewhere [12], all the films were amorphous because of the fact that they were not annealed after deposition. This result is consistent with our high resolution transmission electron microscopy data published elsewhere [11]. The RBS spectra were recorded when the films were irradiated with 2 MeV $^4\text{He}^+$ ions. The shape of the spectra and the chemical elements were the same from all the films. The typical RBS spectrum, for the film deposited at 8 000 laser pulses, is shown in Figure 6.1. The smooth curve (red) represents the best-fit simulated using Rutherford universal manipulation program (RUMP). The energy peaks at ~ 0.7 , ~ 1.35 , ~ 1.65 eV are from O, Al and Sr respectively and are in agreement with the peak positions observed by Sengiku et al. [5]. The Eu^{2+} and Dy^{3+} energy peaks overlap each other at ~ 1.75 eV. The stoichiometry of the films ($\text{Sr}:\text{Al}:\text{O}$; $0.98:1.9:4 \approx 1:1.9:4.1$) was comparable to that of the commercial powder ($\text{Sr}:\text{Al}:\text{O}$; $1:2:4$). A homogeneous distribution of Sr, Al, and O was also confirmed by Auger electron spectroscopy depth profiles. The thicknesses of the films estimated from the RBS data were in the range of $0.2\text{-}0.7\ \mu\text{m}$.

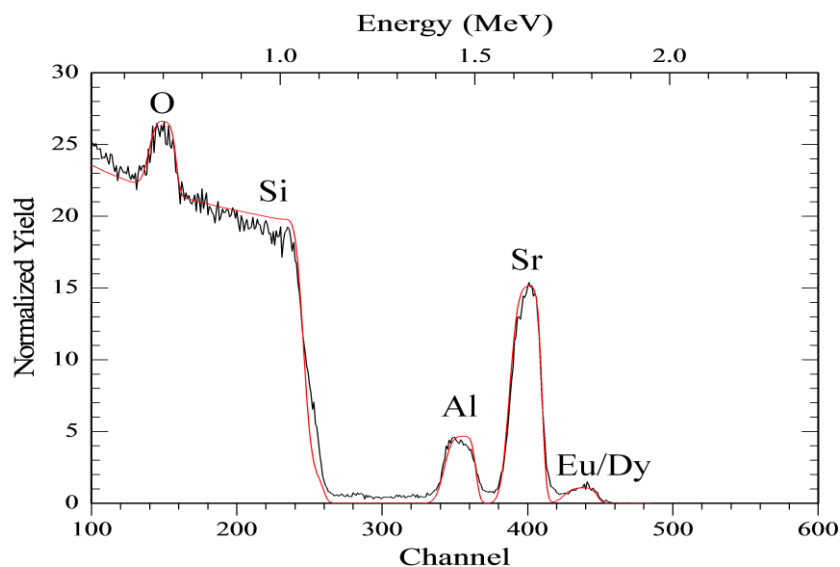
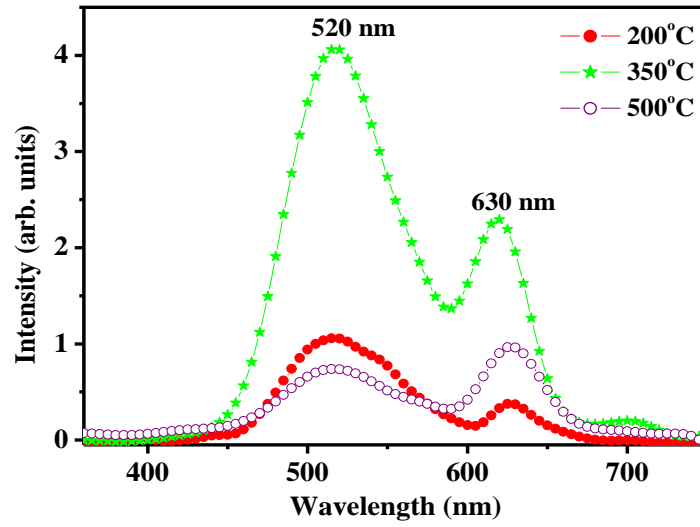


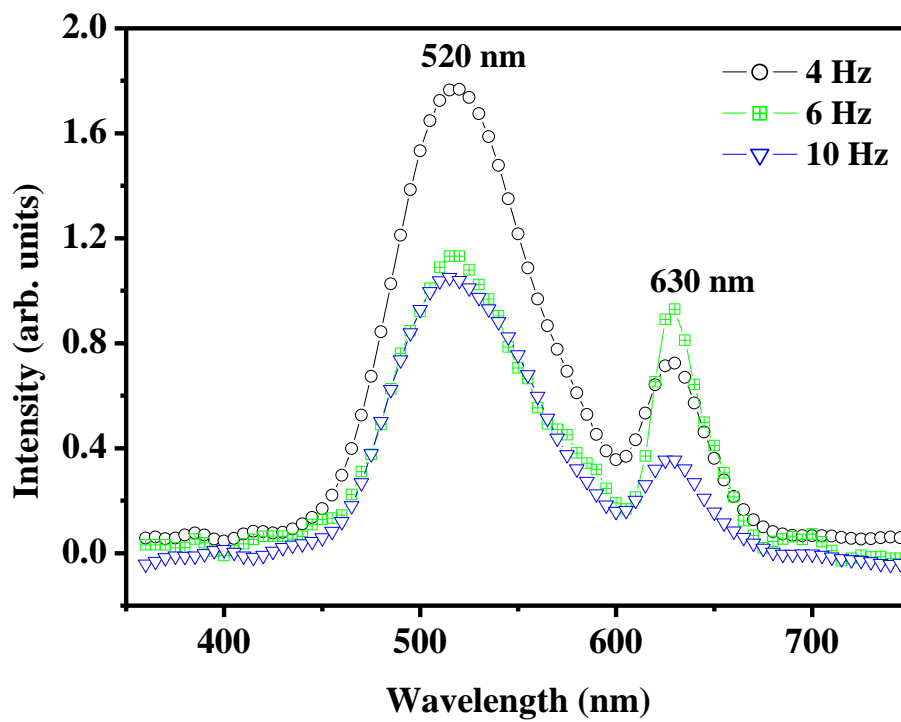
Figure 6.1. RBS spectrum of the film deposited with 8 000 laser pulses.

Photoluminescence (PL) emission (excited at 320 nm) spectra for the films deposited at different substrate temperatures, pulse repetition rates and base pressures, when all other parameters were fixed, are shown in figures 6.2(a)-(c). Generally, all the films showed stable green emission with a maximum at ~520 nm. This emission can be ascribed to the $4f^65d \rightarrow 4f^7(^8S_{7/2})$ transitions of the Eu^{2+} ions. A minor red emission was observed at 630 nm and this can be ascribed to the $^5D_0 \rightarrow ^7F_2$ transitions of unreduced Eu^{3+} ions, which is known to be always present in small amounts in the host matrix. Note that the optical transitions were not determined in this study and were assigned according to the literature cited [1-11]. The role of Dy^{3+} is to enhance green phosphorescence at 520 nm by increasing the number of electron traps and their trap depths in the vicinity of Eu^{2+} [13]. In Figures 6.2 (a)–(c) the maximum PL intensity from the 520 nm peak was observed from the films deposited at a substrate temperature of 350° C, a pulse repetition rate 4 Hz, and base pressure of 2.7×10^{-5} mbar. The peak intensities of the broad and line emissions at 520 and 630 nm, respectively, for the films deposited at 9.2×10^{-6} , 2.7×10^{-5} and 8.8×10^{-4} mbar [Fig. 6.2(d)] were almost the same.

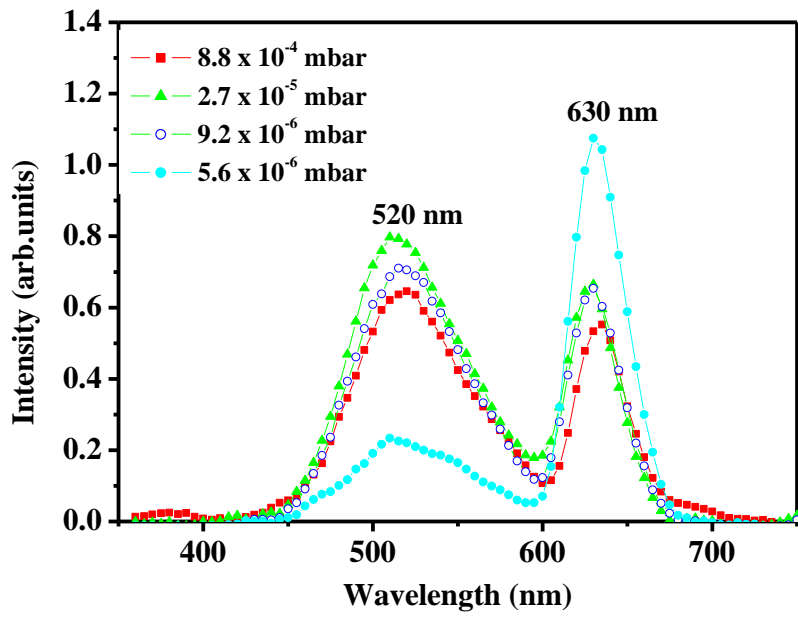
For the films deposited at the base pressure of 5.6×10^{-6} mbar (Fig 6.2(c)), the PL intensity of the 520 nm peak was almost quenched while the intensity of the 630 nm peak increased considerably. Based on these results, it is reasonable to conclude that Eu^{2+} ions were oxidized to Eu^{3+} in some of the films when deposition parameters were varied. The afterglow properties of the brightest films in each set of the deposition parameters of Figure 6.2 were compared to give results given in Figure 6.3. It is evident from the results of Figure 6.3 (a) that the oxidation does not only affect the status of $\text{SrAl}_2\text{O}_4:\text{Eu}^{2+}, \text{Dy}^{3+}$ as the green emitting phosphor, but it also reduces its phosphorescence lifetimes. These films were first excited by the monochromatic xenon lamp at 320 nm and the decay data was collected when the excitation was cut off. The decay (fast, medium and slow) components, were attributed to the short survival time of an electron in Eu^{2+} , intermediate and deep trap centres of Dy^{3+} , respectively, Zhong et al [14]. The traps may also arise from oxygen related defects [15]. The curves were fitted using the third order exponential decay equation given by equation 2.3 and the fitted data are listed in Table 6.2. Figure 6.3 (b) shows the fast, medium and slow decay constants in a logarithmic scale intensity for the film that was deposited at 350° C.



(a)

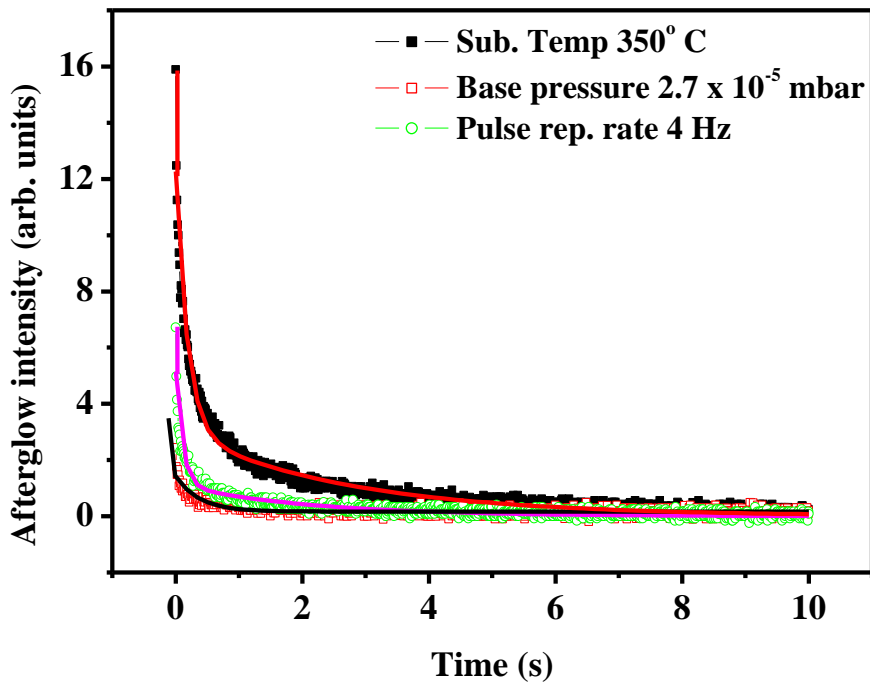


(b)



(c)

Figure 6.2. PL spectra of the films deposited at different (a) substrate temperatures, (c) pulse repetition rates, and (c) base pressures.



(a)

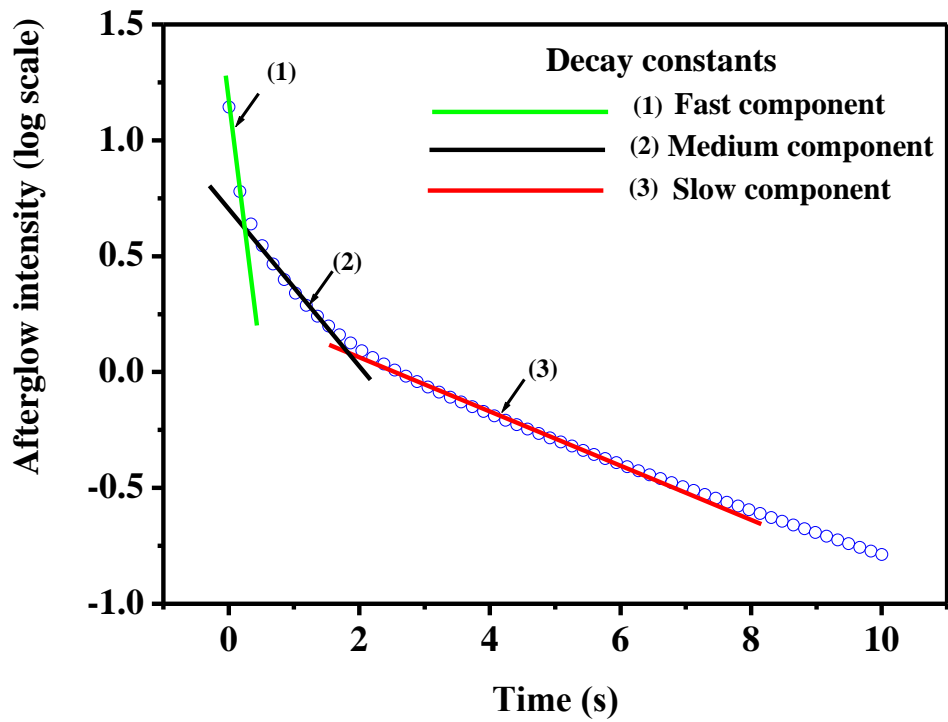


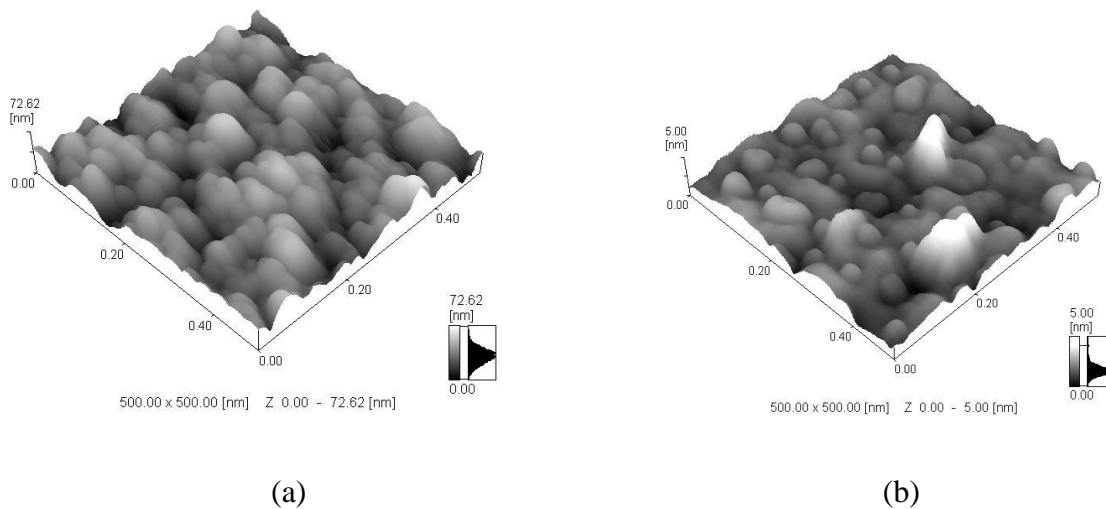
Figure 6.3. (a) Exponential decay curves for the films deposited at the substrate temperature of 350° C, 4 Hz pulse repetition rate, and 2.7 x 10⁻⁵ mbar (b) Logarithmic graph for the film deposited at the substrate temperature 350° C.

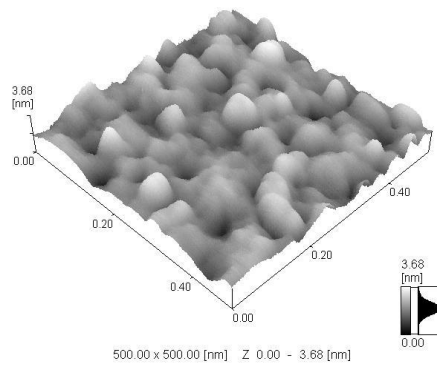
Table 6.2. Decay curves for films deposited at 350° C, 4 Hz pulse rate, and 16000 laser pulses.

Parameters	Half life times		
	τ_1 (s)	τ_2 (s)	τ_3 (s)
(a) 350° C	0.004 ± 0.001	0.375 ± 0.001	5.65 ± 0.05
(b) 4 Hz	0.003 ± 0.001	0.112 ± 0.001	2.18 ± 0.05
(c) 2.7 x 10 ⁻⁵ mbar	0.004 ± 0.001	0.019 ± 0.001	1.43 ± 0.05

The decay time values of the films were in order of seconds and were much shorter than the values obtained from the commercial powder (not shown) which lasted for several minutes after cutting off the excitation. The film that gave superior PL properties in Figure 6.2 is the one that gave higher initial afterglow intensity and higher decay constant times.

Figure 6.4 compares the AFM images of the same films to investigate the relationship between film morphologies of the three films in Figure 6.3 with their corresponding results of Figure 6.2. It can be observed that the film deposited at 350° C gave AFM images with better defined grains that the rest. It is well known that films with well-defined grains give rougher and brighter PL emissions than those with poorly-defined grains [10]. For that matter the AFM images compares very well with the PL results from Figure 6.2, whereby the films prepared at substrate temperature 350° C and base pressure 2.7×10^{-5} mbar gave the highest and the least PL intensities respectively.





(c)

Figure 6.4 AFM images of the films deposited at the substrate temperature of (a) 350° C (b) frequency 4 Hz; and (c) base pressure 2.5×10^{-5} mbar

6.4 CONCLUSIONS

Thin films of $\text{SrAl}_2\text{O}_4:\text{Eu}^{2+},\text{Dy}^{3+}$ phosphor were successfully grown by the pulsed laser deposition technique. The films were grown on Si (100) substrates and the structure, surface topography and photoluminescence properties were examined as functions of deposition parameters. The parameters which were varied during deposition include substrate temperature, pulse repetition rate and base pressure. All the films were amorphous and the surface morphology, roughness and the PL intensity were influenced by the deposition parameters. The green photoluminescence intensity of the films with well-defined grains (rougher) surfaces was higher than that of the films with poorly-defined (smoother) surfaces. There was evidence of oxidation of Eu^{2+} to Eu^{3+} in some of the films as confirmed by the PL data.

REFERENCES

1. T. Peng, H. Yang, X. Pu, B. Hu, Z. Jiang, *Chunhua, Mater. Lett.* **58**, (2004) 352.
2. Y. Zhang, Z. Chen, Z. Zhou, *J. Electrochem. Soc.* **153**, (2006) 86.
3. C. Chang, D. Mao, *Thin Solid Films*, **460** (2004) 48.
4. H. Suematsu, M. Sengiku, K. Kato, M. Mitome, K. Kimoto, Y. Matsui, W.H. Jiang, K. Yatsui, Y. Ogura, K. Kato, K. Shinbo and F. Kaneko. *Thin Solid Films*, **407**, (2002) 136.
5. M. Sengiku, Y. Oda and W. Jiang. *Jpn. J. Appl. Phys.* **140** 2B, (2001)1035.
6. K. Kato, Y. Ogura, M. Sengiku, K. Shinbo, F. Kaneko, Y. Oda and K. Yatsui. *Jpn. J. Appl. Phys.* **140** 2B, (2001)1038.
7. Tsutai, T. Kamimura, K. Kato, F. Kaneko, K. Shinbo, M. Ohta and T. Kawakami. *Electr. Eng. Jpn.* **132**, (2000) **7**.
8. K. Kato, I. Tsutai, T. Kamimura, F. Kaneko, K. Shinbo, M. Ohta and T. Kawakami. *J. Lumin.* **82**, (1999) 213.
9. Z. Fu, S. Zhou, Y. Yu, S. Zhang, *Chem. Phys. Lett.* **395**, (2004) 285.
10. P.D. Nsimama, O.M. Ntwaeaborwa, E. Coetsee, H.C. Swart, *Physica B: Physics of Condensed Matter.* **404**, (2009) 4489.
11. O.M. Ntwaeaborwa, P.D. Nsimama, J.T. Abiade, E. Coetsee, H.C. Swart, *Physica B: Physics of Condensed Matter.* **404**, (2009) 4436.
12. J.M. Ngaruiya, S. Nieuwoudt, O.M. Ntwaeaborwa, J.J. Terblans, H.C. Swart, *Mater. Lett.* **62**, (2008) 3192.
13. F. Clabau, X. Rocquefelte, S. Jobic, P. Deniard, M.-H. Whangbo, A. Garcia, T. Le Mercier, *Chem. Mater.* **17**, (2005), 3904-3912.
14. H. Zhong, X. Zeng, *S. Afr. J. Chem.* **61**, (2008) 22.
15. B.M Mothudi, O.M. Ntwaeaborwa, J.R Botha and H.C. Swart, *Physica B: Physics of Condensed Matter*, **404**, (2009) 4440

CHAPTER 7

THE EFFECT OF DIFFERENT GAS ATMOSPHERES ON THE LUMINESCENT PROPERTIES OF PULSED LASER ABLATED $\text{SrAl}_2\text{O}_4:\text{Eu}^{2+},\text{Dy}^{3+}$ THIN FILMS.

7.1 INTRODUCTION

Nanostructure materials are being actively explored nowadays because of their size induced novel characteristics and applications ranging from micro tips to optoelectronics. To exploit the optical properties of these materials and to meet the ever-increasing demands of energy, tremendous emphasis is being placed on alternate sources of energy conservation and low power driven display devices. Afterglow phosphors are materials that are readily excited by ambient lights and continuously radiate visible light for many hours at high brightness levels [1]. Recently, strontium aluminate phosphors activated by Eu^{2+} , Dy^{3+} ions have attracted a lot of attention since they show excellent properties such as high quantum efficiency, long persistence of phosphorescence and good chemical stability [2]. In most of the reported works [3-7], the $\text{SrAl}_2\text{O}_4:\text{Eu}^{2+},\text{Dy}^{3+}$ phosphors have been prepared and investigated in the form of powders. However, for various industrial applications such as device fabrication and surface coatings it is also important to investigate the performance of these phosphors in the form of thin films. Moreover, it is well documented that thin film phosphors have several advantages over powders, such as higher lateral resolution from smaller grains, better thermal stability, reduced out gassing, and better adhesion to solid substrates [8].

Amongst the techniques used to prepare luminescent thin films, PLD has several attractive features, including stoichiometric transfer of the target material, generation of quality plume of energetic species, hyper thermal reaction between the ablated cations and molecular O_2 in the ablation plasma and compatibility with background pressures ranging from UHV to 100 Pa [8]. The plasma fabricated during pulsed laser ablation is very energetic, and its mobility can be easily controlled by changing processing parameters [9]. The presence of a background gas in the chamber has a strong influence on the quality of the plasma produced

by the laser. The gas can modify the kinetic energy and the spatial distribution of the ejected species present in the plasma, and it may also induce compositional changes in the deposited films [10]. Plume collisions may also provide an increase in the vibrational energy of molecular species [11]. Thus, the gas affects the spatial distribution, the deposition rate, the energy and distribution of ablated particles thereby controlling the cluster formation, cluster size, cluster energy and particle distribution [11]. Dauscher et al. [12] investigated the influence of argon atmosphere on the microstructural properties of $\text{Ca}_x\text{CO}_4\text{Sb}_{12}$ films prepared by pulsed laser deposition and found that the films deposited in argon atmosphere were more delaminated than those prepared in vacuum. The report from Supab et al. [13] on laser ablated ZnO nanorods showed that the growth rate of nanostructures in oxygen atmosphere was slower than in argon atmosphere.

In the current chapter, we report on the influence of vacuum, Ar and O_2 atmospheres on the morphology, structure, photoluminescence (PL) and cathodoluminescence (CL) properties of pulsed laser deposited (PLD) $\text{SrAl}_2\text{O}_4:\text{Eu}^{2+},\text{Dy}^{3+}$ thin films. The annealing effects on the PL and structural properties of the thin films are discussed. A detailed report on the influence of working atmosphere on the properties of the pulsed laser deposited $\text{SrAl}_2\text{O}_4:\text{Eu}^{2+},\text{Dy}^{3+}$ thin films is presented.

7.2 EXPERIMENTAL DETAILS

The Si (100) wafers used as substrate were first cleaned as described elsewhere [14]. A commercial $\text{SrAl}_2\text{O}_4:\text{Eu}^{2+},\text{Dy}^{3+}$ phosphor powder obtained from Phosphor Technology (UK) was pressed without binders to prepare a pellet that was used as an ablation target. The target was annealed at 600°C for 24 hours in air to remove water vapour and other volatile compounds that might be trapped in the pellet before placing it on the target holder of the PLD system. The deposition chamber was evacuated to a base pressure of 8×10^{-6} mbar. The Lambda Physic 248 nm KrF excimer laser was used to ablate the phosphor pellet in vacuum, Ar (4.53×10^{-1} mbar) and O_2 (4.53×10^{-1} mbar) atmospheres. A Baratron Direct (Gas Independent) Pressure/Vacuum capacitance Manometer (1.33×10^{-2} - 2.07×10^5 mbar) was used for the high pressure measurements. The laser energy density, number of pulses and laser frequency were set to 0.74 J/cm^2 , 12000 and 10 Hz respectively. The substrate temperature was fixed at 200°C , and the target to substrate distance was 6 cm. The ablated area was 1 cm^2 . The Shimadzu Superscan SSX-550 system was used to collect the Scanning

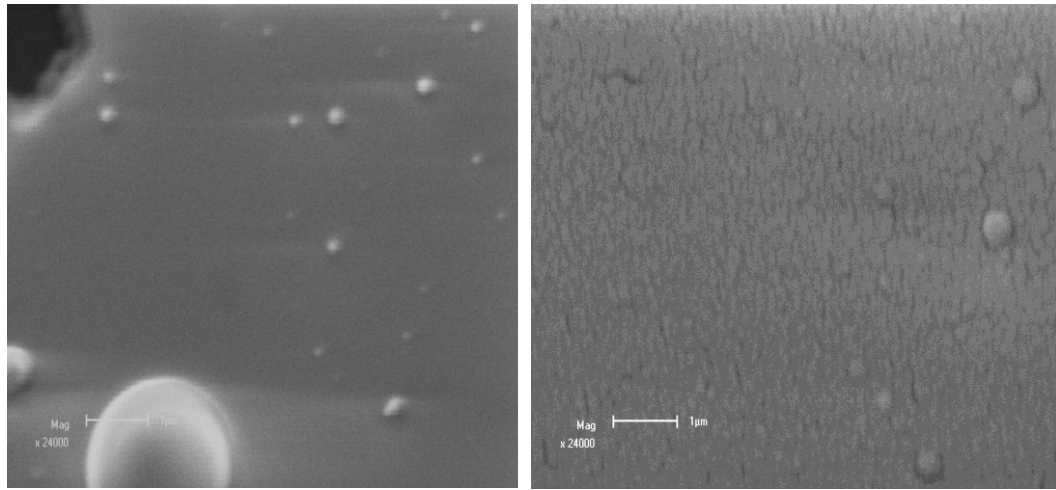
Electron Microscopy (SEM) micrographs, and Energy Dispersive X-ray Spectroscopy (EDS) data. Atomic Force Microscopy (AFM) micrographs were obtained from the Shimadzu SPM - 9600 model. X-ray diffraction data was collected by using a SIEMENS D5000 diffractometer using $\text{CuK}\alpha$ radiation of $\lambda = 1.5405$ nm. PL excitation and emission spectra were recorded using a Cary Eclipse fluorescence spectrophotometer (Model: LS 55) with a built-in xenon lamp and a grating to select a suitable wavelength for excitation. The excitation wavelength was 320 nm and the slit width was 20 nm. The afterglow curves for the films were also obtained with the Cary Eclipse spectrophotometer.

After, the thin films were characterized; they were annealed in vacuum at 800°C for 2h using a locally designed annealing system. The PL and XRD characterization of the films was repeated on the annealed films. Also the AES depth profile analysis was done on the annealed films and was done by argon sputtering with a 2 kV, 2 μA ion beam, 2x2 mm raster area, and sputter rate of 8.5 nm per min.

7.3 RESULTS AND DISCUSSION

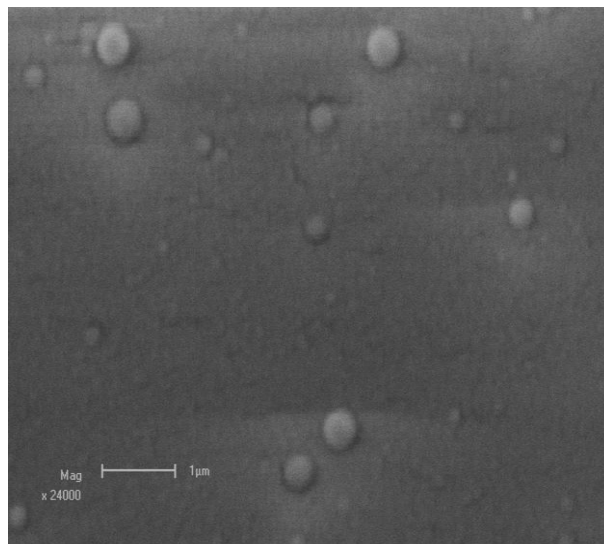
7.3.1 SEM RESULTS

Figure 7.1 shows the SEM pictures of the films prepared in different working atmospheres. The film deposited in vacuum, shown in Figure 7.1 (a), had a smooth surface with numerous bigger spherical particles. The film that was deposited in the O_2 atmosphere, in Figure 7.1(b), had a rougher surface with small cracks on the surface. The film deposited in Ar atmosphere (Figure 7.1(c)) had a much rougher surface packed with larger number of spherical particles than that of the film deposited in the O_2 atmosphere. The SEM pictures suggest that the surfaces of the films prepared in the gas atmosphere are much more rougher than that deposited in vacuum. The increase in surface roughness in the O_2 and Ar atmospheres is due to the enhanced particulate formation in the plume, which is a typical characteristic of high-pressure laser ablation [14]. AES depth profiles (not shown) indicated that the thicknesses of the films were 890 nm, 610 nm and 640 nm for the vacuum, O_2 and Ar films, respectively.



(a)

(b)



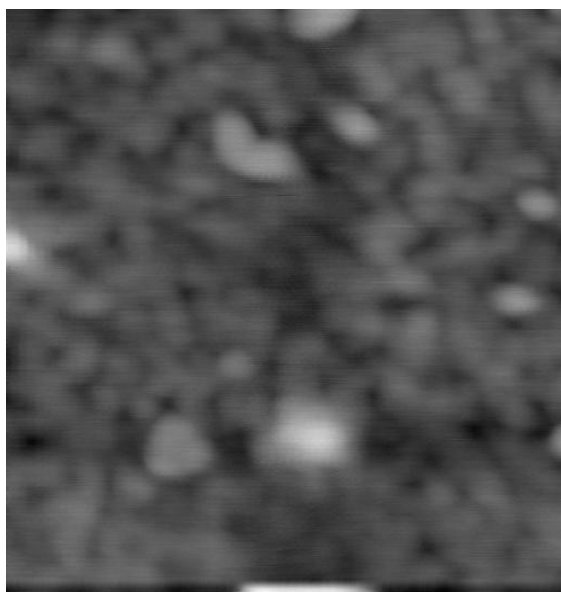
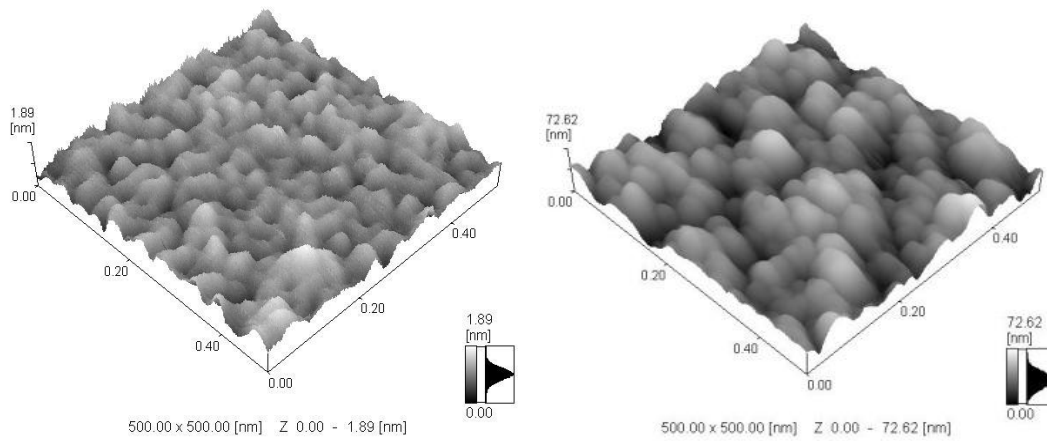
(c)

Figure 7.1. The SEM pictures for SrAl₂O₄:Eu²⁺,Dy³⁺ films deposited in (a) vacuum, (b) O₂ and (c) Ar atmospheres.

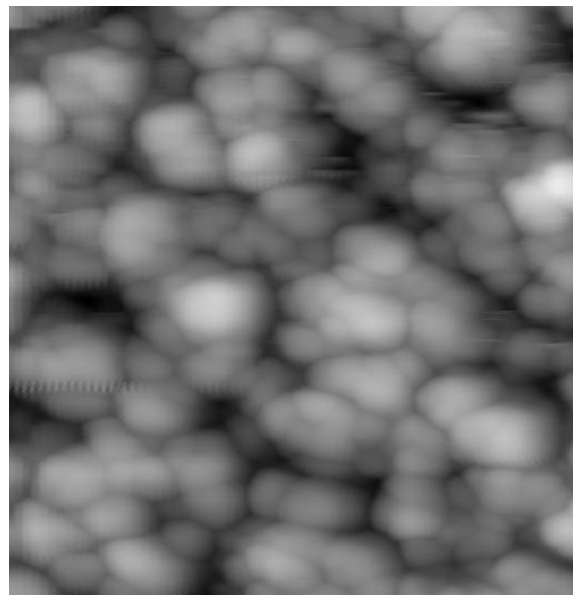
7.3.2 AFM RESULTS

Figure 7.2 shows the AFM pictures of the films deposited in the different atmospheres. The film prepared in vacuum is characterized by a poorly defined grains, possibly resulting from the destruction of the deposited film due to re-sputtering by the fast moving plume particles. Well defined boundaries of cylindrical grains are observed in the surface of the film deposited in the O₂ atmosphere, because the plume speed was somehow reduced by the gas molecules to allow a better nucleation process of the film particles on the substrate. The film that was deposited in the Ar atmosphere shows better defined grain boundaries with well-

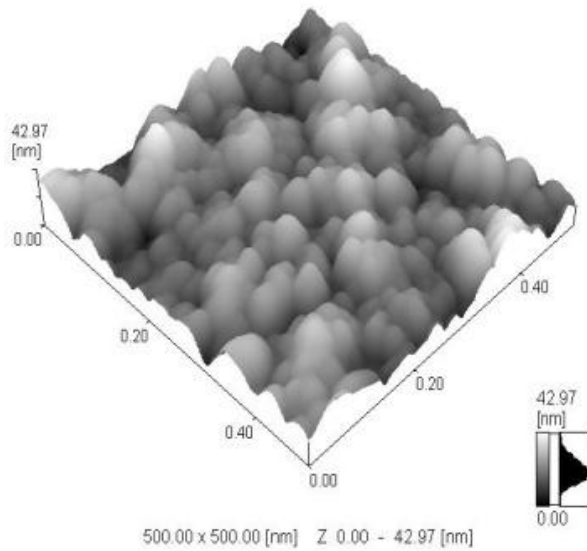
packed spherical nano (25-31 nm) grains. The 2-dimension high resolution AFM pictures show well packed grains for the films deposited in the O₂ and Ar atmospheres with relatively rougher surfaces than the one deposited in vacuum. The RMS values of the films were 3.63nm, 7.18nm and 7.20 nm for the vacuum, O₂ and Ar films, respectively.



(a)



(b)



(c)

Figure 7.2. The 3-dimension and 2-dimension high resolution AFM micrographs (same scale) of the PLD $\text{SrAl}_2\text{O}_4:\text{Eu}^{2+},\text{Dy}^{3+}$ thin films deposited in (a) vacuum, (b) O_2 and (c) Ar atmospheres.

The mean free path of the particles in a low ambient pressure is longer compared to the mean free path at higher ambient pressures. More collisions between the ultrafine particles (vaporized particles close to the target) at a higher ambient pressure can lead to nucleation

and growth into bigger particles before arrival at the substrate. In vacuum there are virtually no collisions between the particles before reaching the substrate. Longer residing time of the particles in the plume, as in the case at higher ambient pressures, may lead to bigger evenly distributed particles [16].

7.3.3 XRD RESULTS

The XRD results for the as-deposited thin films are shown in Figure 7.3. All the films were amorphous (or at least crystallites were too small to give rise to diffraction peaks). Similar structures were reported elsewhere [17, 18] for laser ablated $\text{SrAl}_2\text{O}_4:\text{Eu}^{2+},\text{Dy}^{3+}$ unannealed thin films.

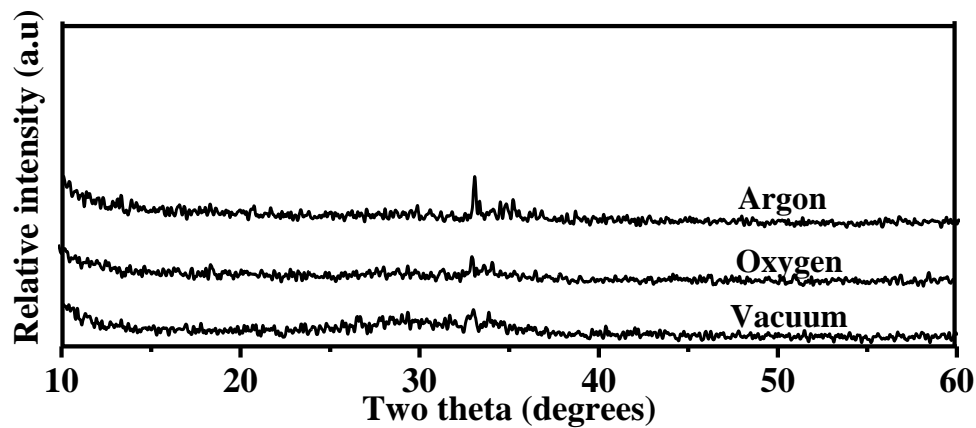


Figure 7.3. The XRD spectra of the $\text{SrAl}_2\text{O}_4:\text{Eu}^{2+},\text{Dy}^{3+}$ thin films deposited in different atmospheres.

No significant differences in the XRD patterns are observed from the three samples. The slight change in the noise level of the spectra in the 30 to 35 region was also obtained from the substrate and is therefore not from the thin film. Previous high resolution transmission microscopy (HRTEM) images [19] confirmed the amorphous structure of the thin film. The stoichiometry of the films was comparable to that of the commercial powder (Sr:Al:O-1:2:4) as determined with Rutherford backscattering spectroscopy (RBS) [20]. A homogeneous distribution of Sr, Al, and O was also confirmed by Auger electron spectroscopy depth profiles.

7.3.4 PHOTOLUMINESCENCE RESULTS

The room temperature PL results for the $\text{SrAl}_2\text{O}_4:\text{Eu}^{2+},\text{Dy}^{3+}$ films deposited using different atmospheres are shown in Figure 7.4. Both the emission and excitation spectra are shown. All the samples were excited at 320 nm using a monochromatized xenon lamp. The green emission peaks that were observed at 515 nm from all the films are ascribed to the $4f^65d^1 \rightarrow 4f^7$ transitions of Eu^{2+} [21]. The intensity of the unannealed film deposited in the Ar atmosphere was the highest followed by the one prepared in the O_2 atmosphere.

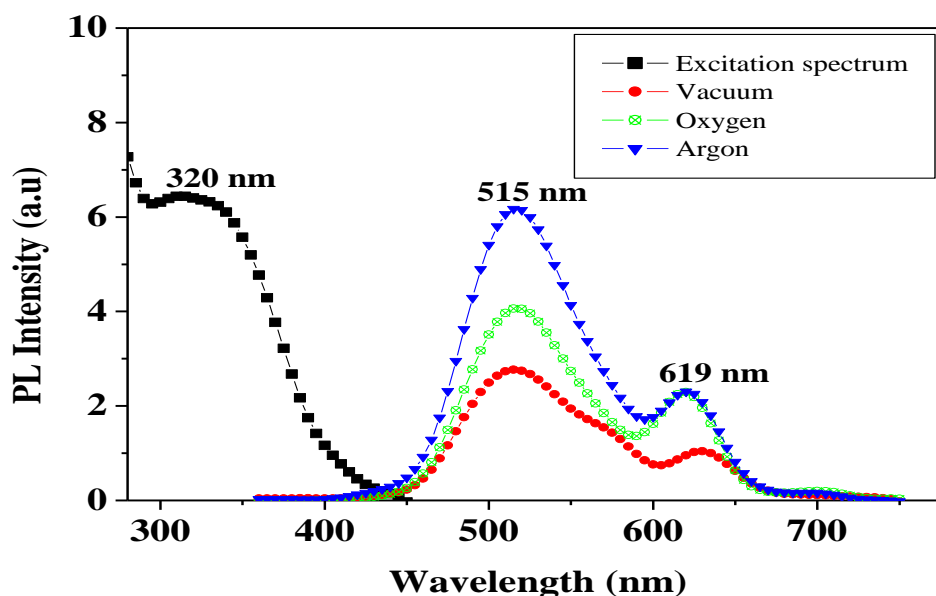


Figure 7.4. The excitation spectrum and emission spectra for PLD $\text{SrAl}_2\text{O}_4:\text{Eu}^{2+},\text{Dy}^{3+}$ thin films at different deposition atmospheres.

The lowest intensity was recorded from the unannealed film prepared in vacuum. Minor emission peaks associated with residual Eu^{3+} [22, 23] were also observed at 619 nm and 630 nm for the films deposited in the gas atmospheres and in vacuum respectively. The red emissions are coming from Eu^{3+} transitions [22]. A shoulder at 560 nm for the vacuum sample is also visible, which is ascribed to Eu^{2+} transitions. It should be mentioned that O_2 atmosphere should favour the stabilization of Eu^{3+} cations (oxidation), while vacuum should play the opposite role and favour Eu^{2+} (reduction). The relative ratios of the 515 nm to 619-630 nm peaks (Eu^{2+} to Eu^{3+} ratio) clearly support this observation. Zhang et al. [24] found that the oxygen contained in the BaSO_4 , which was the impurity in BaAl_4S_7 host material lead to poor blue-emitting performance. It was also found that although BaAl_2S_4 and BaAl_4S_7

are both member of the Ba-Al-S compounds, shifts in the PL emission peaks from the dopant Eu^{2+} occurred [24]. The presence of impurities affected the PL spectra of the film. A shift of the $\text{SrAl}_2\text{O}_4:\text{Eu}^{2+},\text{Dy}^{3+}$ main peaks toward shorter wavelengths was measured by Kim [25] for the phosphors prepared by the co-precipitation method, due to the quantum size effect of the nano-sized particles, compared with those produced by the solid-state reaction method. Luan et al. [26] investigated the influence of different Al/Sr ratios of strontium aluminate phosphors on the emission wavelength. They synthesized a series of strontium aluminate phosphors with different Al/Sr ratios from 1.0 to 12.0 by the solid-state method and found that the emission spectra of the samples shifted from a yellow green to blue-ultraviolet wavelengths with the increase of the Al/Sr ratios. Si-N can be introduced into $\text{Sr}_2\text{Al}_2\text{SiO}_7$ to replace Al-O [27]. Due to the presence of the nitrogen, the shrunk lattice becomes more rigid and the covalency of the $\text{Eu}_{\text{Sr}}-(\text{O}, \text{N})$ bond is increased. $\text{Sr}_2\text{Al}_{2x}\text{Si}_{1+x}\text{O}_{7-x}\text{N}_x:\text{Eu}^{2+}$ shows a broadband emission band from 480 to 565nm depending on both Eu concentration and x. With an increase in x, the emission band of Eu^{2+} shows a significant red shift.

For a high Eu concentration, a new excitation band was also found at about 460 nm. The dominant emission band alternatively changes from an intrinsic emission band (486 nm) associated with the 5d-4f transition of Eu^{2+} to another emission band (560 nm) originating from energy transfer of the Eu ions and/or an electron transition at different crystal-field components of the 5d state within a single Eu^{2+} ion [27]. Both the low-temperature product $\text{SrAl}_2\text{O}_4:\text{Eu}^{2+}\text{Dy}^{3+}$ and the high temperature product $\text{Sr}_4\text{Al}_{14}\text{O}_{25}:\text{Eu}^{2+}\text{Dy}^{3+}$ show photoluminescence peaking at 480 and 505 nm, respectively [28]. When compared to the powder obtained in conventional method, the nano-sized powders revealed a blue shift in the emission spectrum due to the decrease in grain size.

In a previous study it was found that the 630 nm peak due to the Eu^{3+} was much more pronounced than the 515-520 nm peak for the lower number of laser pulses (thinner films) [18]. With all these in mind it might be speculated at this stage that the shift in the emission wavelength of the Eu^{3+} emission might also be due to a combination of emission of the Eu^{3+} in E_2O_3 (due to oxidation in the oxygen atmosphere – although no proof of this was found) or other impurity species, due to the oxygen deposition atmosphere, and from $\text{SrAl}_2\text{O}_4:\text{Eu}$. The crystal field due to the amorphous versus crystalline structure must also be kept in mind. The nano size of the particles formed during deposition also can play a role. The higher PL intensities from the films deposited in the gas atmospheres can be ascribed to the films'

relatively rougher surface as observed from the AFM pictures in Figure 7.2. It is well known that rough surfaces increases the probability of light emission from the surface by limiting the chances of total internal reflection at the film-substrate interface [29].

7.3.5 LONG AFTERGLOW CHARACTERISTICS

Figure 7.5 shows the long afterglow (phosphorescence) characteristics of the thin films deposited in vacuum, O₂ and Ar atmospheres. Consistent with the PL data in Figure 7.4, the film prepared in Ar atmosphere has the highest initial intensity followed by the film prepared in the O₂ atmosphere. The phosphorescence of SrAl₂O₄:Eu²⁺,Dy³⁺ is believed to originate from the photo-oxidation of Eu²⁺ cation under UV-irradiation [19, 22]. According to this model, an electron from the 4f⁷ ground state is excited to the 4f⁶5d¹ level of Eu²⁺ followed by an electron capture from the valence band reducing Eu²⁺ to Eu⁺. The hole generated in the valence can migrate and be captured by Dy³⁺ converting it to Dy⁴⁺. Relaxation to the ground state, which is accompanied by green emission, is triggered by the thermo-activated promotion of an electron from the valence band to the first unoccupied levels of Dy⁴⁺ followed by a migration of the trapped hole to the photon-generated Eu⁺ cation [21].

The films were further characterized by the fast, intermediate and slow decays of the afterglow characteristics [17], since they are indicative of the different rates of decay for the films. The decay curves were fitted according to the equation (2.3) and gave decay constants listed in Table 7.1.

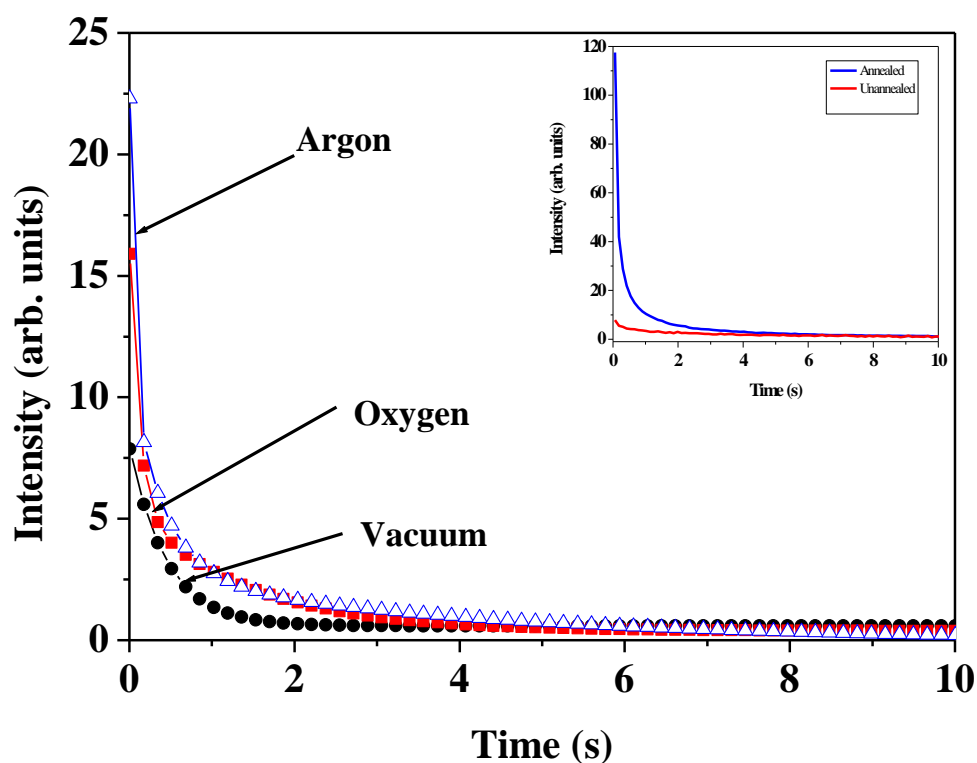


Figure 7.5. The afterglow curves for PLD SrAl₂O₄:Eu²⁺,Dy³⁺ thin films deposited at different atmospheres. The inset shows the comparison of the afterglow intensity of the annealed (800° C) and unannealed vacuum thin films.

Table 7.1. Decay constants for films deposited at the different deposition atmospheres

Working atmosphere	Decay Constants		
	τ_1 (s)	τ_2 (s)	τ_3 (s)
(a) Vacuum	0.0011 ± 0.0001	0.19065 ± 0.0001	3.04 ± 0.05
(b) Oxygen	0.0391 ± 0.0001	0.41957 ± 0.0001	3.75 ± 0.05
(c) Argon	0.0359 ± 0.0001	0.39535 ± 0.0001	3.85 ± 0.05
(d) Vacuum (A*)	0.0695 ± 0.0001	0.7261 ± 0.0001	10.12 ± 0.05

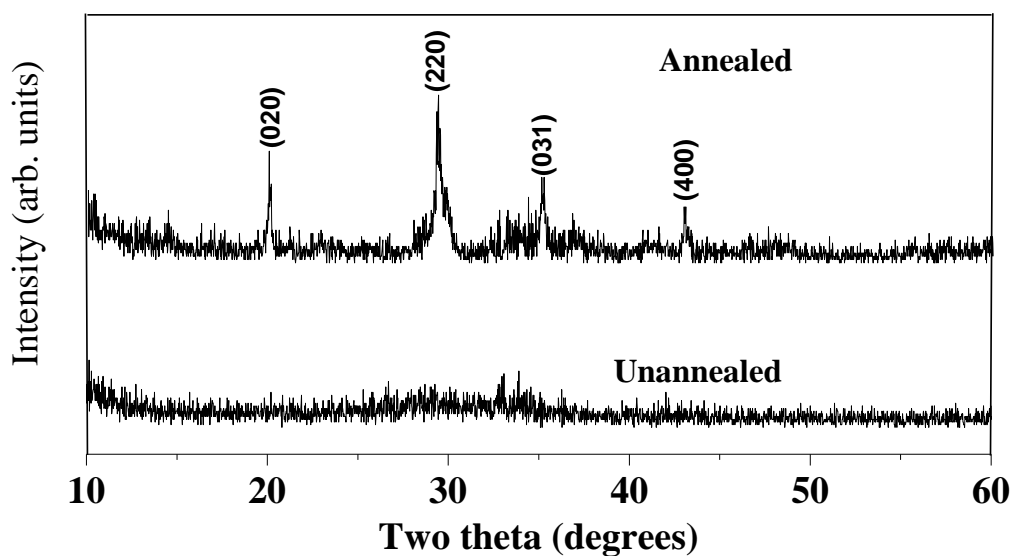
Where A* stands for annealed.

It is clear from Table 1 that the decay constants for the O₂ and Ar samples are longer than that of the vacuum sample. A further improvement in the decay constant was obtained for the

vacuum sample annealed at 800° C. It is well known that for long afterglow persistence, Eu^{2+} acts as a luminescent center and Dy^{3+} acts as trap levels which capture the free electrons, release the trapped holes and recombine with electrons, which accompanies luminescence. The emission lifetime will be influenced by the depth of the trap level and the trap types. According to these results the gas atmospheres did play a role in the trap level concentration and also in the possible trap types.

7.3.6 THE XRD AND PL RESULTS FOR THE ANNEALED FILM

The XRD results for the vacuum deposited unannealed and annealed (in vacuum at 800° C) films are shown in Figure 7.6 (a). It can be observed from the results that the annealed film had a monoclinic crystal structure, with common peaks of the standard SrAl_2O_4 (JCPDS 34-379) peaks as opposed to the amorphous structure of the unannealed film.



(a)

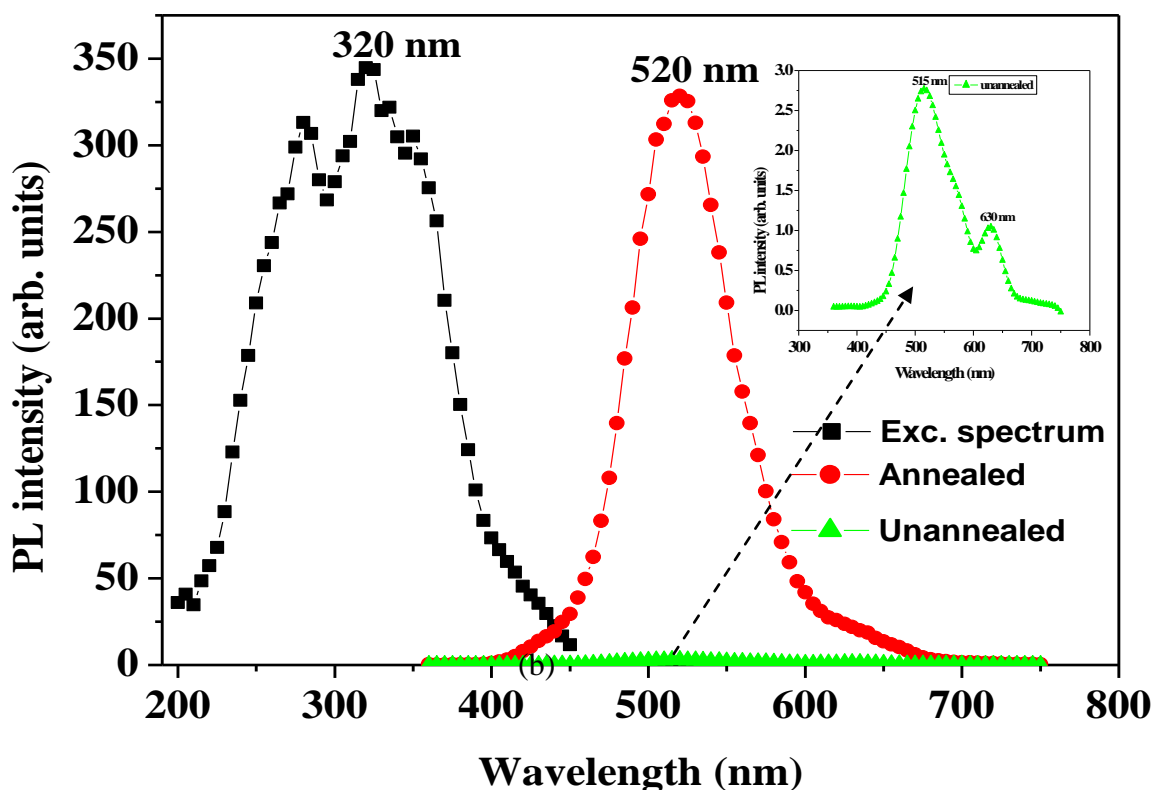


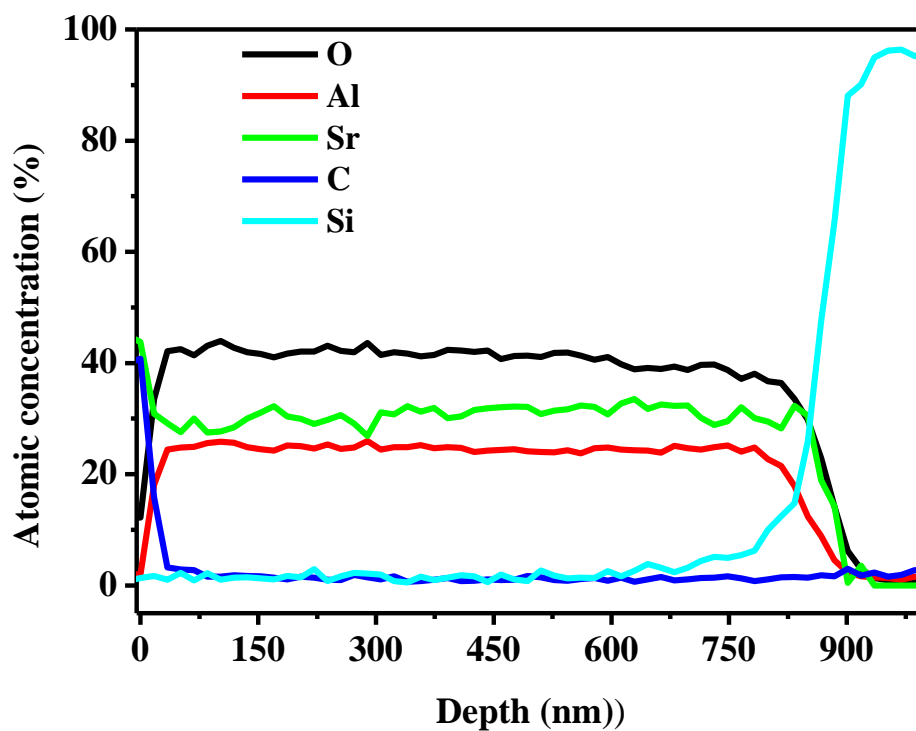
Figure 7.6. (a) The XRD and (b) PL results for the $\text{SrAl}_2\text{O}_4:\text{Eu}^{2+}, \text{Dy}^{3+}$ thin film deposited in vacuum before and after annealing at 800°C in vacuum.

The PL results for the unannealed and annealed film deposited in vacuum are shown in Figure 7.6 (b). The PL intensity of the film increased significantly after annealing in vacuum at 800°C . This increase in the PL intensity is attributed to improvement in crystallinity of the films upon annealing as observed in the XRD results in Figure 7.6 (a). The green emission peak from the annealed film was at 520 nm, while that of the unannealed film (inset graph) was at 515 nm. We attribute the red-shift on the peak position to the increase in grain particles resulting from improved crystallinity of the annealed film. The PL of the Ar and O_2 films annealed at 800°C were completely quenched (the explanation forms part of another study). The decay curve, Figure 7.5 inset, also shows an improvement in decay times as indicated in Table 7.1.

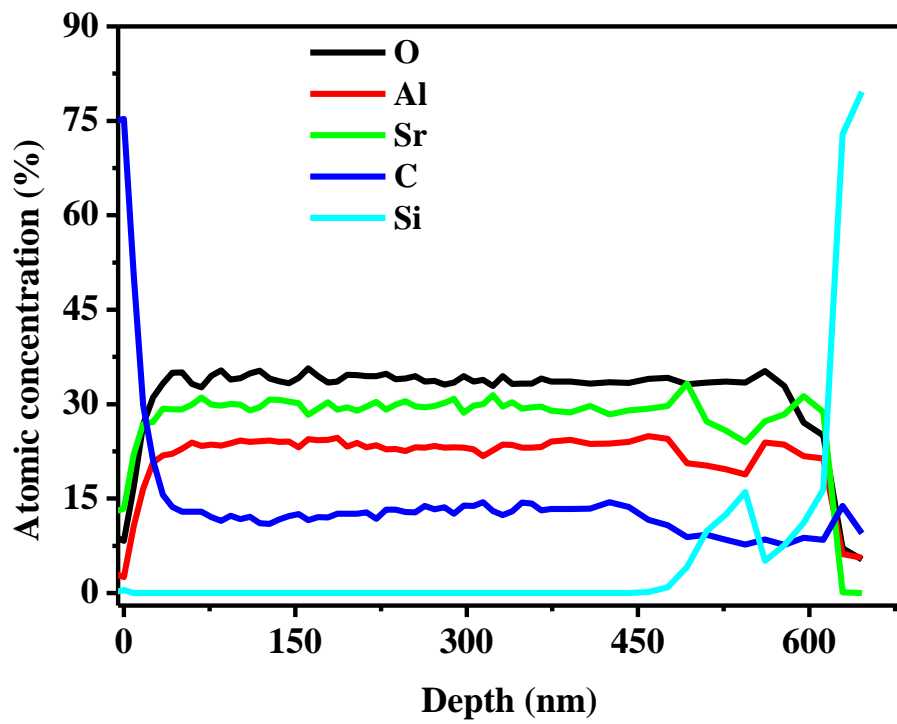
The depth profiles for the annealed films were determined to study the relation between their PL properties with the elemental depth profile analysis and the results are presented in the next section.

7.3.7 DEPTH PROFILE ANALYSIS

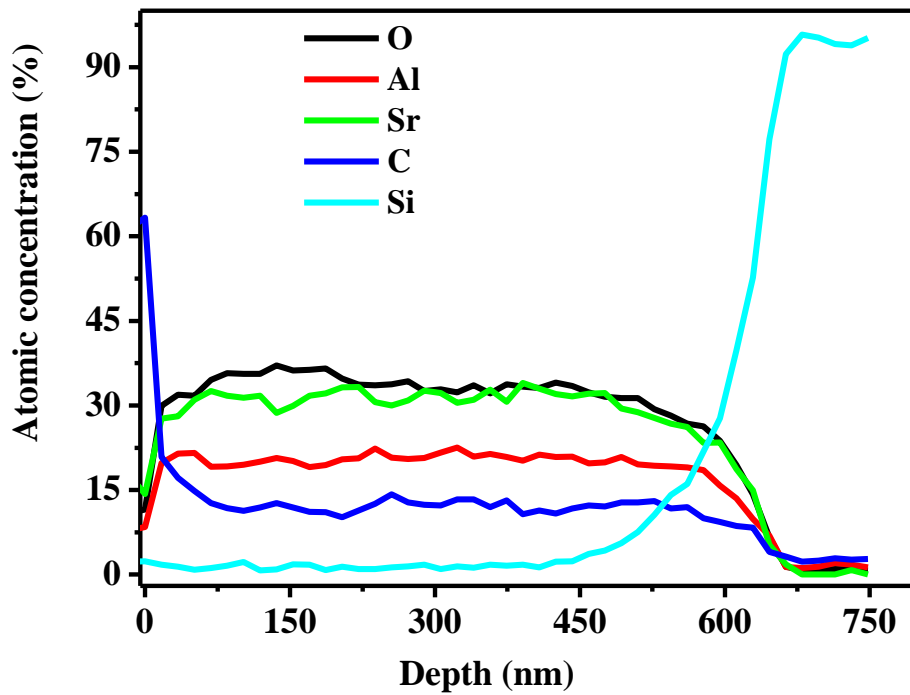
The depth profiles for the annealed thin films deposited in vacuum, oxygen and argon atmospheres are shown in Figure 7.7 (a)-(c). In all the depth profiles, the main elements in $\text{SrAl}_2\text{O}_4:\text{Eu}^{2+},\text{Dy}^{3+}$ material, i.e. Sr, Al and O were found. There were also an adventitious C and Si from the substrate. The dopants Eu, and Dy could not be detected due to their small amounts in the material. In all the cases, C decreased abruptly in the first 5 minutes before attaining a constant value. Another general case is that of having Si signal rising up sharply after reaching the substrate in the depth profile analysis. It can be observed from the results that, the depth profile of the vacuum annealed film Figure 7.7 (a) has a uniform elemental composition of all of the elements with time/depth.



(a)



(b)



(c)

Figure 7.7 The depth profiles for $\text{SrAl}_2\text{O}_4:\text{Eu}^{2+}, \text{Dy}^{3+}$ thin film phosphors prepared in (a) vacuum, (b) oxygen atmosphere and (c) argon atmospheres.

Both Si and C were at the bottom across the whole thickness. It is a different case with the annealed films deposited in the gas atmospheres, (Figure 7.7 (b)-(c)) whereby the carbon diffused into the films and its percentage composition remained at around 15 % throughout the rest of the time/depth. It can be proposed that the C diffusion in the annealed films deposited in the gas atmosphere is their rougher surfaces which captured more adventitious carbon than the smooth surface of the vacuum film. Upon annealing the C might have sank down and end up diffusing into the film. It is more likely that the diffusion of C into the film created luminescence killers, which lead to the poor PL properties of the annealed films deposited in the gas atmospheres. The depth profile of the film deposited in the oxygen atmosphere suggests the formation of another compound after nm, which calls for more investigations on the bonding in the films in future work.

7.4 CONCLUSION

Long afterglow $\text{SrAl}_2\text{O}_4:\text{Eu}^{2+},\text{Dy}^{3+}$ thin film phosphors were successfully ablated on Si (100) substrates by the pulsed laser deposition technique. Stable green emission, with a maximum peak at 515 nm associated with the $4f^65d^1 \rightarrow 4f^7$ transitions of Eu^{2+} was detected from all the unannealed films. The working atmosphere has a severe influence on the PL properties of the films. The unannealed films prepared in the gas atmospheres gave better PL and afterglow properties than the film prepared in vacuum. The unannealed films were all amorphous. The crystallinity and PL properties of the sample ablated in vacuum greatly improved after annealing in vacuum at 800°C , giving a very bright green emission. The depth profile results suggest that the poor PL properties of the annealed films deposited in the gas atmospheres is coming from the diffusion of C into the film. It can be proposed that the C diffusion in the annealed films deposited in the gas atmosphere is because of their rougher surfaces which captured more adventitious carbon than the smooth surface of the vacuum film. Upon annealing the C might have sank down and end up diffusing into the film.

REFERENCES

1. P. Sharma, D. Haranath, Harish Chander, Sukhivir Singh, Appl. Surf. Sci. **254** (2008) 4052.
2. S-D. Han, Krishan C. Singh, T-Y. Cho, H-S. Lee, D. Jakhar, J. P. Hulme, C-H. Han, J-D. Kim, II-S. Chun, J. Gwak, Journal of Luminescence **128** (2008) 301.
3. Y-L. Chang, H-I. Hsiang, M-T. Liang, Journal of Alloys and Compounds **461** (2008) 598.
4. P.D. Sarkisov, N.V. Popovich, A.G. Zhelnin, Glass and Ceramics **60** (2003) 9.
5. T. Peng, L. Huajun, H. Yang, J. Mater. Chem. & Phys **85** (2004) 68.
6. T. Peng, H. Yang, X. Pu, B. Hu, Z. Jian, C. Yan, Mater. Lett. **58** (2004) 352.
7. X. Li, Y. Qu, X. Xie, Z. Wang, R. Li, Mater. Lett. **60** (2006) 3673.
8. D.P. Norton, Materials Science and Engineering R **43** (2004) 139.
9. Z.G. Zhang, F. Zhou, X.Q. Wei, M. Liu, G. Sun, C.S. Chen, C.S. Xue, H.Z. Zhuang, B.Y. Man, Physica E **39** (2007) 253.
10. J. Gonzalo, R. Gómez San Román J. Errière, C.N. AFonso, R. Pérez Casero, Appl. Phys. A **66**, (1998) 487.
11. A. Bailini, P.M. Ossi, A. Rivolta, Appl. Surf. Sci. **253** (2007) 7682.
12. A. Dauscher, M. Puyet, B. Lenoir, D. Colceag, M. Dinescu, Appl. Phys. A **79** (2004) 1465.
13. S. Choopun, H.Tabata, T. Kawai, J. Cryst. Growth **274** (2005) 167.
14. E. Coetsee, H.C. Swart, J.J. Terblans, O.M. Ntwaeaborwa, K.T. Hillie, W.A. Jordaan, U. Buttnerk, Opt. Mater. **29** (2007) 1338.
15. S.S. Kim, B-T. Lee, Thin Solid Films **446** (2004) 307.
16. L. Chen, Particles generated by pulsed laser ablation, in D. B. Chrisey, G. K Hulber (Eds), Pulsed Laser Deposition of Thin Films, John Wiley & Sons, Inc, New York, (1994) chap. no. 6, p. 167 and 184.
17. K. Sato, S. Komuroa, T. Morikawa, H. Aizawa, T. Katsumata, S. Harako, X. Zhao, J. Cryst. Growth **275** (2005) 1137.
18. P.D. Nsimama, O.M. Ntwaeaborwa, E. Coetsee and H.C. Swart, Phys. B, Condens. Matter **404** (2009) 4489.
19. O.M. Ntwaeaborwa, P.D. Nsimama, S. Pitale, I. Nagpure, V. Kumar, E. Coetsee, J.J. Terblans, H.C. Swart, P.T. Sechogela, J. Vac. Sci. Technol. A **28** (2010) 901.

20. O.M. Ntwaeaborwa, P.D. Nsimama, J.T. Abiade, E. Coetsee, H.C. Swart, *Phys. B: Phys. Condens. Matter* **404** (2009) 4436.
21. D. Jia, *Optical Materials* **22** (2003) 65.
22. H. K. Yang, K.S. Shim, B.K. Moon, B.C. Choi, J.H. Jeong, S.S. Yi, J.H. Kim, *Thin Solid Films* **516** (2008) 5577.
23. F. Clabau, X. Rocquefelte, S. Jobic, P. Deniard, M-H. Whangbo, A. Garcia, T. Mercier, *Sol. State Sci.* **9** (2007) 608.
24. D. Zang, Y. Zhinong, W. Xue, T. Zhang, Z. Ding, W. Wang, *J. Rare Earths* **28** (2010) 185.
25. J.S. Kim, *J. of Ceram. Proc. Res.* **10** (2009) 443.
26. L. Luan, C.F. Guio, D.X. Huang, *J. Inorg. Mater.* **24** (2009) 53.
27. Y. Q. Li, N. Hirosaki, R-J. Xie, M. Mitomo, *Sci. Technol. Adv. Mater.* **8** (2007) 607.
28. C. Chang, Z. Yuan, D. Mao, *J. Alloys Compds.* **415** (2006) 220.
29. S.L. Jones, D Kumar, K-G Cho, R Singh, P.H. Holloway, *Displays* **19** (1999) 151.
30. J.M.Ngaruiya, S.Nieuwoudt, O.M.Ntwaeaborwa, J.J.Terblans, H.C.Swart, *Mater.Lett.* **62** (2008) 3192.
31. F. Clara, X. Rocquefelte, S. Jobic, P. Deniard, M.H. Whangbo, A. Garcia, T.L. Mercier, *Chem. Mater.* **17** (2005) 3909.
32. B.M. Mothudi, O.M. Ntwaeaborwa, J.R. Botha, H.C. Swart, *Phys. B:Condens. Matter* **404** (2009) 4440.

CHAPTER 8

ELEMENTAL COMPOSITION AND CATHODOLUMINESCENT STUDIES OF PULSED LASER ABLATED $\text{SrAl}_2\text{O}_4:\text{Eu}^{2+}, \text{Dy}^{3+}$ THIN FILMS

8.1 INTRODUCTION

Stuffed tridymite $\text{SrAl}_2\text{O}_4:\text{Eu}^{2+}, \text{Dy}^{3+}$ is a chemical stable phosphor applied extensively in the long-persistent phosphorescence [1]. It possesses better, safe, excellent photo-resistance, very bright and long-lasting photoluminescence with no radiation, which has resulted in an unexpectedly large field of applications such as luminous paints in highway, airport, buildings and ceramics products. In addition, it can also be applied in textile, dial plates of glow watch, warning signs, escape routes, etc [2]. Common techniques for preparing $\text{SrAl}_2\text{O}_4:\text{Eu}^{2+}, \text{Dy}^{3+}$ include the sol-gel [2], solid-state reaction [3], combustion [4], detonation [5], etc. Most of the reported works are on powder samples. However, thin film phosphors have several advantages over powders, such as higher lateral resolution from smaller grains, better thermal stability, reduced out gassing, and better adhesion to the solid surface [6]. Amongst the techniques used to prepare luminescent thin films, PLD has several attractive features, including stoichiometric transfer of the target material, generation of quality plume of energetic species, hyper thermal reaction between the ablated cations and molecular O_2 in the ablation plasma, and compatibility with background pressures ranging from UHV to 100 Pa [7].

The composition and chemical state of film surfaces and inter-faces strongly influence many natural properties (e.g., aerosols, particles, particulates, and mineral phases). For that matter, it is increasingly important to understand the full complexity of many natural systems and to characterize the complexities that can now be designed into a wide variety of synthetic structures, including nanometer-sized features [8]. There has been a continuing search for methods capable of determining composition and structure of complex heterogeneous materials, shallow surface layers, interfaces and heterogeneities on the microscopic (>100

nm) and nano-scale (<100 nm) level [9]. The beam analytical and the scanning probe techniques are valuable tools for understanding the complex architecture of nanoscale structures. A full understanding requires combined use of the two experimental approaches. Beam methods provide more specific analytical information while scanning probe methods are powerful as visualization/imaging tools [9]. Auger electron spectroscopy (AES) has become an almost indispensable tool for the chemical characterization of thin films, owing to its fairly sensitive detection of light and heavy elements with moderate matrix effects, its high spatial resolution in the sub-micrometer range, and its ease of combination with cathodoluminescence. Surface-related phenomena in $\text{SrAl}_2\text{O}_4:\text{Eu}^{2+},\text{Dy}^{3+}$ thin films is not well documented in the literature.

This chapter reports on the AES and EDS elemental surface analysis and cathodoluminescent studies of $\text{SrAl}_2\text{O}_4:\text{Eu}^{2+},\text{Dy}^{3+}$ thin films prepared by the pulsed laser deposition technique in different deposition atmospheres.

8.2 EXPERIMENTAL DETAILS

The $\text{SrAl}_2\text{O}_4:\text{Eu}^{2+},\text{Dy}^{3+}$ thin films were prepared as described in Section 7.2. The SEM images were captured by the PHI 700 Auger Nanoprobe. The vacuum annealed film was mounted on a carousel of the (AES) system, such that the surface normal was 30° from the Auger cylindrical mirror analyzer (CMA) axis, and 60° from the axis to a quartz view port for CL measurements. The PHI model 545 Auger electron spectrometer was used to monitor the surface composition during prolonged electron bombardment. The thin film was bombarded with a primary electron beam (2 keV, 10 μA) at an O_2 pressure of 1.3×10^{-6} mbar. Auger peak-to-peak height (APPH) data were collected with a single pass CMA in the derivative mode, using a peak-to-peak modulation of 4 eV for monitoring elemental composition changes. The AES and the CL data were collected simultaneously. The CL and AES degradation data were collected for about 19 hours (130 C/cm^2). The Shimadzu Superscan SSX-550 system was used to collect the Energy Dispersive x-ray Spectroscopy (EDS) data.

8.3 RESULTS AND DISCUSSION

8.3.1 THE SEM RESULTS

Figure 8.1 shows the SEM images for the annealed films deposited at different backgrounds, i.e. in vacuum (a), in oxygen (b) and in argon (c). The images are given in both the 2 μm and 0.500 μm marker scales. It can be observed from the results that the film that was deposited in vacuum is smooth and non-uniform as can be evidenced by the lower marker scale SEM images (a). The SEM images for the films deposited in the gas atmospheres shows rougher surfaces than that deposited in vacuum. The low resolution of the film deposited in oxygen (b) has a number of spherical phosphor particulates on the surface, contrary to the film deposited in the Ar atmosphere which has a surface free from particulates. From the 0.500 μm marker scales films (a) and (b) it is clear that film (c) deposited in argon atmosphere is slightly rougher than the other.

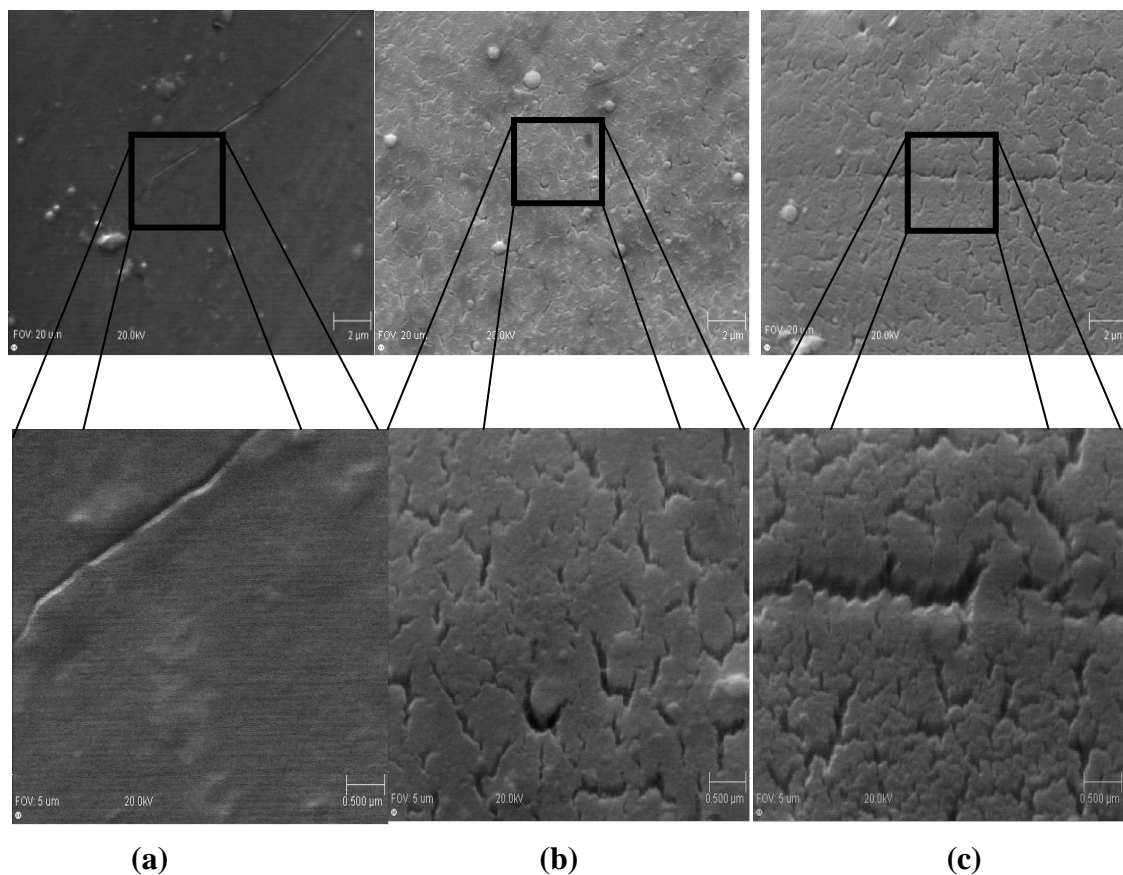


Figure 8.1. SEM images (2 and 0.500 μm marker scales) for $\text{SrAl}_2\text{O}_4:\text{Eu}^{2+}, \text{Dy}^{3+}$ thin films deposited in (a) Vacuum (b) O_2 and (c) Ar atmospheres.

This result is similar to that of Supab et al. [10] who found that the FE-SEM laser ablated ZnO images of films deposited in the argon atmosphere had rougher surfaces than that deposited in the oxygen counterpart.

The EDS result for the film deposited in the Ar atmosphere (the brightest film) is shown by Figure 8.2 with an inset representing the EDS spectrum in the range 0-2 KeV. It can be observed from the results that all the main elements of the $\text{SrAl}_2\text{O}_4:\text{Eu}^{2+},\text{Dy}^{3+}$, i.e. Sr, Al and O were identified in the film material. The Sr peak was embedded on the peak of Si. Similar EDS spectra were recorded from the other two films.

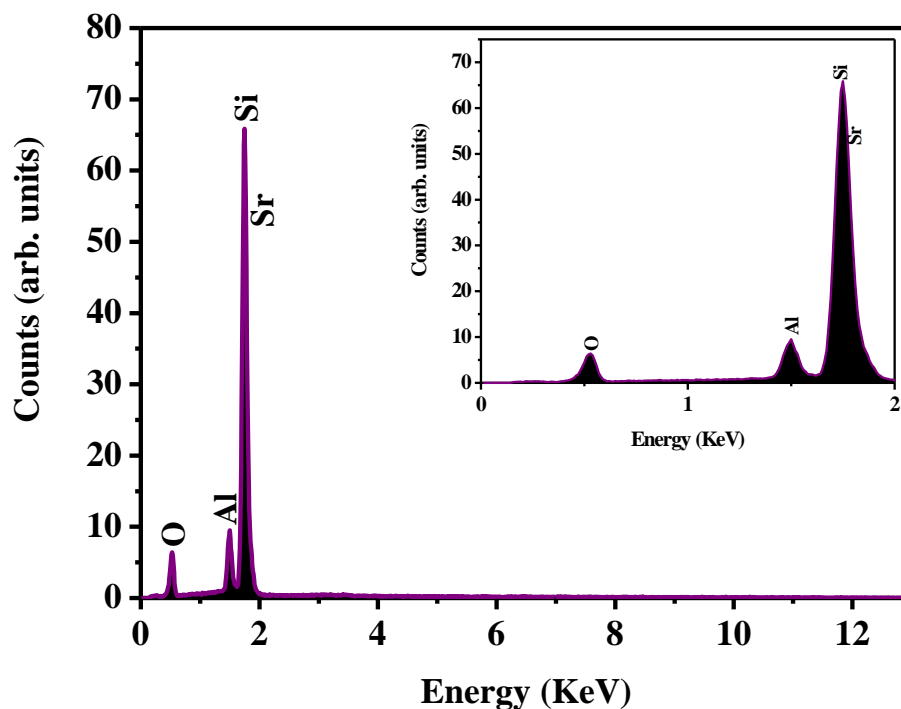


Figure 8.2: the EDS spectra for the $\text{SrAl}_2\text{O}_4:\text{Eu}^{2+},\text{Dy}^{3+}$ film deposited in the Ar atmosphere.

The dopant elements (Eu and Dy) could not be detected due to the small amounts present in the strontium aluminate material.

8.3.2 THE AES RESULTS

Figure 8.3 shows the AES spectra for the undegraded and degraded annealed vacuum deposited film. The surface of the undegraded film displayed a high concentration of C, coming from the atmospheric contamination. It is clear that the C was almost completely removed during the degradation process.

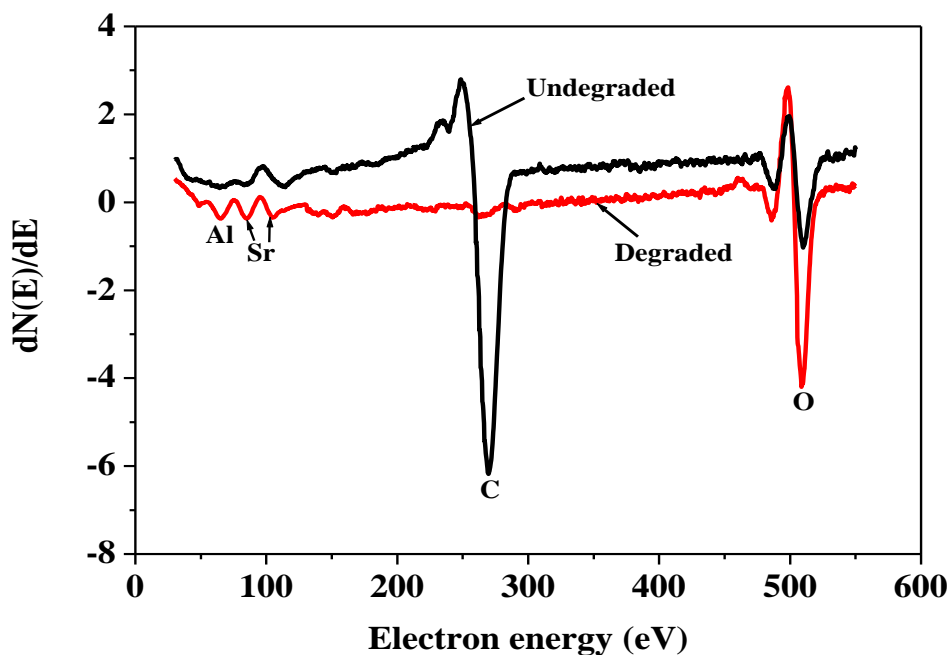


Figure 8.3. The Auger electron spectrum for the degraded and undegraded laser ablated $\text{SrAl}_2\text{O}_4:\text{Eu}^{2+}, \text{Dy}^{3+}$ film prepared in vacuum.

Electron stimulated surface chemical reactions (ESSCRs) took place during electron bombardment. During the ESSCR process, the electron beam dissociates the O_2 and other background species such as H_2O to atomic species which subsequently react with C to form volatile compounds (CO_x , CH_4 , etc.) [11]. During the removal of C from the surface the O peak increase considerably and the Al and Sr peaks become more visible. The O and the low energy Sr and Al peaks became more prominent after removal of the C. Figure 8.4 shows the variation of element/oxygen APPH ratios as a function of the electron dose at a base pressure of 1.33×10^{-6} mbar O_2 . The ratios were determined from the APPH versus electron bombardment time data. It is clear from the results that the ratios of Al and Sr APPHs to that of O increased slightly during removal of the C from the surface. The C/O ratio decreased

with the increase in the electron dose. The sharp decrease in the C/O APPH ratio was due to removal of C from the surface through volatile species as measured with a residual gas analyzer.

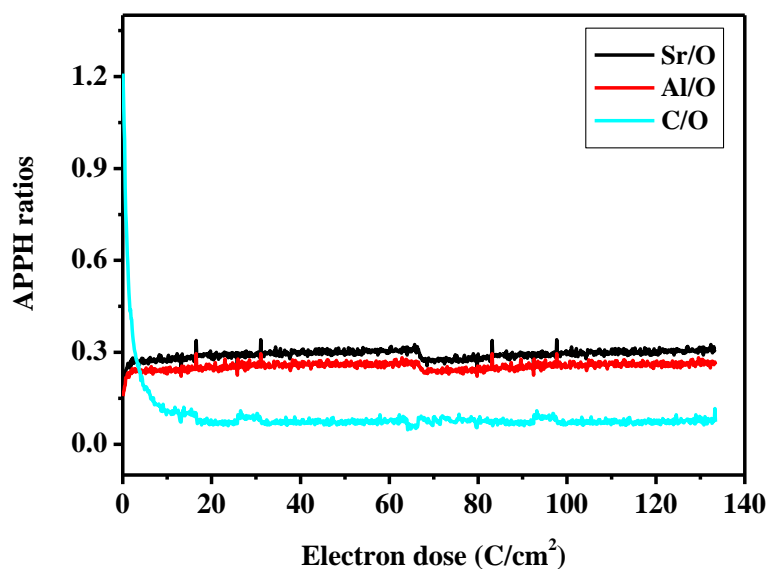
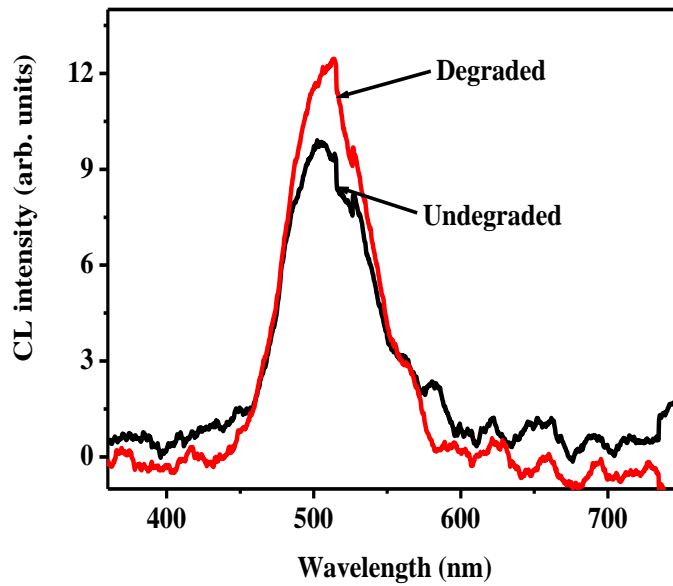


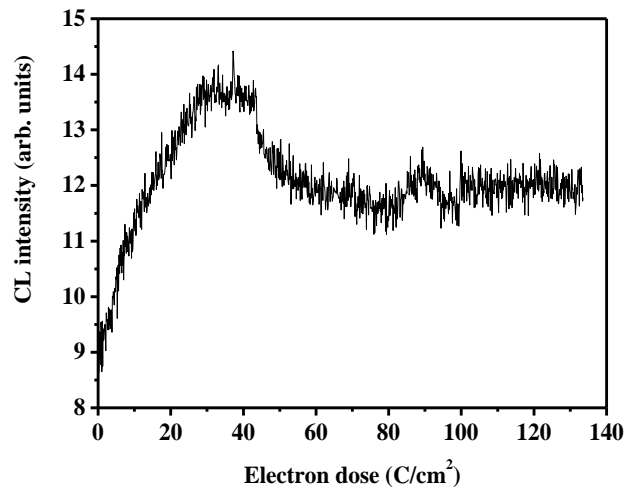
Figure 8.4. The variation of elements to oxygen APPH ratios for the $\text{SrAl}_2\text{O}_4:\text{Eu}^{2+},\text{Dy}^{3+}$ film deposited in vacuum.

8.3.3 CL RESULTS

The CL results for the annealed film prepared in vacuum are shown in Figures 8.5 (a) and (b). In both spectra, there is only one green emission peak at around 507 nm attributed to the $4f^65d^1 \rightarrow 4f^7 \text{Eu}^{2+}$ ion transitions. The CL intensity of the film after electron bombardment for almost 19 hours was higher than the undegraded film, Figure 8.5 (a). Figure 8.5 (b) shows the variation of the CL intensity as function of electron dose at 1.33×10^{-6} mbar O_2 . Initially, the CL intensity increased with the electron dose as the carbon layer from atmospheric contamination was removed from the film surface (if compared with APPH ratio of C/O, Figure 8.4). After reaching the maximum CL intensity value, it started decreasing with the further increase of the electron dose. The decrease in CL intensity with electron irradiation is due to the formation of a non-luminescent layer on the film surface as a result of electron stimulated surface chemical reaction (ESSCR) process.



(a)



(b)

Figure 8.4 (a). The CL intensity for the undegraded and degraded $\text{SrAl}_2\text{O}_4:\text{Eu}^{2+},\text{Dy}^{3+}$ film and (b) the variation of the CL intensity with the electron dose for the same film.

In our earlier work [12] we reported the formation of SrO and Al_2O_3 on the surface during the electron bombardment process. The vacuum annealed $\text{SrAl}_2\text{O}_4:\text{Eu}^{2+},\text{Dy}^{3+}$ thin film showed a high stability to the electron beam after stabilizing at about 12 units upon 19 hours (130 C/cm^2) of electron beam irradiation. This suggests the potentiality of this material to be used in electron beam operated devices.

8.4 CONCLUSION

The elemental surface analysis and cathodoluminescence of pulsed laser deposited $\text{SrAl}_2\text{O}_4:\text{Eu}^{2+},\text{Dy}^{3+}$ annealed thin films have successfully been done. The SEM images of annealed films deposited in the gas atmospheres gave rougher surfaces than the vacuum annealed film. Both the EDS and AES elemental composition results gave the main elements of strontium aluminate. The degraded $\text{SrAl}_2\text{O}_4:\text{Eu}^{2+},\text{Dy}^{3+}$ thin films had very low C and higher O_2 concentration as a result of the ESSCR process. In the APPH ratios versus electron dose results, there were a decrease in C/O and an increase in Sr/O and Al/O ratios with an increase in the electron dose. The C was removed from the film as volatile species as a result of the ESSCR process. The CL intensity of the annealed film was very stable on further electron bombardment. The $\text{SrAl}_2\text{O}_4:\text{Eu}^{2+},\text{Dy}^{3+}$ material can be considered to be one of the potential candidates for electron beam operating device application based on its high stability to the electron bombardment.

REFERENCES

1. Y-L. Chang, H-I. Hsiang, M-T. Liang, *J. of Alloys and Comp.* **461** (2008) 598.
2. T. Peng, L. Huajun, H. Yang, *J. Mater. Chem. & Phys* **85** (2004) 68.
3. P.D. Sarkisov, N.V. Popovich, A.G. Zhelnin, *Glass and Ceramics* **60** (2003) 9.
4. T. Peng, H. Yang, X. Pu, B. Hu, Z. Jian, C. Yan, *Mater. Lett.* **58** (2004) 352.
5. X. Li, Y. Qu, X. Xie, Z. Wang, R. Li, *Mater. Lett.* **60** (2006) 3673.
6. J.S. BAe, K.S. Shim, S.B. Kim, J.H. Jeong, S.S. Yi, J.C. Park, *J. Cryst. Growth* **264** (2004) 290.
7. D.P. Norton, *Materials Science and Engineering R* **43** (2004) 139.
8. D.R. Baer, A.S. Lea, J.D. Geller, J.S. Hammond, L. Kover, C.J. Powell, M.P. Seah, M. Suzuki, J.F.Watts, J.Wolstenholme, *J. Electron Spectros. & Relat. Phenom.* **176** (2010) 80.
9. F. Adams, L. Van Vaeck, R. Barrett, *Spectrochimica Acta Part B* **60** (2005) 13.
10. S. Choopun, H. Tabata, T. Kawai, *J. of Cryst. Growth* **274** (2005) 167.
11. H. C. Swart, T. A. Trottier, J. S. Sebastian, S. L. Jones, P. H. Holloway, *J. Appl. Phys.* **83** (1998) 4578.
12. H.C. Swart, E. Coetzee, J.J. Terblans, O.M. Ntwaeaborwa, P.D. Nsimama, F.B. Dejene and J.J. Dolo, *J. Appl. Phys. A*, doi:10.1007/s00339-010r-r5915-6.

CHAPTER 9

AUGER ELECTRON/X-RAY PHOTOELECTRON AND CATHODOLUMINESCENT SPECTROSCOPIC STUDIES OF PULSED LASER ABLATED $\text{SrAl}_2\text{O}_4:\text{Eu}^{2+}, \text{Dy}^{3+}$ THIN FILMS

9.1 INTRODUCTION

For persistent luminescence, alkaline earth aluminates (with a general formula MAl_2O_4 , where $\text{M} = \text{Ba}, \text{Ca}$ or Sr) co-doped with divalent europium (Eu^{2+}) and trivalent dysprosium (Dy^{3+}) ions are by far the most studied phosphorescent materials in the past decade. In most case, these materials give bright blue-green phosphorescence with an afterglow decay time lasting for minutes-hours. In the case of green phosphorescence, SrAl_2O_4 has emerged as the most preferred host for Eu^{2+} and Dy^{3+} ions. A ground breaking record of the afterglow decay time exceeding 30 hours from the green-emitting $\text{SrAl}_2\text{O}_4:\text{Eu}^{2+}, \text{Dy}^{3+}$ phosphor was reported by Matsuzawa et al. [1] and Katsumata et al. [2]. Unlike traditional sulphide phosphors, persistent afterglow from the $\text{SrAl}_2\text{O}_4:\text{Eu}^{2+}, \text{Dy}^{3+}$ phosphor could be achieved without incorporation of radioactive isotopes. It therefore shows that this phosphor does not only exhibit high brightness and long afterglow but it is also safe for the environment. In addition, $\text{SrAl}_2\text{O}_4:\text{Eu}^{2+}, \text{Dy}^{3+}$ has been reported to be more stable, chemically, than sulphide phosphors.

On the basis of closeness in ionic radii, Eu^{2+} ions are expected to occupy Sr^{2+} in the SrAl_2O_4 matrix. Photoluminescence data from $\text{SrAl}_2\text{O}_4:\text{Eu}^{2+}, \text{Dy}^{3+}$ showed that there are two emission peaks associated with Eu^{2+} transitions. The most intense peak was observed at $\sim 520 - 530$ nm and the second less intense peak observed only at low temperatures (below room temperature) was found to be located at $\sim 545-580$ nm. Ngaruiya et al [3] observed two emission peaks from cathodoluminescence data of commercial $\text{SrAl}_2\text{O}_4:\text{Eu}^{2+}, \text{Dy}^{3+}$ powder phosphor collected at room temperature in an ultra high vacuum (UHV) chamber. The two peaks were attributed to Eu^{2+} occupying two different crystallographic sites of Sr^{2+} . The two sites are believed to be chemically indistinguishable which makes it difficult to establish the

preferred occupation of any of the site to the other making it difficult to assign the two peaks in respect to these sites. For a better understanding of the correlation between the structure and luminescent properties, a multidisciplinary investigation is needed. The aim of this study was therefore to combine Auger/x-ray photoelectron and cathodoluminescent spectroscopic investigations in order to determine the correlation between structure and luminescent properties. The Auger and cathodoluminescent study conducted on the commercial $\text{SrAl}_2\text{O}_4:\text{Eu}^{2+},\text{Dy}^{3+}$ powder phosphor showed that the CL intensity was quenched within 5 seconds of electron irradiation suggesting that the powders were highly charging [3]. In the case of thin films, bright and stable green cathodoluminescence was observed at ~ 521 nm when the films were irradiated with a beam of electrons in the UHV chamber [4]. The Auger and the CL measurements were taken simultaneously during the electron beam irradiation, and the x-ray photoelectron measurements were taken from the films before and after irradiation. The CL intensity was shown to degrade at different rates when the measurements were taken at different oxygen pressures. The x-ray photoelectron analyses of the electron beam irradiated/degraded and unirradiated/undegraded films were consistent with the speculation that there are two different crystallographic sites of Sr^{2+} . In addition, the new oxide layer that could have contributed to the CL intensity degradation was formed on the film surfaces. Among other things, these films were evaluated for industrial and technological applications such as surface coatings and device fabrications.

This chapter reports on the AES, CL, CL degradation and XPS results of $\text{SrAl}_2\text{O}_4:\text{Eu}^{2+},\text{Dy}^{3+}$ thin films.

9.2 EXPERIMENTAL DETAILS

$\text{SrAl}_2\text{O}_4:\text{Eu}^{2+},\text{Dy}^{3+}$ thin films were prepared by using the pulsed laser deposition technique as described elsewhere [4]. The $\text{SrAl}_2\text{O}_4:\text{Eu}^{2+},\text{Dy}^{3+}$ was deposited in vacuum at a pressure of 10^{-6} Torr, substrate temperature of 200°C , frequency of 8 Hz and fluency of $1.2 \pm 0.2\text{ J cm}^{-2}$. A Lambda Physic 248 nm KrF excimer laser was used to ablate the phosphor pellet. A total number of 8000 pulses were used to ablate the thin films. The films were mounted on a carousel of the Auger electron spectroscopy (AES) system, such that the surface normal was 30° from the Auger cylindrical mirror analyzer (CMA) axis, and 60° from the axis to a quartz view port for luminescence measurement. The CL and Auger data were collected using the

same primary electron beam of 2 keV and 10 μA (730 μm diameter beam, 2.4 mA/cm^2 current density). The electron irradiation during the AES and CL data collection was prolonged for 14 hours. The data was collected either at base pressure of 3.6×10^{-9} Torr or after backfilling with oxygen gas to 1×10^{-7} Torr and 1×10^{-6} Torr. The Auger peak-to-peak height (APPH) data were collected with a single pass CMA in the derivative mode, using a peak-to-peak modulation of 4 eV for monitoring elemental composition changes. Data for the CL measurements were collected via an optical fiber set attached to one of the ports of the UHV chamber and a computer. The Ocean Optics S2000 spectrometer type with OOI Base32 computer software was employed for the CL data collection. The XPS data for the undegraded and degraded films were collected by using the PHI 5000 XPS Versa probe (monochromatic $\text{AlK}\alpha$ lines). A dark spot on the SXI (Secondary X-ray Image) clearly pointed out the degraded area for the XPS analyses. The 100 μm diameter, 25 W, 15 W, 15 KV energy X-ray beam was used to analyse the Sr 3d, O1s and Al 3d binding energy peaks (pass energy 11.75 eV, analyser resolution ≤ 0.5 eV). XPS measurements were done in the middle of the degraded spot as well as on the undegraded area. The possible chemical states were identified with the Multipack version 8.2C computer software [5] by using Gaussian-Lorentz fits. Crystal structures were drawn with the Diamond software [6].

9.3 RESULTS AND DISCUSSION

9.3.1 THE AUGER ELECTRON SPECTROSCOPY (AES) RESULTS

The AES spectra for films degraded at the three different pressures showed similar trends. The AES spectra in Figure 9.1 are representatives of the undegraded and degraded spots. The degraded spectrum was obtained on the spot degraded for 93 C/cm^2 at 1×10^{-6} Torr O_2 . The C measured on the undegraded spot was possibly coming from atmospheric contamination during handling, exposure to ambient and cracking of organics and /or hydrocarbon gases on the surface by the electron beam [7]. It is clear that C was completely removed from the surface after 14 hours of electron beam irradiation. It is most likely that C desorbed from the surface after reacting with volatile atomic species to form gaseous compounds such as CO_x or CH_4 . The O peak, however, increased during the electron bombardment indicating that an oxide layer was formed on the surface. A small shift of the O Auger peak from 2-3 eV indicates that the surface was charging [8] during prolonged electron bombardment.

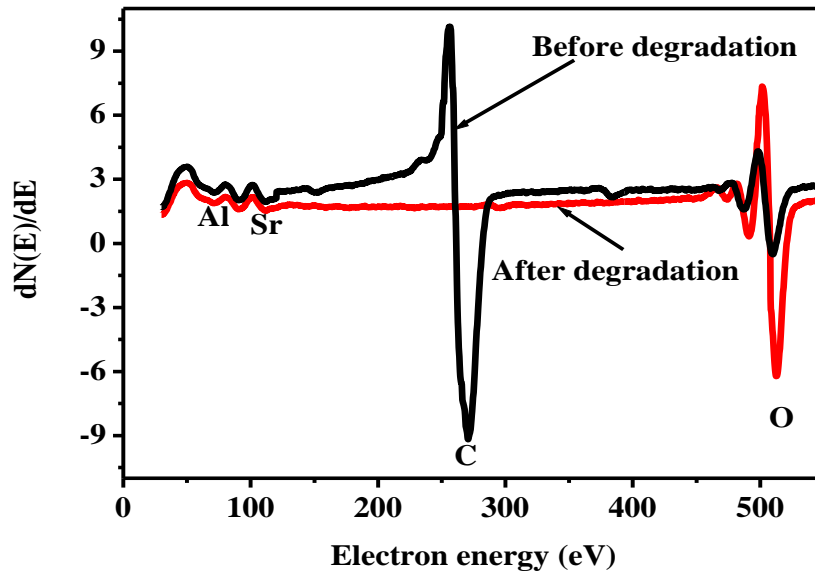
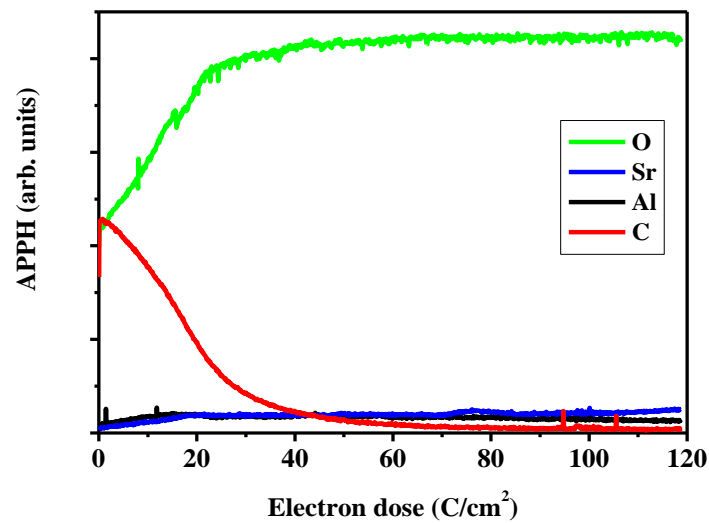
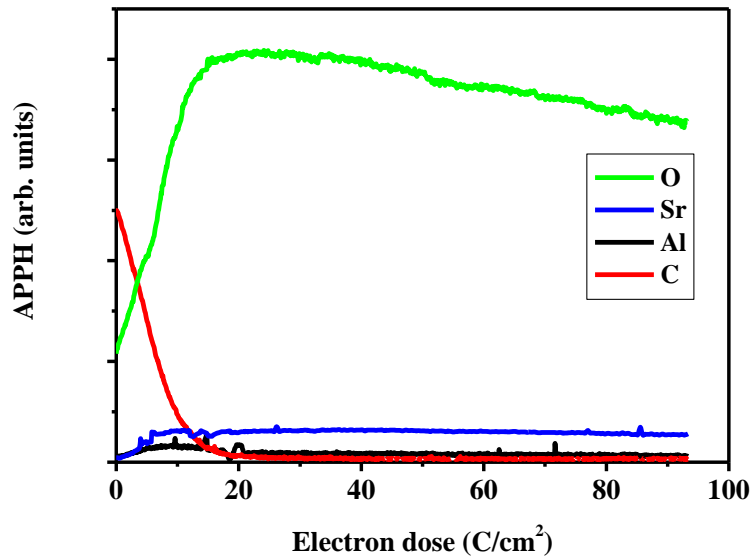


Figure 9.1. The AES spectra before and after degradation of $\text{SrAl}_2\text{O}_4:\text{Eu}^{2+}, \text{Dy}^{3+}$ thin films at 1.33×10^{-6} Torr O_2 .

Figure 9.2 shows the APPH for the $\text{SrAl}_2\text{O}_4:\text{Eu}^{2+}, \text{Dy}^{3+}$ thin films degraded at a base pressures of (a) 3.6×10^{-9} Torr and an oxygen pressure of (b) 1.0×10^{-6} Torr.



(a)



(b)

Figure 9.2. The variation of APPH values with the electron dose for $\text{SrAl}_2\text{O}_4:\text{Eu}^{2+}, \text{Dy}^{3+}$ thin films degraded at a base pressures of (a) 4.79×10^{-9} mbar and an oxygen pressure of (b) 1.33×10^{-6} mbar O_2 .

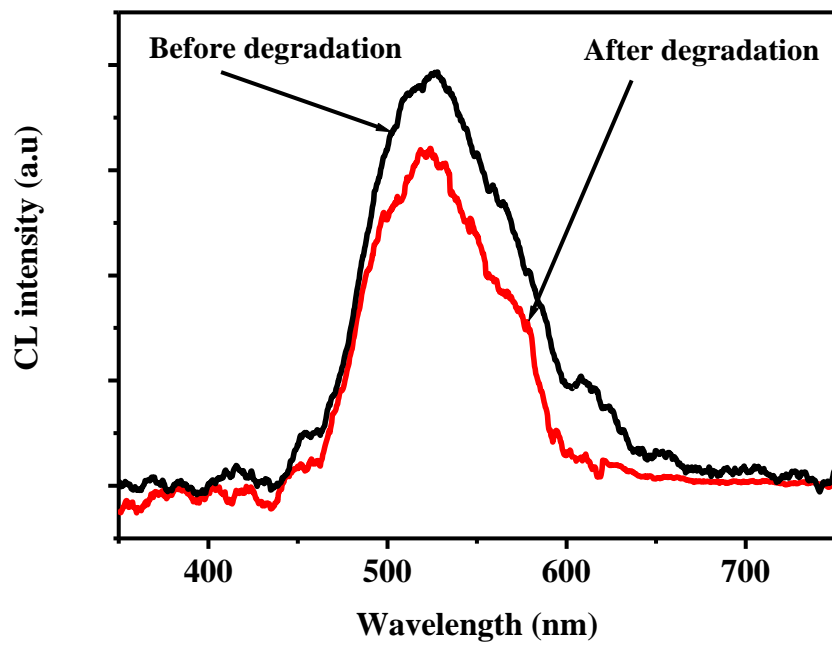
At base pressure (4.79×10^{-9} mbar) the APPH of the O signal increased sharply during the first 30 C/cm^2 electron dose and was almost stable for the remainder of the experiment as shown in Figure 9.2(a). The Sr and Al Auger peaks increased slightly during the first 30 C/cm^2 electron dose and was almost stable for the remainder of the experiment as shown in Figure. 9.2(a). The Sr and Al Auger peaks increased slightly during the first 15 C/cm^2 electron dose and then stabilized for the rest of the experiment. Consistent with the Auger data in Figure 9.1, the C peak decreased from the start to the end of the electron beam irradiation. In the presence of oxygen (1.33×10^{-6} mbar O_2) as shown in Figure 9.2(b), the C, Sr, and Al Auger peaks followed the same pattern as that of Figure 9.2(a) while the O Auger peak decreased steadily after the initial increase during the first 30 C/cm^2 . C was also completely removed within 25 C/cm^2 . The increase in APPH signals of Sr, Al and O during the first 30 C/cm^2 can be attributed to the formation of non luminescent Al- and Sr-oxides on the surface due to the ESSCR process. During the ESSCR process, the electron beam dissociates the oxygen gas as well as water vapour from their background gases into atomic species, which then reacts with the surface atoms to form different chemical layers as explained previously [8]. The desorption of O_2 with increasing electron dose during the

beam irradiation at 1.33×10^{-6} and 1.33×10^{-7} mbar O_2 could be attributed to the Knotek-Feibelman mechanism of electron stimulated desorption of atoms from solids [8, 9]. The dopant elements Eu, and Dy could not be detected by AES due to their low concentrations.

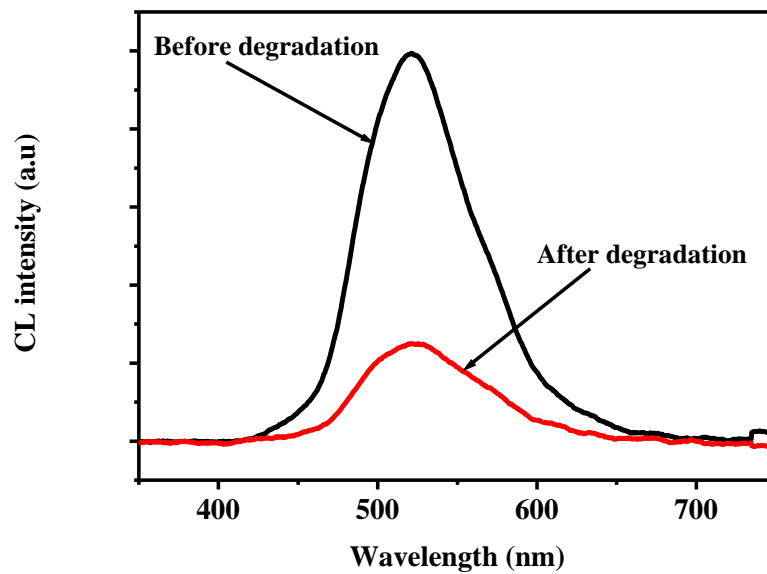
9.3.2 CL RESULTS

Figure. 9.3 (a) and (b) shows the CL spectra of the $SrAl_2O_4:Eu^{2+},Dy^{3+}$ thin films before and after degradation at 4.79×10^{-9} mbar (base pressure) and 1.33×10^{-6} mbar O_2 respectively. In all cases the film gave a green emission with a maximum peak at ~ 521 nm. The emission is attributed to the $4f^65d^1 \rightarrow 4f^7$ transitions of Eu^{2+} [4]. Comparing the degradation rates of Figures 9.3 (a) and (b), it is clear that the rate was much slower at the base pressure compared to higher oxygen pressure. Figure 9.4 compares the decrease in the CL intensity as a function of electron dose at different vacuum pressures. There is firstly a rapid drop in intensity, within the first few seconds. This could be due to surface charge occurring at the onset of irradiation, which increases the probability of sweeping apart the electron-hole pairs before recombination [8] resulting in the loss of the CL intensity. Then a decrease in the CL intensity continued with time.

The CL degradation curve for the film degraded at base pressure (4.79×10^{-9} mbar) showed a similar pattern to that degraded at 1.33×10^{-7} mbar O_2 , but with less degradation. For the film degraded at 1.33×10^{-6} mbar O_2 , there was initially a decrease in the CL intensity due to the removal of C from the surface. During the removal of C from the surface, the CL intensity increased slightly before it decreased at a higher rate. The fact that the decrease in the CL intensity was faster at higher oxygen pressure (1.33×10^{-6} mbar O_2) suggests that the rate of formation of the non-luminescent oxide layers was also high at higher oxygen pressures. The degradation of the CL intensity during electron irradiation can be explained by a combination of the power loss in a non-luminescence oxide surface layer and the injection of point defects into the near surface region as explained previously [8, 11].



(a)



(b)

Figures 9.3. (a) The CL spectra for the undegraded and degraded spots of $\text{SrAl}_2\text{O}_4:\text{Eu}^{2+}, \text{Dy}^{3+}$ thin films at the base pressure of (a) 3.6×10^{-9} Torr. (b) Oxygen pressure of 1×10^{-6} Torr.

Figure 9.5 shows the Gaussian fit of the undegraded CL peak at 521 nm. The fitted data gave rise to two peaks at 512 and 550 nm which are attributed two Eu^{2+} occupying two different sites of Sr^{2+} . As explained in the next section, the XPS data collected from degraded and undegraded data confirms the existence of the two Sr^{2+} sites.

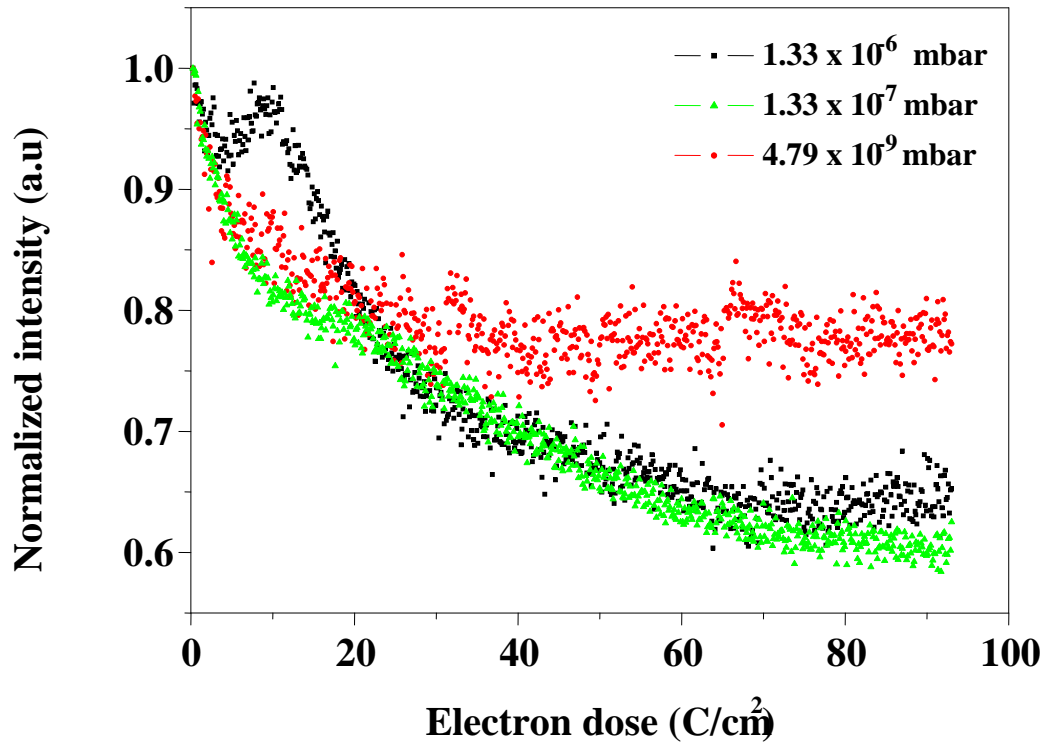


Figure 9.4. The normalized CL degradation for $\text{SrAl}_2\text{O}_4:\text{Eu}^{2+}, \text{Dy}^{3+}$ thin film degraded at the different pressures.

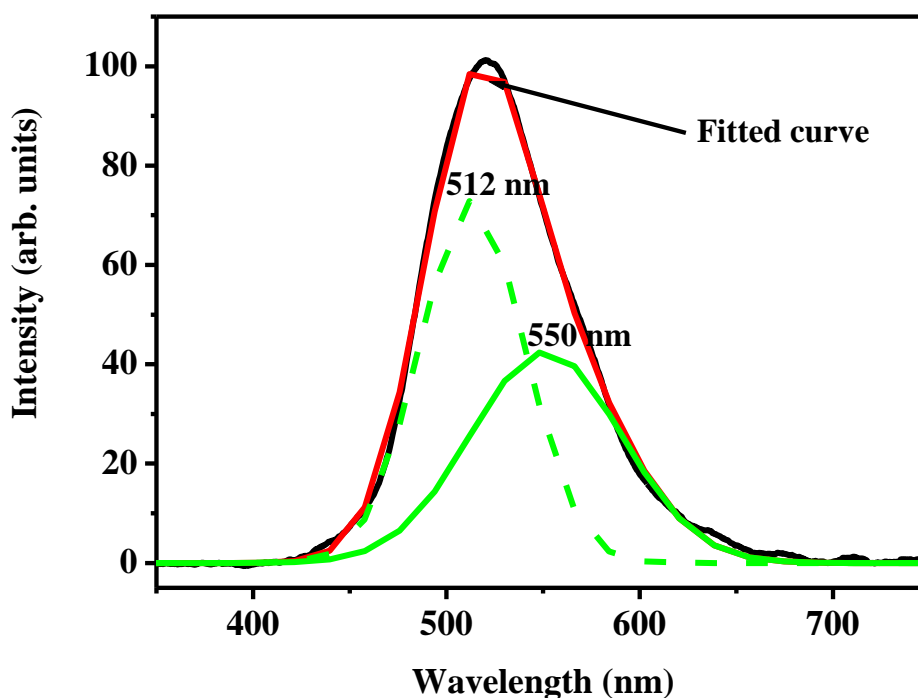
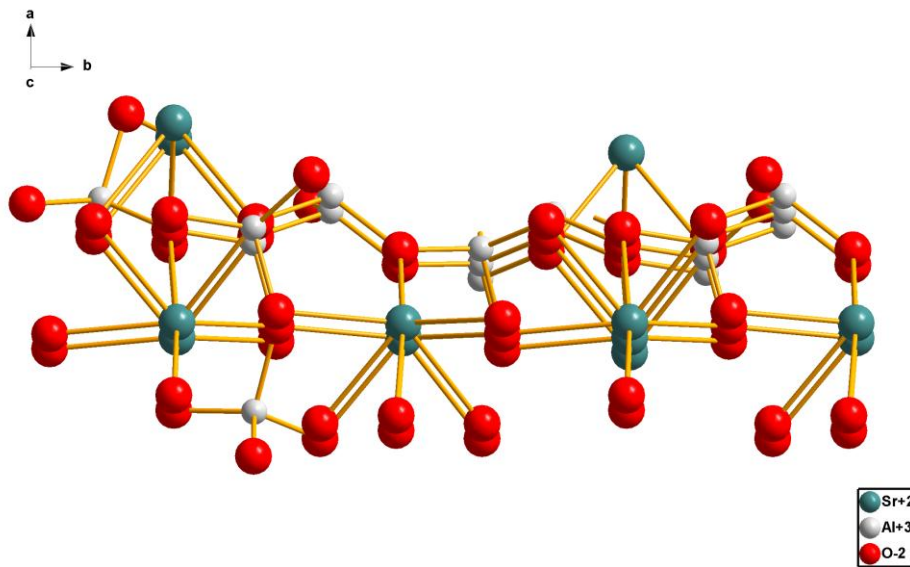
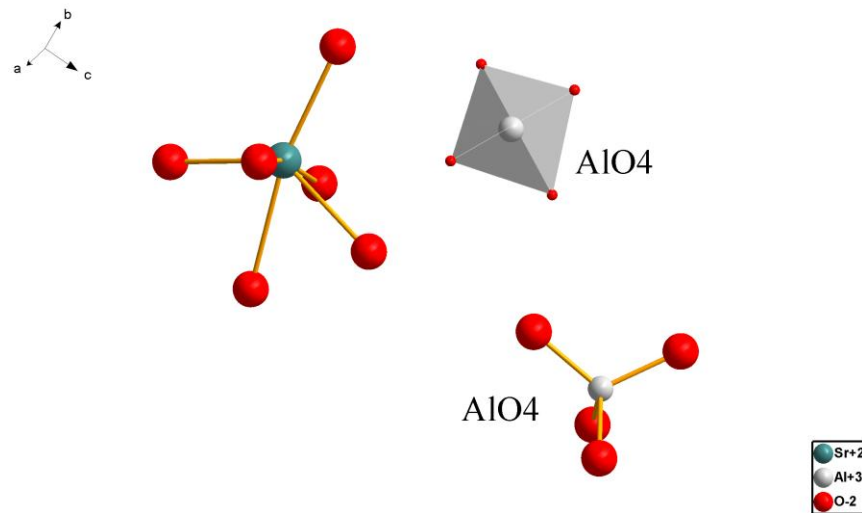


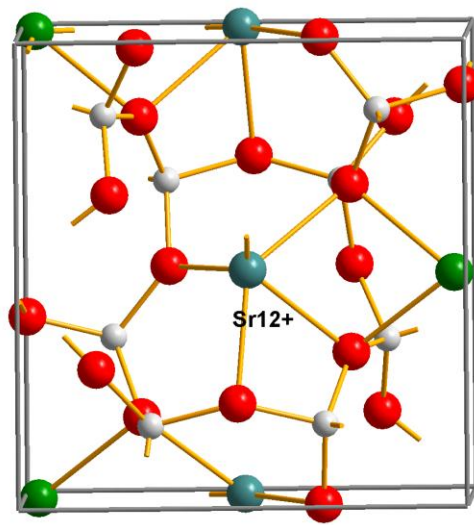
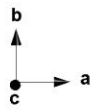
Figure 9.5. The Gaussian fit of the CL emission spectrum of undegraded $\text{SrAl}_2\text{O}_4:\text{Eu}^{2+}, \text{Dy}^{3+}$ thin film at the oxygen pressure of 1×10^{-6} Torr..

9.3.4 THE XPS RESULTS

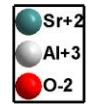
The XPS chemical oxidation states depend mainly on the sites of the alkaline earth ion, i.e., Sr^{2+} in the crystal structure. SrAl_2O_4 belongs to the tridymite-like structure. The typical structure is formed with a three-dimensional frame-work of corner sharing AlO_4 tetrahedra. The connection network of atoms in SrAl_2O_4 is as shown in Figure 9.6(a) and (b) [6]. Each oxygen ion is shared by two aluminium ions so that each tetrahedron has one negative charge. The charge balance is achieved by the large divalent cation Sr^{2+} , which occupies interstitial site within the tetrahedral frame-work. The structure of the low-temperature phase has a three-dimensional network of corner-sharing AlO_4 tetrahedra, which has channels in the a- and c-directions where Sr^{2+} ions are located [12]. Figure 9.6(c)-(f) shows the Sr^{2+} ion locations at different projections. There are two crystallographically different sites for Sr^{2+} represented by (Sr_1) and (Sr_2), which have identical coordination numbers (i.e. $6+1$). The distance between two successive strontium ions is alternately 3.9 and 4.6 Å [13]. The two environments differ only by a slight distortion of their square planes. However the distances between the strontium ion and its neighboring oxygen ions are different for the two strontium

sites. The oxygen ions are rather close to the one strontium site, whereas the oxygen ions are at a much larger distance from the other strontium site [13]. This can be revealed by the parallel projections of the polyhedral forms for the two directions (c) and (a) shown in Figure 9.6 (d) and (f).

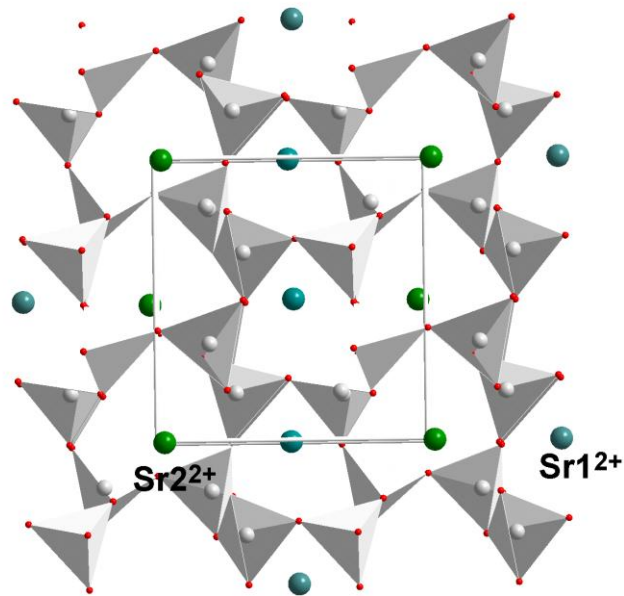




Sr22+

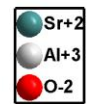


(c)



Sr22+

Sr12+



(d)

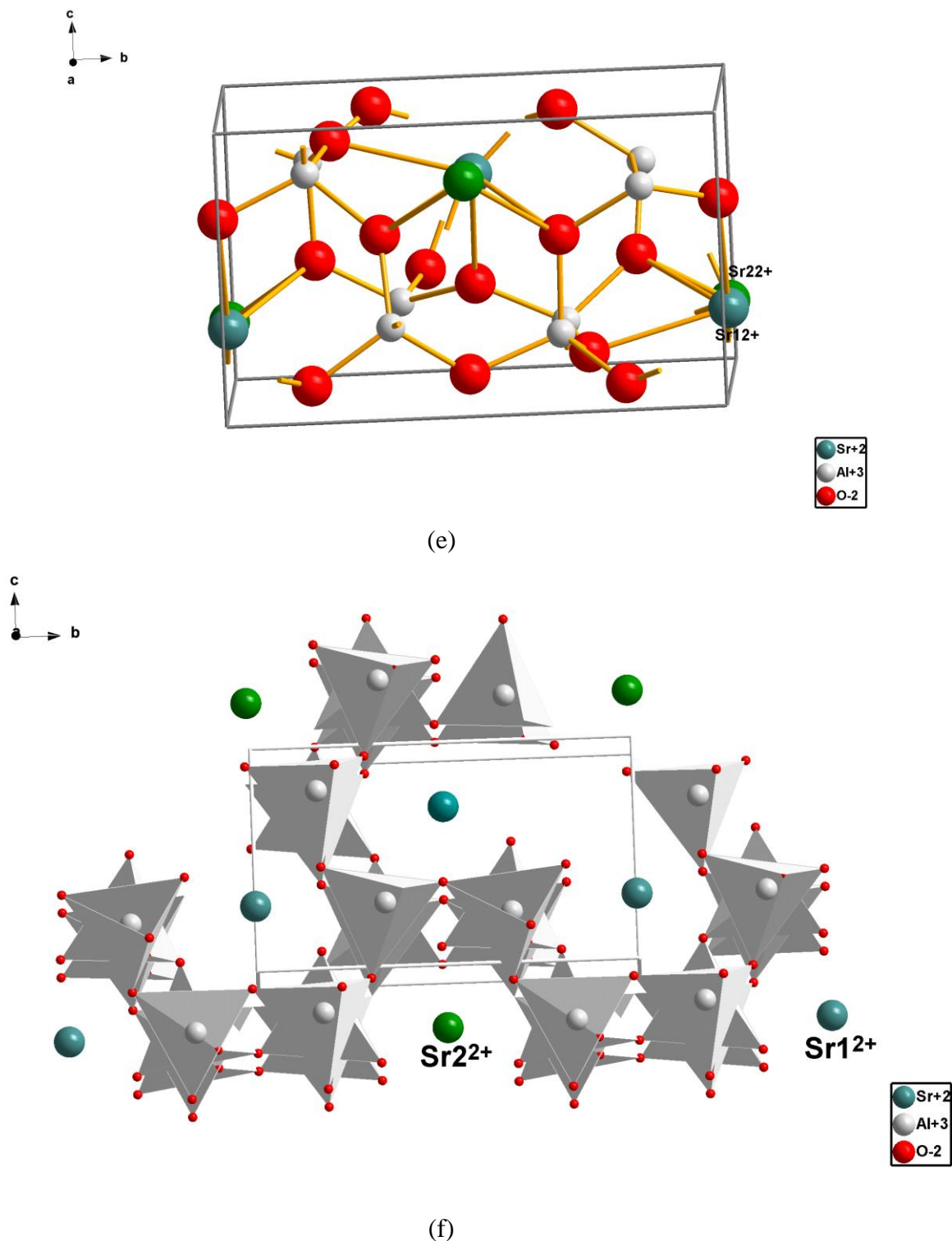


Figure 9.6. (a) and (b) shows the arrangement of atoms in the SrAl₂O₄ crystal (c), (d), (e) and (f) show the two sites of Sr²⁺ (Sr₁-blue and Sr₂-green) in the c- and a- direction respectively (JCPDS 34-379 or ICSD 26466)

The Sr²⁺ and Eu²⁺ ions are very similar in their ionic size (i.e., 1.21 and 1.20 Å respectively [13]). Consequently, when occupied by Eu²⁺ ions, the two different Sr²⁺ ions located at the two

different Sr^{2+} sites will have very similar local environments [12]. The monoclinic SrAl_2O_4 , being stable at temperatures below 950 K is a distorted form of a hexagonal SrAl_2O_4 . The distortion involves a reduction in the symmetry of the trigonally distorted rings. The structure of hexagonal SrAl_2O_4 has all of the tetrahedral rings equivalent and trigonally distorted [12].

The XPS results from Figure 9.7 represent the undegraded and degraded spectra of the $\text{SrAl}_2\text{O}_4:\text{Eu}^{2+}$, Dy^{3+} thin films. They are given in the order; (a) Al 2p, (b) Sr 3d, and (c) O1s. The general difference between the XPS spectra of the undegraded and degraded films is the absence of the C peak (C1s) in the degraded film as opposed to the undegraded one (not shown). In Figure 9.7(a) there are only two peaks for the Al 2p oxidation state, namely SrAl_2O_4 (74.3 eV) and a peak at 74.8 eV, which is associated with Al_2O_3 [14]. The degraded film has a more intense Al_2O_3 peak than the undegraded one. The increase in Al_2O_3 is due to the oxide formation on the film surface as a result of ESSCR process as observed in the APPH results.

The oxidation states of Sr 3d are represented by Figure 9.7 (b). The undegraded film spot recorded two SrAl_2O_4 peaks, i.e., $\text{SrAl}_2\text{O}_4\text{-}3d_{5/2}$ and $\text{SrAl}_2\text{O}_4\text{-}3d_{3/2}$ from the two Sr^{2+} sites. The degraded spot gave two Sr- $3d_{5/2}$ (133.2 and 134.3 eV) and two Sr- $3d_{3/2}$ (134.9 and 135.8 eV) peaks, which are associated with the Sr from the two sites in the SrAl_2O_4 and two more peaks at 135.2 ($3d_{5/2}$) and 136.5 eV ($3d_{3/2}$) coming from SrO [15]. The SrO was formed as a result of the ESSCR process. A similar result was reported by Swart et al. [16]. The chemical states of oxygen (O1s) are shown in Figure 9.7(c). It can be noted that for the undegraded film only two binding energy peaks were identified, i.e., SrAl_2O_4 [this work-530.6 eV] and Al_2O_3 at 532.0 eV compared to literature 531.8 eV [17], while the degraded film had another peak at 529.8 eV coming from SrO [15, 18] and also a more pronounced Al_2O_3 peak. It is therefore clear that SrO and Al_2O_3 were formed on the surface of the degraded films.

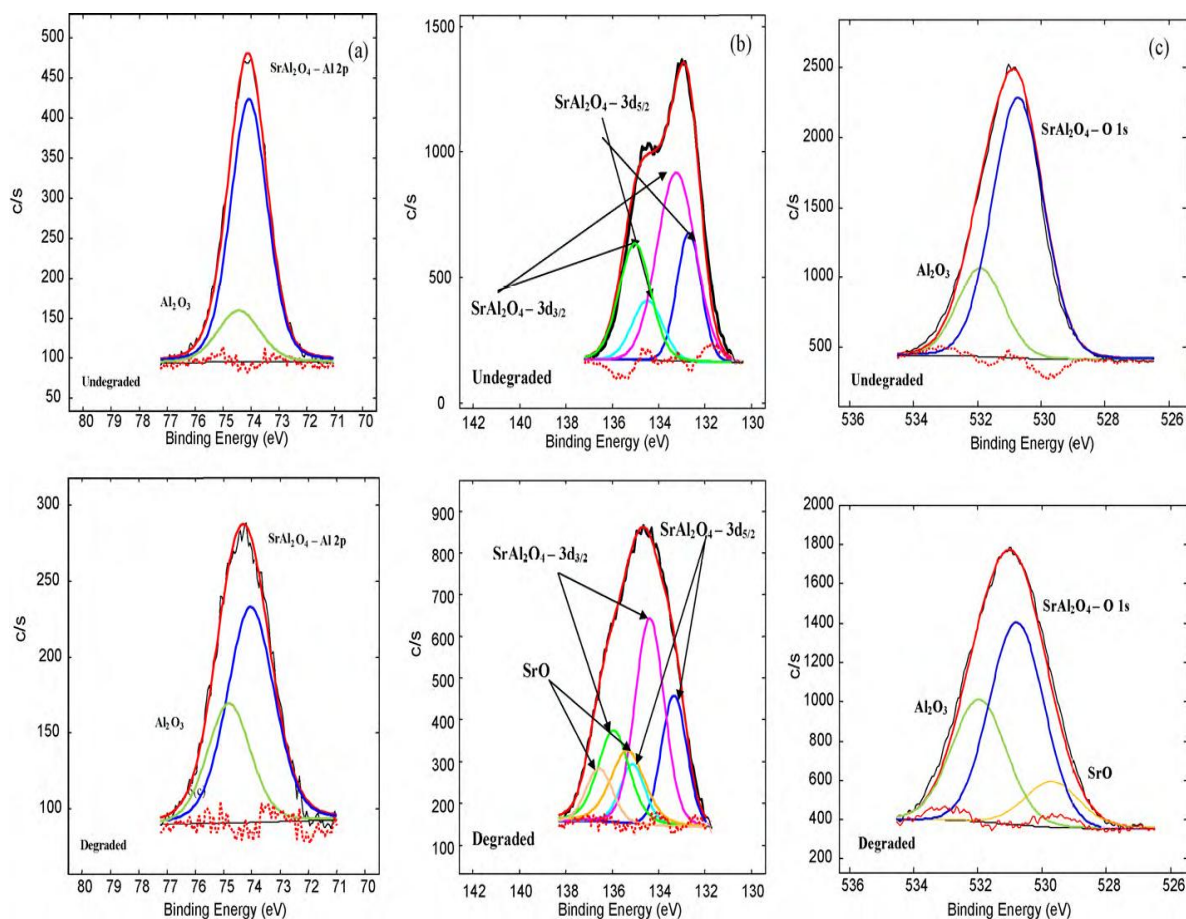


Figure 9.7. The undegraded and degraded XPS results for (a) Al 2p, 6(b) Sr 3d, 6(c) C1s, and (d) O1s for the $\text{SrAl}_2\text{O}_4:\text{Eu}^{2+}, \text{Dy}^{3+}$ thin films.

This serves as another proof that prolonged electron bombardment of several phosphors resulted in the degradation thereof due to the ESSCR process.

9.4 CONCLUSION

Laser ablated $\text{SrAl}_2\text{O}_4:\text{Eu}^{2+}, \text{Dy}^{3+}$ thin films have been successfully degraded using the Auger electron spectroscopy combined with the CL facility. The base pressure plays a great role in the degradation of $\text{SrAl}_2\text{O}_4:\text{Eu}^{2+}, \text{Dy}^{3+}$ thin films. The APPH signals of O and Sr increased with the increase in the electron dose of the electron irradiation. A similar trend was observed in the Al APPH signal though at a less extent due to the formation of Al_2O_3 . The APPH signal of C decreased with the increase in the electron dose of the electron beam. The ESSCR process is responsible for the CL degradation of the films. The CL intensity decreased with the increase in the electron dose due to formation of a non-luminescent layer (SrO and Al_2O_3)

on the film surface. The electron beam dissociates molecular species, particularly; H₂O to atomic species which subsequently react with C to form volatile compounds (Co_x, CH₄, SO₂ etc.). The XPS results have proved the presence of SrO and Al₂O₃ on the degraded film spots.

REFERENCES

1. T. Matsuzawa, Y. Aoki, N. Takeuchi, Y. Murayama, *J. Electrochem. Soc.* **143** (1996) 2670.
2. T. Katsumata, T. Nabae, k. Sasajima, S. Komuro, T. Morikawa, *J. Electrochem. Soc.* **144** (1997) L243.
3. J.M. Ngaruiya, S. Niewoudt, O.M. Ntwaeaborwa, J.J. Terblans, H.C. Swart, *Mater. Lett.* **62** (2008) 3192.
4. P. D. Nsimama, O.M. Ntwaeaborwa, E.Coetsee, H.C.Swart, *Phys. B: Condens. Matter* **404** (2009).
5. PHI MultipakTM, Version 8.2C, Part number 706570, Software for Complete AES and XPS Data Reduction, Copyright 2007, Ulvac-PHI, Inc.
6. Diamond Version 3.0d, Copyright © 1997-2005 Crystal Impact GbR, Bonn Germany.
7. J.S. Sebastian, H.C. Swart, T.A. Trottier, S.L. Jones and P.H. Holloway, *J. Vac. Sci. Technol. A* **15** (1997) 2349.
8. H. C. Swart, T. A. Trottier, J. S. Sebastian, S. L. Jones, P. H. Holloway, *J. Appl. Phys.* **83** (1998) 4578.
9. O. M. Ntwaeaborwa, H. C. Swart, R. E. Kroon, P. H. Holloway and, J. R. Botha, *J. Phys. Chem. Solids* **67** (2006) 1749.
10. O. M. Ntwaeaborwa, H. C. Swart, R. E. Kroon, J. R. Botha, and P. H. Holloway, *J. Vac. Sci. and Technol. A* **25** (2007) 1152.
11. H. C. Swart, J. S. Sebastian, T. A. Trottier, S. L. Jones, P. H. Holloway, *J. Vac. Sci. A* **14** (1996) 1697.
12. H. Ryu, K.S. Bartwal, *Physica B* **404** (2009) 1714.
13. D. Ravichandran, Shikik T. Johnson, S. Erdei, Rustum Roy, William B. White, *Displays* **19** (1999) 197.
14. J.C. Klein, D.M. Hercules, *J. Catal.* **82** (1983) 424.
15. H. van Doveren, J.A. Verhoeven, *J. Electron Spectrosc. Relat. Phenom.* **21** (1980) 265.
16. H.C. Swart, E. Coetzee, J.J. Terblans, O.M. Ntwaeaborwa, P.D. Nsimama, F.B. Dejene and J.J. Dolo, *J. Appl. Phys. A*, doi:10.1007/s00339-010r-r5915-6.
17. C.D. Wagner, D.E. Passoja, H.F. Hillery, T.G. Kinisky, H.A. Six, W.T. Jansen, J.A. Taylor, *J. Vac. Sci. Technol.* **21** (1982) 933.

18. XPS International Inc., Handbook of the Elements and Native Oxides, XPS International, Inc., 1999.

CHAPTER 10

SUMMARY AND SUGGESTIONS FOR FUTURE WORK

10.1 THESIS SUMMARY

Thin films of $\text{SrAl}_2\text{O}_4:\text{Eu}^{2+},\text{Dy}^{3+}$ phosphor were successfully prepared using the pulsed laser deposition technique. The Lambda Physic 248 nm KrF excimer laser was used to ablate the phosphor pellets. The AFM and SEM were employed for morphological and topographical analysis. The XRD and HRTEM were used in structural analysis. The PL data were obtained from the He-Cd 325 nm laser PL system and the xenon-lamp Cary Eclipse fluorescence spectrophotometer. The CL data were obtained from the CL system connected to the AES system. The elemental composition analysis of the films was done by using, the AES, XPS, RBS and EDS. The AES and XPS were employed for depth profile analysis.

The morphological, topographical, PL and CL properties of the thin films varied with the deposition parameters, namely, substrate temperature, pulse repetition rate, base pressure and the working atmospheres. The optimum substrate temperature for highly emitting $\text{SrAl}_2\text{O}_4:\text{Eu}^{2+},\text{Dy}^{3+}$ films has been found to be on the 350-400° C range. The films deposited using lower pulse repetition rates gave better PL properties than those deposited at higher repetition rates. $\text{SrAl}_2\text{O}_4:\text{Eu}^{2+},\text{Dy}^{3+}$ thin films ablated using higher number of pulses have superior PL and afterglow properties to the lower number of pulses counterparts. The film that was deposited at the base pressure of 2.7×10^{-5} mbar base gave the brightest green emission of all the films deposited by varying the base pressure. The results suggest that the film deposited at lower base pressure (5.6×10^{-6} mbar) favoured the oxidation of Eu^{2+} into Eu^{3+} and ended up giving a brighter red emission peak and weak green emission peak. As-deposited films prepared in the gas atmospheres gave AFM images with well-defined grains. The average particle sizes for films deposited in gas atmospheres were ranging from 25 nm to 40 nm. The as-deposited film prepared in vacuum had poorly-defined AFM images. The as-deposited films prepared in the gas atmospheres gave better PL and afterglow properties than the film deposited in vacuum. Generally, films with rougher surfaces and well-defined grains

gave better PL and afterglow properties. All the green PL emissions of $\text{SrAl}_2\text{O}_4:\text{Eu}^{2+},\text{Dy}^{3+}$ thin films are attributed to the $4f^65d^1 \rightarrow 4f^7$ Eu^{2+} transitions, while the red emissions are attributed to the $^5\text{D}_0 \rightarrow ^7\text{F}_2$ Eu^{3+} transitions.

The XRD and HRTEM results of the as-deposited $\text{SrAl}_2\text{O}_4:\text{Eu}^{2+},\text{Dy}^{3+}$ thin films were all amorphous. Upon annealing at 800°C in vacuum for 2 hours, the PL of the films deposited in the gas atmospheres worsened. However, the PL properties of the annealed vacuum deposited thin film improved considerably, due the improved crystal structure upon annealing. The crystal structure was similar to that of the monoclinic SrAl_2O_4 .

The CL spectra of $\text{SrAl}_2\text{O}_4:\text{Eu}^{2+},\text{Dy}^{3+}$ thin films gave green emission peaks ranging from 507 nm-522 nm coming from the $4f^65d^1 \rightarrow 4f^7$ Eu^{2+} ion transitions. The films showed a high stability to the electron beam irradiations; It took up to 19 hours (130 C/cm^2) of electron bombardment (electron dose) to decrease to a stable lower CL intensity value. The CL degradation of the films was increasing with the increasing chamber pressure. The degradation was due to the formation of the non-luminescent layer on the film surface during electron bombardment as a result of the ESSCR process.

The AES elemental composition results for the undegraded and degraded gave all the main elements in the $\text{SrAl}_2\text{O}_4:\text{Eu}^{2+},\text{Dy}^{3+}$ material, i.e. Sr, Al and O. The AES APPH results showed an increasing O, Sr and Al signals and a decrease in the C signal with the increase in the electron dose. The increase in O, Sr and Al signals was due to formation of SrO and Al_2O_3 on the surface of the film as a result of the electron stimulated surface chemical reaction (ESSCR) process on the film surface. During the ESSCR process, the electron beam dissociates the O_2 and other background species such as H_2O to atomic species which subsequently react with C to form volatile compounds (CO_x , CH_4 , etc.).

The XPS results for the undegraded spots of $\text{SrAl}_2\text{O}_4:\text{Eu}^{2+},\text{Dy}^{3+}$ thin films were characterized by the Al2p, Sr3d and O1s oxidation states. The oxidation states existed in form of SrAl_2O_4 and Al_2O_3 . The degraded spots had similar oxidation states but with an increase in the Al_2O_3 peak intensity and an additional SrO peak. Both SrO and the increase in the Al_2O_3 peak resulted from the ESSCR process. The Sr3d oxidation state was split into Sr3d_{3/2} and Sr3d_{5/2} due to the two sites of Sr^{2+} in the crystal host.

The RBS results showed stoichiometric ratios of elements in pulsed laser SrAl₂O₄:Eu²⁺,Dy³⁺ thin films (Sr:Al:O; 1:1.9:4.1) comparable to the commercial powder (Sr:Al:O; 1:2:4). The dopants also could be identified suggesting RBS to be a powerful technique for dopant identification and analysis.

10.2 SUGGESTIONS FOR FUTURE WORK

The work presented in this thesis is very valuable to the literature of laser ablated $\text{SrAl}_2\text{O}_4:\text{Eu}^{2+},\text{Dy}^{3+}$ thin films. The CL spectra and CL degradation studies have been reported from this work for the first time. The XPS results have also been communicated to the science world for the first time. However, there are some investigations which need more attention to get more light on some of the findings.

With regards to the deposition conditions, it is important to investigate more on the changes of oxygen, argon and nitrogen with the PL properties of $\text{SrAl}_2\text{O}_4:\text{Eu}^{2+},\text{Dy}^{3+}$ thin film phosphors. A wider range of the gas pressures (0.1^{-2} Torr) is needed for better optimizations. Other deposition parameters which are of interest are the target-substrate, the laser-target distance and the substrate type. It is important to do some more investigations on the in-situ post deposition analysis on the films and compare with the ex-situ annealing to determine the better annealing process for better PL and afterglow properties of $\text{SrAl}_2\text{O}_4:\text{Eu}^{2+},\text{Dy}^{3+}$ films.

In connection with the effect of annealing on the films deposited in different deposition atmospheres, we found that the properties of the films deposited in the gas atmospheres and annealed gave poorer PL properties than the as-deposited. It is of great importance that further studies must be done on the obtained unexpected results by annealing the films at different substrate temperatures, e.g. 200, 400 and 600° C. Annealing in different atmospheres such as argon, nitrogen can also be interesting.

In the current work, all the depositions were done by using a 248 nm KrF laser source. It will be interesting to use another source of laser with higher energy such as 193 nm ArF in the course of seeing how the properties of $\text{SrAl}_2\text{O}_4:\text{Eu}^{2+},\text{Dy}^{3+}$ thin films will change.

It will also be of interest to do further investigation on the AES of $\text{SrAl}_2\text{O}_4:\text{Eu}^{2+},\text{Dy}^{3+}$ thin films including the residual gas analyzer (RGA) results.

Also more studies should be done on the CL degradation, namely; the influence of beam voltage and beam current on the CL degradation of $\text{SrAl}_2\text{O}_4:\text{Eu}^{2+},\text{Dy}^{3+}$ thin films, establishing a relation governing the ESSCR of $\text{SrAl}_2\text{O}_4:\text{Eu}^{2+},\text{Dy}^{3+}$ phosphor.

Coating the surface of phosphors is one of the measures of decreasing the degradation rate. The coating is supposed to be thin enough to be transparent to low energies and should not influence the chromaticity and brightness of the phosphor [1]. The coating layer should have a good bandgap alignment with the material to be protected. Furthermore, it should consist of light elements and low density to exhibit minimal losses in electron penetration and should also have a penetration depth higher than the film material to be protected [2]. So, I would suggest future CL degradation on the $\text{SrAl}_2\text{O}_4:\text{Eu}^{2+},\text{Dy}^{3+}$ thin films to involve coatings of thin layers of the following frequently used materials, SiO_2 , MgO , SnO_2 , In_2O_3 , Al_2O_3 , CdO to try to reduce the CL degradation. Heat treatments on the coatings should also be applied to improve the coating stability whenever necessary.

REFERENCES

1. E. Coetsee, H. C. Swart, and J. J. Terblans, *J. Vac. Sci. Technol. A* **25** (2007)1226.
2. W. Park, B.K. Wagner, G. Russell, K. Yasuda, and C.J. Summers, *J. Mater. Res.* **15** (2000) 2288.

PUBLICATIONS RESULTING FROM THIS WORK

1. O.M Ntwaeaborwa, M.S. Dhlamini, J.J Terblans, B.M Mothudi, P.D. Nsimama, H.C Swart, Proceedings of the 14th International Workshop on Organic and Inorganic Electroluminescence & 2008 International Conference on the Science and Technology of Emissive Displays and Lighting, 9-12 September 2008, Italy (Rome) pp 177 – 179 (ISBN 88-8286-194-5).
2. P.D. Nsimama, O. M. Ntwaeaborwa, E. Coetsee, H.C. Swart , Phys. B; Condens. Matter, **404** (2009) 4489-4492.
3. O .M. Ntwaeaborwa, P.D. Nsimama, E. Coetsee, H.C. Swart, Phys. B; Condens. Matter, **404** (2009) 4436-4439.
4. O. M. Ntwaeaborwa, P.D. Nsimama, S. Pitale, I. M. Nagpure, V. Kumar, E. Coetsee, J. J. Terblans, P. T. Sechogela and H. C. Swart, J. Vac. Sci. Tech. A **28** (2010) 901-905.
5. H.C. Swart, E. Coetsee, J.J. Terblans, O.M. Ntwaeaborwa, P.D. Nsimama · F.B. Dejene, J.J. Dolo, Appl. Phys A, **101** (2010) 633.
6. P.D. Nsimama, O. M. Ntwaeaborwa, H.C. Swart, Appl. Surf. Sci. **257** (2010) 512-517.
7. P.D. Nsimama, O. M. Ntwaeaborwa, H.C. Swart, J. Lumin. **131** (2011), 119.

PRESENTATIONS IN CONFERENCES/WORKSHOPS

1. O.M Ntwaeaborwa, M.S Dhlamini, J.J Terblans, B.M Mothudi, P.D Nsimama, H.C Swart, "Phonon mediated energy transfer from ZnO nanoparticles to SiO₂:PbS", 14th International Workshop on organic and Inorganic Electroluminescence & 2008 International Conference on the Science and Technology of Emissive Displays and Lighting, 9-12 September 2008, Pagni de Tivoli- Rome (Italy).
2. O.M Ntwaeaborwa, M.S Dhlamini, J.J Terblans, B.M Mothudi, P.D Nsimama, H.C Swart, "Phonon mediated energy transfer from ZnO nanoparticles to SiO₂:PbS", 14th International Workshop on organic and Inorganic Electroluminescence & 2008 International Conference on the Science and Technology of Emissive Displays and Lighting, 9-12 September 2008, Pagni de Tivoli- Rome (Italy).
3. O.M Ntwaeaborwa, H.C Swart, R.E Kroon, M.S Dhlamini, J.J Terblans, B.M Mothudi, P.D Nsimama, M-M Biggs, P.H Holloway, AVS 55th International Symposium and Exhibitions, 19-24 October 2008, Boston-Massachusetts (USA).
4. O.M Ntwaeaborwa, RE Kroon, MS Dhlamini, BM Mothudi, PD Nsimama, M-M Biggs, PS Mbule, HC Swart, "Sol-gel synthesis, characterization and luminescence properties of ZnO-PbS nanocomposite", 3rd NanoAfrica Conference, 1- 4 February 2009, Pretoria (South Africa).
5. P.D. Nsimama, O.M. Ntwaeaborwa, E. Coetsee and H.C Swart, "The influence of the number of pulses on the morphological and photoluminescence properties of SrAl₂O₄:Eu²⁺, Dy³⁺ thin films prepared by pulsed laser deposition", Physica B, 3rd South African Conference on Photonic Materials, 23-27 March 2009, Mabula Game Lodge, Limpompo, South Africa.
6. O.M. Ntwaeaborwa, P.D.Nsimama, J.T. Abiade, E. Coetsee and H.C Swart, "The effects of substrate temperature on the structure, morphology and photoluminescence properties of pulsed laser deposited SrAl₂O₄:Eu²⁺, Dy³⁺ thin films", Physica B, 3rd South African Conference on Photonic Materials, 23-27 March 2009, Mabula Game Lodge, Limpompo, South Africa.
7. P.D. Nsimama, O. M. Ntwaeaborwa, H.C. Swart, "The influence of deposition parameters on the properties of SrO₂Al₄:Eu²⁺, Dy³⁺ thin film phosphors prepared by the pulsed laser technique", The 2nd ALC Student Workshop, 2nd-5th July 2009, Kariega Game Reserve-Port Elizabeth, South Africa.
8. P.D. Nsimama, O.M. Ntwaeaborwa, E. Coetsee and H.C Swart, "The influence of deposition parameters on the properties of SrO₂Al₄:Eu²⁺, Dy³⁺ thin film phosphors prepared by the pulsed laser technique: Working atmosphere" SAIP Conference, 7th-11th July 2009, UKZN, Durban, South Africa.
9. O.M. Ntwaeaborwa, P.D. Nsimama, S. Pitale, I. Nagpure, V. Kumar, E. Coetsee, J.J. Terblans, H.C. Swart, P. Sechogela, "Photoluminescence properties of SrAl₂O₄:Eu²⁺, Dy³⁺ thin phosphor films grown by pulsed laser deposition" AVS 56th International Symposium and Exhibition, November 8-13, 2009, San Jose, California.

10. H.C. Swart, E Coetzee, JJ Terblans, OM Ntwaeaborwa, PD Nsimama, FB Dejene and JJ Dolo, "Cathodoluminescence degradation of PLD thin films", COLA 2009, 22nd-27th November 2009, Singapore.
11. P.D. Nsimama, O.M. Ntwaeaborwa, H.C. Swart, "Characterization of SrAl₂O₄:Eu²⁺, Dy³⁺ prepared by pulsed laser deposition", 3rd African Laser Center (ALC) Student Workshop, 23-26 September 2010, Zevenwacht Wine Estate, Stellenbosch, South Africa.
12. P.D. Nsimama, O.M. Ntwaeaborwa, H.C. Swart, "Elemental composition analysis, morphological and photoluminescence Studies of pulsed laser deposited SrAl₂O₄:Eu²⁺, Dy³⁺ , SAIP Annual Conference, 28 Sept.-01st October 2010, CSIR, Pretoria, South Africa.